Discovery and Development of Antibodies for Drug Delivery Across the Blood-Brain Barrier

By

Loukas Goulatis

A dissertation submitted in partial fulfillment of the

requirements for the degree of

Doctor of Philosophy

(Chemical and Biological Engineering)

at the

UNIVERSITY OF WISCONSIN-MADISON

2018

Date of final oral examination: 11/07/2018

The dissertation is approved by the following members of the Final Oral Committee:

Eric V. Shusta, Professor, Chemical and Biological Engineering

John Yin, Professor, Chemical and Biological Engineering

Regina M. Murphy, Professor, Chemical and Biological Engineering

David M. Lynn, Professor, Chemical and Biological Engineering

Michael R. Taylor, Assistant Professor, Pharmacy

Discovery and Development of Antibodies for Drug Delivery Across the Blood-Brain Barrier

Loukas Goulatis

Under the supervision of Professor Eric V. Shusta in Chemical and Biological Engineering, University of Wisconsin - Madison

Abstract

The cure and management of the majority of diseases affecting the brain is hampered by the blood-brain barrier (BBB). In the brain endothelia adjacent endothelial cells are sealed together, redirecting molecular trafficking from the paracellular route to the transcellular trafficking. This leads to the barrier's selectivity that maintains brain homeostasis allowing the selective passage of nutrients, but at the same time preventing the vast majority of therapeutics from entering the brain from the blood. In order to treat diseases of the central nervous system harsh, invasive procedures are typically employed. The lack of effective treatments motivates the development of non-invasive methods for brain drug delivery. A widely researched method for non-invasive delivery across the BBB is to target via antibodies the brain's endogenous transport mechanisms particularly transporters that utilize receptor mediated transcytosis (RMT) to ferry therapeutics into the brain. Current RMT systems suffer from low trans-BBB transport capacity, as well as ubiquitous expression throughout the periphery, necessitating the research for novel antibody-RMT pairs. However, the search for such antibody-RMT pairs is at best, problematic, due to a lack of human BBB models of high fidelity that can force a selection campaign towards delivery of transcytosis-capable antibodies. In this work, we aim to discover and develop such brain penetrating antibodies.

First, we describe a novel, combinatorial methodology to screen a phage display antibody library against a stem cell-derived model of the human BBB specifically for transcytosing antibodies. The *in vivo*-like selectivity of the model and its human origin, combined with the power of display technologies allow us to perform screens to find the ‘’needle in a haystack’’ that is an antibody that can traffic across the BBB *in vivo*, and target antigens with human relevance. We move forward to describe the production, purification, and validation for both *in vitro* and *in vivo* brain transport of our lead antibodies. A panel of novel antibodies able to transport across the BBB through RMT mechanisms is identified and evaluated.

Next, we aim to develop an antibody functionalization platform to integrate our brain penetrating antibodies and enable further downstream *in vivo* evaluation. To this end, we describe the optimization of a semi-synthetic protein functionalization platform developed previously in our laboratory. Through fusing antibodies with an intein, a protein segment able to splice itself, and secreting the fusion in yeast it is possible to append site-specifically a chemical handle to the protein of interest thereby enabling a controlled functionalization. This process, termed express protein ligation (EPL), is limited by total protein secretion, and intein cleavage efficiency. By optimizing key amino acid residues at the protein-intein interface critical for cleavage and culture conditions we increase the total capacity of our system for site-specific protein functionalization. Thus, this body of work presents the development of brain penetrating antibodies from early lead discovery to protein functionalization, paving the way for potential applications for brain drug delivery.

Acknowledgments

I would like to take this opportunity to thank all the people that made this body of work possible. Funding provided from the Defense Threat Reduction Agency (DTRA) allowed us to perform scientific studies. I would like to thank the Palecek, Murphy, and Reed labs for offering their equipment as well as advice when most needed, as well as Jackie Cooper who maintained the flow cytometer and microscope I used on a regular basis. Next, I would like to thank all the members of the Shusta lab that I had the pleasure of working with during the past five years. I would like to thank in particular Dr. Thomas Mallott, Dr. Jason Lajoie, Angelica Rodriguez, Dr. Vijesh Bhute, and Dr. Scott Canfield for sharing offices with me and making my time at work enjoyable. Finally, professor Eric Shusta for advising me through the process and being the voice of optimism when discussing and planning the next steps of my PhD.

This journey would not be possible, and certainly far less enjoyable without the friends and people that made for all the fun and support during these five years; I would like to thank them now. My friends back home Vasileios Chantziaras, Maria Tsoutsou, and Aggelos Giamas, and particularly Vasileios Theodosiadis whose work schedule made it feasible to always have someone to chat with despite the hours of time difference. The friends I made in Madison, Travis and Hannah Nelson, Kevin Barnett, Frank Nguyen, Parth Mangrolia, Michael Risbeck, Joe Chada, Dan McClelland, and Nestor Hernandez. Prashant Kumar and Duygu Gerceker not only proved to be great friends, but I would not be able to finish my studies without them spending many hours listening to my presentations and offering advice. And of course, the Greeks that made if feel like home when needed, Kostas Mavrakakis, Lampros Perogamvros, Vaggelis Dhmou, George

Koutsakis, Tasos Pateras, and George Bokas. Importantly, Charalambos Michael to whom I will always be grateful for meeting me when I came to America, and Marla and the rest of the Kougias family that made Chicago feel like home away from home. I would also like to thank professors Alexander Chroneos and Lefteri Tsoukalas for being my unofficial mentors through these years, from my grad school applications all the way down to getting a PhD.

Most importantly I would like to thank my parents Ioannis Goulatis and Inna Volkova, and my grandmother Valentina Volkova. Nothing in my life would be possible without them. Ευχαριστώ . Спасибо.

Table of Contents

List of Figures:

List of Tables:

Chapter 1 – Discovery and Development of antibodies as vectors for Blood-Brain Barrier Drug Delivery

1.1 Introduction

Treatment of central nervous system (CNS) disorders represents one of the major challenges facing public health. With the increase in life expectancy worldwide, the aging population in developed countries, and the late life onset of many of these diseases it is estimated that the toll of these disorders, both financial and societal, will only continue to increase [1]. The hurdle in treating such diseases lies two major areas, drug design, and drug delivery. Responsible for the latter, and most troublesome area, is the Blood-Brain barrier (BBB) that forms a continuous layer of cells lining brain vasculature. A healthy BBB prevents the crossing of the majority of chemical molecules and proteins into the brain allowing only small gaseous molecules or lipophilic agents to freely diffuse across the lipid bilayer, thereby regulating brain homeostasis [2]. Thus, the majority of large molecules that are found from pharmaceutical screens to be effective are effectively excluded from crossing the BBB and exercising their therapeutic effect.

It follows that development of a drug delivery vector that can cross the BBB would be a valuable innovation. To this end, we have employed functional screens to identify antibodies capable to traffic across the BBB in a non-invasive manner. We demonstrated accumulation of our antibodies *in vivo*, as well as the human relevance of our lead candidates (Chapter 3). In Chapter 2, we review the current state of the art of antibody-mediated brain drug delivery with the goal to put in perspective the value and challenges of this technology for addressing treatment of brain disorders.

As our understanding of vector pharmacokinetics and pharmacodynamics, as well as BBB and brain disorders' biology evolves, drug delivery vehicles and therapies move beyond plain 1rst generation antibody therapies [2]. A new generation of therapeutics is under development that utilizes antibodies and peptides as coatings of nanoparticles which themselves possess unique drug delivery properties. Along with nanoparticles' manufacturing technologies, antibody conjugation technologies also continue to develop. In Chapter 4 we describe a platform to chemically functionalize our brain penetrating antibodies through integration with a semi-synthetic platform, as a first step in offering an antibody capable of ferrying a therapeutic into the brain. Chapter 5 contains the first steps into functionalizing our brain penetrating antibodies as proof of concept.

The balance of this introduction surveys the literature and research standing of key fields pertinent to the success of this study.

1.2 Blood-Brain barrier physiology

A unique feature of brain microvascular endothelial cells (BMECs) is the formation of the neurovascular unit that surrounds the vessels and establish and maintains the BBB properties. A typical neurovascular unit is comprised of different cell types interacting with the BMECs that form the BBB. The four main cell types that are assumed to influence the unique BMECs properties are brain astrocytes, pericytes, microglia and neurons [3–5]. These cells regulate BBB development to confer its barrier properties, and capillary blood flow regulation. The role of neurons is more complex, with research showing that the BBB functions is highly influenced by neuronal cues [6]. BBB phenotype is also highly influenced by interaction of the basal lamina of the extracellular matrix with the cerebral microvascular endothelium [6]. Finally, the BBB vasculature expresses a variety of active

efflux transporters on its surface such as those of the ABC family (ATP binding cassette), multi-drug resistance transporters, and importantly the P-glycoprotein (P-gp) transporter that act to remove a wide range of drugs, foreign molecules and their metabolites from the endothelial cells [7].

Defining features distinguishing the brain endothelia from the periphery and renders it impermeable to large molecules is a lack of fenestrations, minimal pinocytotic activity, and the presence of tight junctions (TJ) [6,8]. BMECs are sealed together with the help of a network of specialized intercompartmental membrane proteins that mediate cell-cell contact and bond together endothelial cells: the tight junctions and the adherens junctions [6]. Adherens junctions (AJ), consisting of a number of proteins, serve to provide structural support. Cadherins span the intracellular cleft and are themselves linked to the cell cytoplasm via alpha, beta, and γ-catenin scaffolding proteins [9]. Formation of TJ follows, the manifestation of a healthy AJ phenotype, and disruption of the barrier is subsequent to the AJ disruption [10]. Tight junctions themselves constitute a complex of proteins interacting between overlapping BMECs, such as occludins and various isoforms of claudins that are irreplaceably responsible for BBB integrity and span the intercellular cleft, and junctional adhesion molecules (JAMs)[9]. Peripheral scaffolding proteins such as Z0-1/2/3 and cingulin link occludins and claudins to the cytoskeleton [9]. These interactions of tight junctional proteins with the cytoskeleton are important in barrier properties' regulation, as cytoskeletal rearrangement by external cues can lead to the modification of tight junctional properties and lead to a leaky barrier [8].

Despite its remarkable ''sealing'' properties the BBB is not completely impermeable. The brain constitutes the ''command center'' of the body, and needs to

receive all necessary nutrients, as well as a variety of chemical signals. While small lipophilic molecules (<400Da) diffuse through the lipid membrane of the BMECs large and/or hydrophilic molecules employ alternate, and/or specific, cell assisted routes [11]. For these larger molecules, three main classes of transport systems function at the BBB: absorptive mediated, carrier mediated, and receptor mediated. A diagram of these processes that allow passage of molecules to the brain can be seen in Figure 1.1. Absorptive mediated transcytosis (AMT) is initiated by the absorption of cationic molecules to negatively charged moieties present in the surface that forms the clathrin coated pit and is, therefore, random and non-specific [12]. Nutrient transport is accomplished by a

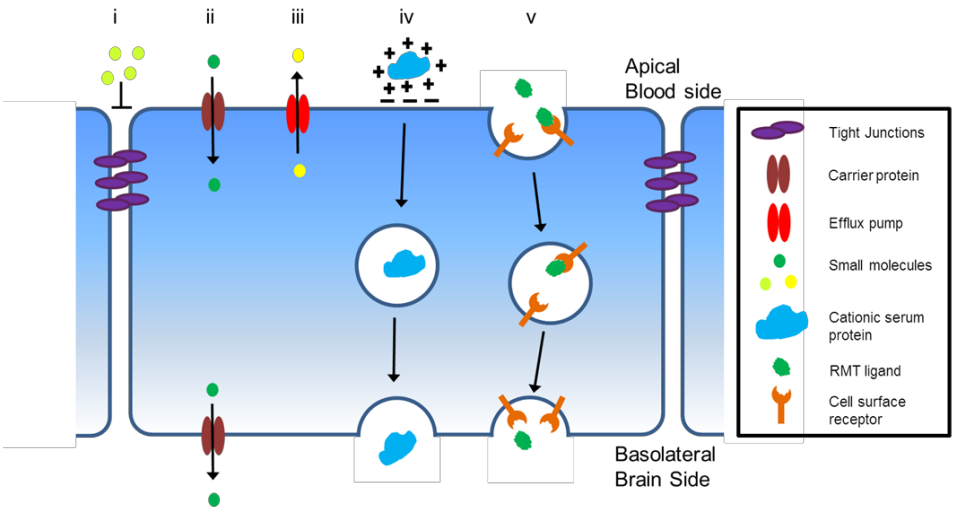

Figure 1.1 BBB transport

Schematic presenting the main classes of transport across the BBB. Large molecules can employ only a fraction of the total processes (Adapted from [14] Lajoie JM, Shusta E V. Targeting Receptor-Mediated Transport for Delivery of Biologics Across the. Annu Rev Pharmacol Toxicol. 2015;55(1):613-631. doi:10.1146/annurev-pharmtox-010814-124852).

specialized system of protein carriers embedded on both the luminal and abluminal surfaces of BMECs. Nutrients such as amino acids and hexoses, amines, carnitines, and monocarboxylates are transported across the BBB via carrier mediated transcytosis (CMT) [13]. In the same category of transport systems belongs various efflux transporters such as P-glycoprotein and various organic anion transporters (e.g. sodium, potassium, bicarbonate, chloride). Selectivity is achieved via the recognition from the receptor of a specific stereochemistry of the molecule [13]. Finally, receptor mediated transcytosis (RMT) is initiated by the specific binding of a ligand to its respective receptor and allows high selectivity[14]. Common routes for RMT include the use of insulin receptor [15], the leptin receptor [16], the LDL receptor [17], and transferrin receptor [18] among others. In RMT a ligand binds with high specificity to a receptor in the BMEC surface and triggers a vesicle formation around the receptor-ligand complex. This is followed by the next step where the complex is internalized in the endothelial cytoplasm and migrates via so far not completely elucidated routes to the basolateral (brain) side. Finally, the vesicle is fused with the basolateral membrane and the cargo is exocytosed [19]. Highly desirable properties of the RMT route are the wide variability of ligands of all sizes and shapes (e.g. symmetric 5kDa insulin to variably-shaped 55kDa LDL particle), and the large size of the vesicles that allows the conjugation of the ligand with a large molecular weight hydrophilic drug, or the use on ligand-coated particle preparations as drug carriers [11]. Moreover, RMT systems allow us to raise antibodies against the respective receptors that do not compete with the natural ligand, leading to increase efficiency and less system toxicity. Known RMT complexes have been utilized to ferry drugs encapsulated in liposomes coated with the targeting moiety, and magnetic nanoparticles with a RMT targeting coat [20]. Despite the

effort to identify high capacity RMT systems that can delivery therapeutics to the brain, the current state-of-the-art approaches targeting TfR, IR, and LDLR face significant issues of limited efficacy and safety liabilities [21]. To this end, the need for novel RMT-antibody pairs is evident and will be the focus of the present study.

1.3 *in vitro* models of the Blood-Brain barrier

In order to identify receptors and antibodies with promising receptor mediated transport across the BBB the use of *in vitro* models of the BBB is invaluable. *In vivo* screens of antibodies are plagued by high background, rendering this avenue ineffective [22]. Further, genomic and proteomic profiling of BBB endothelial cells while successful in identifying new BBB specific receptors [23] have the difficulty of a priori determining which receptors are actually capable of transport. Hence, the use of *in vitro* human BBB models is advantageous in performing functional screens to identify BBB targeting and transcytosing antibodies.

There is a large number of studies employing types of epithelial or non-cerebral origin endothelial cells to study BBB function. Particularly, Madin-Darby canine kidney (MDCK) cells and human umbilical endothelial cells (HUVEC) [24]. Further, primary cultures of endothelial cells isolated from various non-human species such as rat [25], pig [26], mouse [27], and bovine [28] origin are used. In particular, pig and bovine primary cells are available in high quantities and poses good permeability properties [29]. Co-culture with pericytes and astrocytes results in tightening of cell junctions and a corresponding increase in TEER. Brain endothelial cell lines such as RBE4 [30], and Bend3 [31] are heavily employed in research, but their barrier properties and TEER values are poor precluding their use in functional transcytosis screens.

BBB models based on primary human tissue are reported, but due to scarcity of available material their use is limited when a significant and constant supply of cells is needed. Instead, alternative models based on immortalized brain endothelial cells or human-derived stem cells are employed. The most widespread and characterized such immortalized model, hCMEC/D3 [32] has been successfully used to isolate antibody-like molecules able to transcytose the BBB [33]. The most important feature of a BBB model for the present study is the junctional tightness, a marker of low permeability of the model to molecules and particles. This property is often measured as transendothelial electrical resistance (TEER). Besides TEER, it is important that the model poses transporters and receptors commonly found in the *in vivo* human BBB in order to identify reagents with *in vivo* relevance. While hCMEC/D3 express the characteristic tight junction proteins of the BBB the monolayer they form is leaky and hinders functional antibody screens using vectorial transport [34].

Recently, human brain endothelial cells have been derived from stem cell sources such as induced pluripotent stem cells (iPSCs) [35] and human cord blood-derived stem cells of circulating endothelial progenitor and hematopoietic lineages [36]. In the case of iPCS-derived BBB pure, BBB-like, endothelial monolayers are obtained by selective purification of endothelial cells from neural progenitor cells that form a restrictive barrier and have high expression of key junctional proteins such as ZO-1, claudin-5, and occludin, as well as high P-gp, Mrp-1, and BCRP activity[35,37] ; features that help develop a low permeability phenotype. TEER values of this models reach >2000 Ω cm^2 forming a selective barrier that can be used in functional antibody discovery campaigns offering an avenue for developing transcytosis capable antibodies.

1.4 Antibody discovery

The lack of high efflux and specific brain RMT targets has motivated extensive academic and industry efforts to identify alternative RMT systems. There is evidence that due to the unique nature of the blood-brain barrier phenotype and the significant need of the brain for nutrients, there exists an enhanced profile of RMT systems. Further evidence based on genomics studies such as suppression subtractive hybridization (SSH) [38], and serial analysis of gene expression (SAGE) [39] have pointed that the transcription profile of the BBB differs from peripheral organs with many identified enriched genes having unknown function. These findings that combined with recent data showing upregulated transporters in the BBB compared to endothelial cells in liver and lung in mouse provide evidence that there is a high likelihood for the existence of novel BBB RMT systems [40].

The target discovery project can originate from ‘’omic’’ studies including transcriptominal profiling and proteomics experiments that lead to discovery of overexpressed or unique transporters to serve as targets for antibodies in a canonical discovery campaign, nevertheless due to the [23] lack of clear relationship between expression and function of RMT molecules, alternative functional approaches are implemented were the lead targeting molecule is identified without a priori knowledge of the underlying RMT mechanism. Important technical aspects in the search of such a molecule go beyond the choice of an appropriate screening substrate and involve the use of correct selection technology in the form of the antibody display platform.

To meet the demands for antibody discovery, *in vitro* display technologies are an invaluable recourse. The most widely used technology is phage display (Figure 1.2) [41]. The defining characteristic of display technologies is the genotype to phenotype linkage,

where the

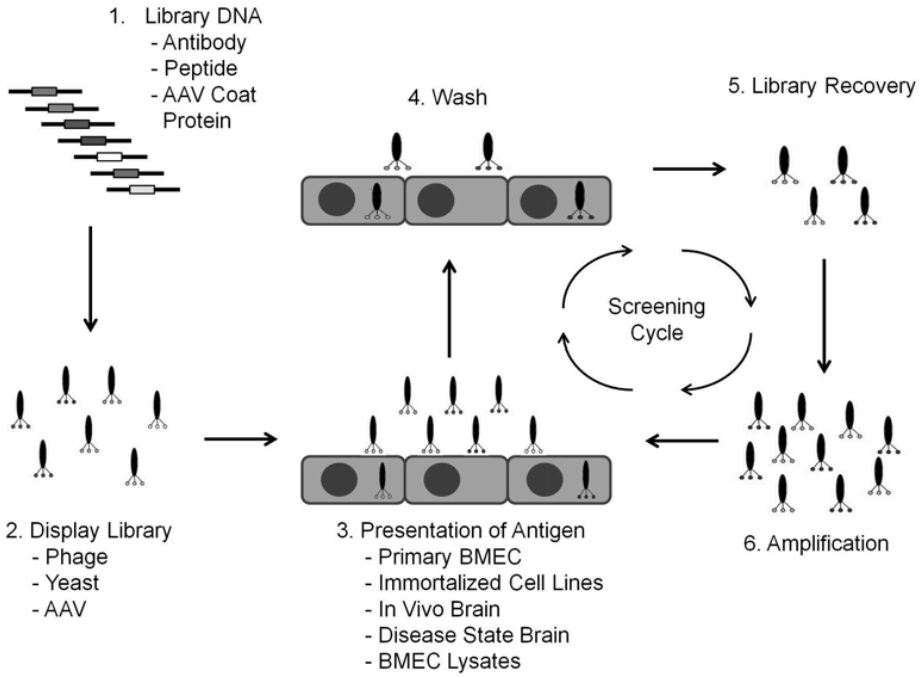

Figure 1.2 Phage Display biopanning

Basic screening methodology for identifying BBB penetrating antibodies through phage display selections. 1. Creation of library of ligands that are displayed on the surface of phage. 2. Display of particles on surface of phage. 3. Panning of phage on appropriate cell substrate that presents the antigens of interest. 4. Washing of non-desired phage particles along with non-specific background binders. 5. Recovery of desired library fraction. 6. Amplification of phage library and preparation for next selection round. Steps 3-6 are repeated till the desired output has been achieved. (Adapted from [78] Stutz C, Zhang X, Shusta E. Combinatorial approaches for the identification of brain drug delivery targets. Curr Pharm Des. 2014;20:1564-1576)

DNA encoding the displayed protein is retained in the displaying organism and recovered after the end of each round of screening along with the particle displaying the selected ligand. Phage display, developed by GP Smith [42], employs filamentous bacteriophage (either M13, fd, or f1) [43] to display peptides or antibodies as fusions to phage coat proteins, particularly the pIII protein that is present at one end of the phage particle. The main characteristic that make phage display so attractive for isolating brain penetrating antibodies are the small size of phage particles that allows internalization and trafficking through brain endothelial cells, allowing screening for function, namely transcytosis.

In a functional combinatorial screen, a library of targeting ligands, peptides or antibodies displayed in an appropriate platform is screened on a BBB-like substrate that can consist of brain endothelial cells of various species. The library mixture is allowed to bind and internalize, followed by extensive washing steps to remove non-specific targeting reagents from the library [44]. The members of the library that are still associated with the cells are recovered, amplified, and the process repeated until the isolation of lead candidates possessing the desired phenotype as assayed in downstream experimental steps. Employing the human cell line hCMEC/D3, Muruganandam *et al.*, identified camelid single domain antibodies from a screen assaying transcytosis across a cell-coated transwell [33]. Two particular reagents, FC5 and FC44 showed considerably stronger affinity *in vivo* towards mouse BBB compared to lungs. FC5 has been used extensively for imaging and therapeutics delivery. In another study a phage displayed human single chain antibody fragment library was screened on hydrocortisone-treated primary rat brain endothelial cells resulting in the identification of three unique antibodies that immunolabeled rat brain vessels *in vivo* [33] further highlighting the power of functional

screens.

Despite previous approaches, the lack of appropriate *in vitro* BBB-like screening substrate that will maintain almost *in vivo* like selectivity precluded the ability to select for true function, instead relying on gearing towards initial steps of transcytosis to get the desired phenotype. A combinatorial *in vitro* screen employing human BBB model closely resembling *in vivo* BBB would open exciting opportunities in identifying a true BBB penetrating antibody with human relevance.

1.5 Antibody functionalization

Discovery and engineering of internalizing antibodies has gained significant momentum as vectors for drug delivery to the brain. The basic concept is that antibodies engage endogenous transport mechanisms available in endothelial cells constituting the BBB to transcytose into the brain where they can excise their therapeutic potential or deliver a payload. Two main venues for drug delivery through antibodies are conjugation with nanoparticles (NPs), and antibody-drug conjugates (ADCs). While significant amount of research has been documented regarding the method of trafficking of particles [45], and antibodies [21] through the BBB, the mechanism of ligand conjugation as well as the fine tuning of NPs' antibody coating is critical for the fate of the therapeutic. In landmark studies binding properties of anti-transferrin receptor antibodies [46] and NPs coating conditions with transferrin [46] were found to heavily influence transcytosis capacity proving that functionalization of brain targeting antibodies, with all the consequential effects on antibody-target binding dynamics, is a critical downstream parameter that requires optimization for successful brain delivery.

Available techniques to conjugate antibodies with NPs or therapeutic moieties usually involve modification of chemical residues within the protein itself to link a target. While there are numerous conjugation strategies [47], the most commonly modified protein residues are lysines, since they tend to be located at the exterior accessible space of proteins and contain a reactive primary amine that is a versatile target for chemical conjugation. Chemical conjugation through primary amines via NHS-ester chemistry results in the formation of a stable amide bond covalently linking the insert with the protein [48]. However, since functional groups are present in multiple locations throughout proteins these methods lead to random integration of the functional entity in the protein and a heterogeneous population. The most severe byproduct of random integration is the often-detrimental alteration of protein activity and function due to changes in structure and conformation, as well as steric hindrance between the protein and inserted molecule.

An alternative strategy consists in site-specific bioconjugation, wherein a specific residue in the protein is employed in the chemical conjugation reaction. This allows control of the number and site of conjugation limiting deleterious effects and alteration of binding properties and producing a homogeneous population while maintaining a preset ratio of antibody to payload [47]. A critical challenge lies in the incorporation of a unique, chemically reactive residue in within the protein to serve as an acceptor for the chemical handle. Attempt to bypass this obstacle involve incorporation of unnatural amino acids [49] and use of modified tRNAs [50]. Due to the labor intensive and low efficiency nature of these techniques, our lab has developed modification through expressed protein ligation (EPL) as a means to deliver uniformly modified proteins following secretion in yeast [51]. In EPL the protein of interest is fused with a protein splicing element known as intein to generate

a reactive thioester at the C-terminus of the target protein [52] that can be further reacted with the chemical handle of interest (Figure 1.3). This method has

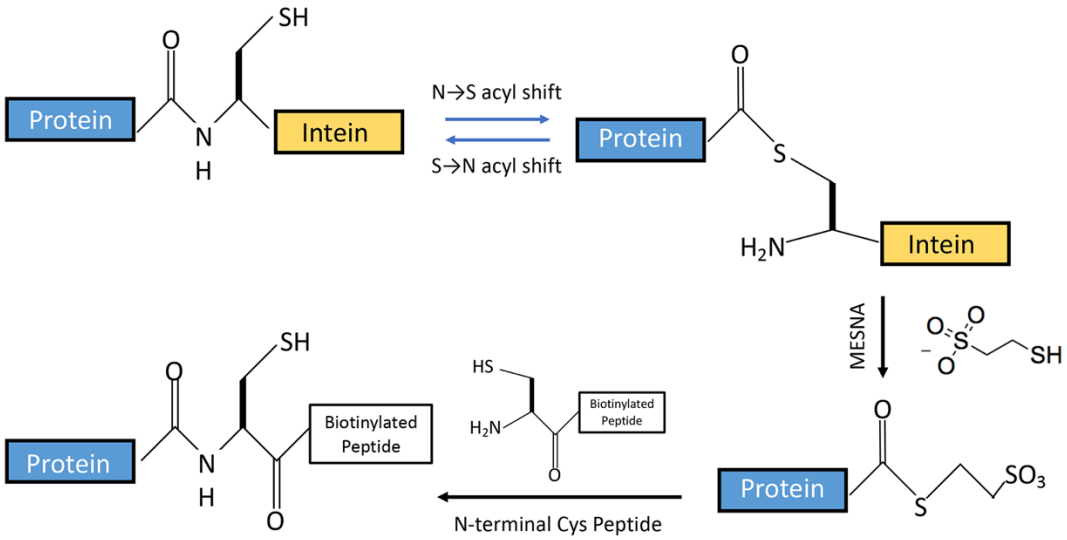

Figure 1.3 Site-specific antibody functionalization

EPL can be used to install chemical entities onto the carboxy-terminus of intein fused proteins. The intein catalyzes a reversible N- to S- acyl shift between the target protein and the intein. This exposes a thioester at the carboxy-terminus of the target protein that is susceptible to attack by a nucleophile. Commonly used nucleophiles, such as thiol-based reagents then react to release the intein and install a carboxy-terminal thioester on the target protein that can be further reacted with an appropriate chemical handle (shown here is a biotin functional group). (Adapted from Goulatis LI, Shusta E V. Protein engineering approaches for regulating blood–brain barrier transcytosis. Curr Opin Struct Biol. 2017;45:109-115. doi:10.1016/j.sbi.2016.12.005)

been used to install functionalities such as aklynes, azides, and fluorophores [53,54]. This technique is particularly powerful in our process to move our brain penetrating antibodies into further *in vivo* studies by providing a suitable platform to append functional groups without the possibility of abolishing activity. To this end, we have worked on optimizing our antibody-intein fusion functionalization process in yeast with the goal of providing a scaffold to integrate our brain penetrating antibodies identified from a discovery campaign.

1.6 Summary

The BBB is a formidable obstacle for successful delivery of therapeutics to the brain. Its unique phenotype requires the development of complex targeting reagents that can deliver drugs non-invasively. Human models of the BBB can mimic the endothelial barrier and provide the pool of potential RMT antigens in antibody discovery campaigns through display selections. With this in mind, we demonstrate the discovery and development of novel brain penetrating antibodies that recognize human and mouse antigens and are validated for their capacity to cross the BBB *in vivo*. We describe their development all the way from selection out of a diverse human antibody library and hit validation *in vitro* and *in vivo*, down to integration with an optimized functionalization platform that enables future *in vivo* validation of their capacity to ferry therapeutics to the brain.

Chapter 2 – Protein Engineering Approaches for Regulating Blood-Brain Barrier Transcytosis

This chapter was adapted from: L. I. Goulatis, and E.V. Shusta, "Protein engineering Approaches for Regulating Blood-Brain Barrier Transcytosis", Curr Opin Struct Biol, 2017. 45: p. 109-115. Motivation for the need to identify novel Blood-Brain Barrier transcytosing antibodies is established, and the state of the art in biologics Blood-Brain Barrier delivery reviewed.

2.1 Introduction

Therapeutic delivery for the treatment of brain diseases is hampered by the physical, transport, and metabolic properties of the blood-brain barrier (BBB). The BBB is comprised of brain microvascular endothelial cells (BMECs) that are stitched together by a network of specialized tight junctions, yielding an impressive physical barrier to blood-to-brain transport. In addition, BMECs lack fenestrae and have minimal pinocytotic activity [6]. These unique properties combine to limit the entry of blood-borne small molecule drugs and biologics into the brain [55]. However, despite its remarkable sealing properties and restriction to drug transport, the BBB is actually selectively permeable to key nutrients such as glucose, iron and lipoproteins that cross the BBB via specific molecular transport systems. This BBB phenotype may hold the solution to the brain drug delivery problem in the form of noninvasive delivery strategies that coopt such endogenous transcellular transport systems. In particular, vectors that target BBB transport systems that rely on the vesicle trafficking network can be used to deliver pharmacologically relevant doses of a variety of therapeutics [56]. Recently, the efficacy of these vectors has been improved by a

combination of protein engineering approaches and a better understanding of intracellular trafficking events. In this review, we will highlight the various transcellular BBB pathways available for noninvasive brain drug delivery and the protein engineering efforts that have been deployed to best utilize the available pathway capacity.

2.2 Trans-BBB brain delivery pathways

Transport mechanisms employing the vesicle-mediated trafficking systems of BMECs can be used to traffic drug cargo into and across the BBB. Several classes of vesicle-mediated transport systems function at the BBB including fluid phase endocytosis, absorptive-mediated endocytosis, and receptor-mediated transport in the form of caveolae- or clathrin- mediated mechanisms [11,57] (Figure 2.1). In the case of employing receptor-mediated systems for drug delivery, an antibody or peptide is usually employed as a targeting vector. A therapeutic can either be attached directly to the targeting vector or loaded into liposomes or nanoparticles (NPs), themselves coated with the targeting vector [14]. After binding and endocytosing into BMECs by one of the aforementioned mechanisms, the vector and attached therapeutic cargo is then trafficked within the endothelial cell, with some cargo ultimately being released into the brain parenchyma by transcytosis (Figure 2.1). Interactions between the targeting vector and the respective transcytosis pathway components are key to determining where the therapeutic traffics and to what extent it may transcytose as discussed in the specific examples below. In this way, therapeutics can enter the central nervous system (CNS) noninvasively from the bloodstream. Below, we break down the various vesicle-mediated transcytosis pathways as they have been employed in BBB drug delivery.

2.2.1 Fluid phase transcytosis

Fluid phase endocytosis serves as a non-specific uptake method allowing cells to internalize extracellular fluid. Endocytosis follows actin cytoskeletal rearrangements that result in formation of membrane ruffles that occasionally fold back on themselves and envelop fluid domains [58]. The resulting vesicles are devoid of coating material required for the curvature of smaller vesicles, distinguishing them as pinocytotic vesicles that can ultimately transcytose and release contents into the brain parenchyma [58] (Figure 2.1). While fluid phase endocytosis is capable of delivering payload across the BBB, challenges include its inherently nonspecific nature, inability to concentrate the

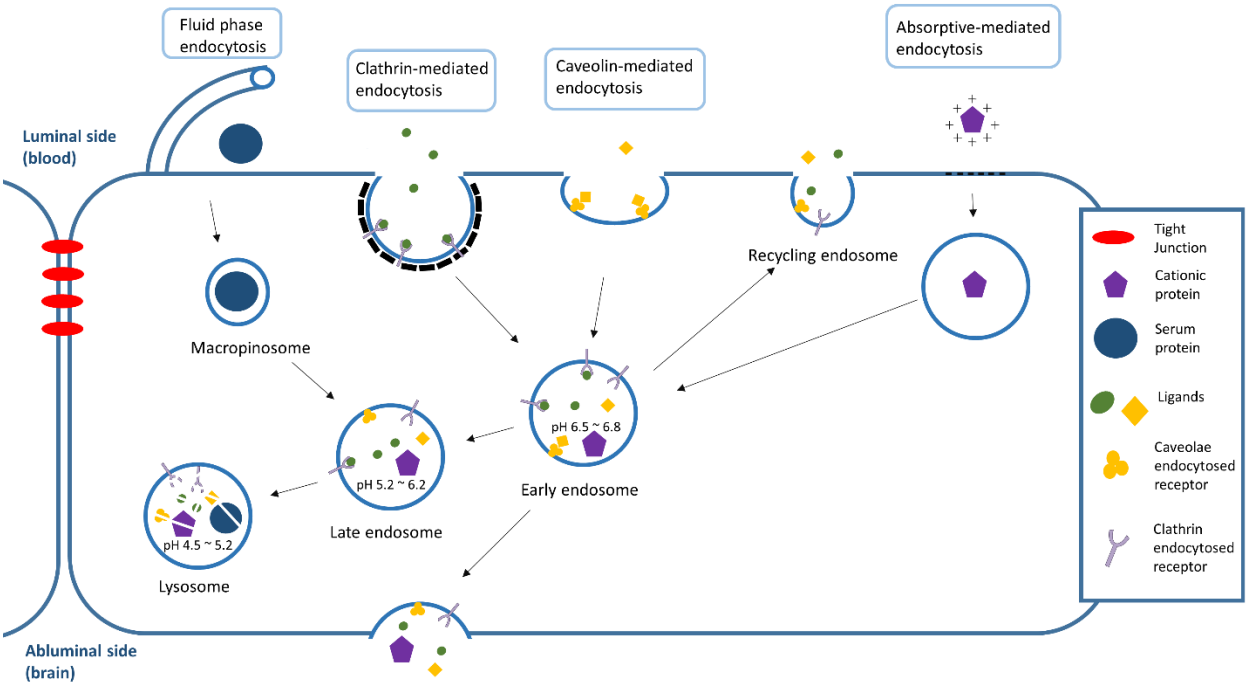

Figure 2.1 Endogenous BBB endocytosis and transcytosis pathways. Fluid phase endocytosis involves the generation of large vesicles that internalize extracellular fluid and soluble proteins. Absorptive-mediated endocytosis is initiated by the nonspecific absorption of cationic molecules to the negatively charged plasma membrane and subsequent trafficking through the endosome towards either degradation, or transcytosis. Clathrin-mediated endocytosis involves the formation of clathrin and adaptor protein complexes that result in the formation of a clathrin-coated vesicles. These vesicles mature to EEs, where cargo can then be sorted and trafficked for recycling, degradation or transcytosis. Caveolae-mediated endocytosis begins with the formation of vesicles that are structurally and functionally different from clathrin-coated vesicles, followed by delivery of the receptor-ligand complex to the EE where it can be further processed for transcytosis.

therapeutic since it involves engulfment of fluid at the prevailing blood concentration, and the difficulty of tuning the transcytosis process. Moreover, one of the unique features of the BBB is that it possesses comparatively few pinocytotic vesicles [59] and therefore, the total trans-BBB flux of therapeutic by this route will be limited. Therefore, much of the trans-BBB delivery focus has been on targetable transport routes.

2.2.2 Absorptive-mediated transcytosis

One approach to add a first level of targeting capability is surface modification of the therapeutic carrier or the therapeutic itself through cationization. AMT is initiated by the absorption of cationic molecules to negatively charged moieties present in the surface of the brain endothelia (e.g. sialo-glycoconjugates and heparan sulfate proteoglycans) [60] (Figure 2.1). Using the model AMT substrate, wheat germ agglutinin, it has been shown that following internalization, cargo is directed towards the endo-lysosomal pathway, with *in vivo* studies showing accumulation also in the inner saccules of the golgi network, a destination not accessible to fluid phase endocytosed cargo [61]. Protein cationization by carboxyl group modification has been performed for albumin and antibodies in order to enhance the delivery of pharmaceutical payloads to the brain [62]. For instance, cationized Immunoglobulin (IgG) and cationized bovine albumin transcytosed into brain following carotid arterial infusion [63]. Further, NPs coated with cationic moieties [64] and cell penetrating peptides (CPPs) such as SynB vectors [65] have been employed to deliver functionalized small molecules, proteins, and nanoparticles across the BBB by AMT. Though AMT allows trans-BBB delivery of drugs in concentrated transcytotic vesicles, it remains a non-specific approach as the therapeutic will also accumulate in the blood

vessels of peripheral organs leading to potential off-target effects. Moreover, the cationization process has the potential to affect the therapeutic activity. Thus, other approaches that both allow drug concentration and employ targeting of specific BBB receptors have been developed.

2.2.3 Clathrin-mediated transcytosis

Upon ligand and receptor engagement, clathrin-mediated transcytosis (CMT) starts with the formation of clathrin-coated pits which are then endocytosed and fused with the early, or sorting endosome (EE) (Figure 2.1). The EE is the main sorting compartment in the endocytic pathway and is the acceptor vesicle for other major endocytosis pathways besides CMT [66]. Membrane cargoes are sorted within the complex EE structure that involves so-called tubular and vacuolar domains. Immediately after the formation of clathrin-coated vesicles, acidification driven by vacuolar H^+-ATPases begins and continues through the endosome-lysosome maturation process. Of particular relevance to CMT-targeting, pH-induced dissociation of ligands from their cognate CMT receptors starts in the EE conditions of pH 6.8-6.1, thereby providing a sorting mechanism separating bound ligand from the fluid phase (Figure 2.1). Cargoes are then spatially sequestered and sorted [67]. The main spherical vacuole matures further to become the late endosome, and finally the acidic pH 4.5 lysosome where any accompanying material is destined for degradation. In contrast, cargo that resides in the tubular domains can either be recycled, directed to different intracellular sites or ultimately transcytosed in polarized cells such as BBB endothelium (Figure 2.1). As will be discussed below, the relative balance between these various pathways is key to maximizing the brain uptake of CMT-targeted therapeutics.

Among the most widely used CMT systems are the transferrin receptor (TfR) [68], the insulin receptor [69], and low-density lipoprotein receptor-related protein receptor 1/2 (LRP) [14] all of which are highly expressed on human brain microvasculature. Another receptor believed to involve CMT processes at the BBB is the cell surface a(2,3)-sialoglycoprotein TMEM-30A that has been targeted by a single domain antibody (sdAb) known as FC5 [33,70]. CMT offers the advantage of selective targeting compared with AMT, although the aforementioned CMT receptors, while abundant at the BBB, are expressed in peripheral endothelia as well. Finally, although CMT can direct transcellular movement of targeted therapeutics, the relative distribution of the various sorting pathways is not necessarily directed towards maximum transcytosis. Thus, engineering strategies that attempt to address this issue have been developed.

2.2.4 Caveolae-mediated transcytosis

Caveolae are flask-shaped membrane invaginations that are structurally and functionally different than clathrin-coated endocytotic structures (Figure 2.1). These primary endocytic vesicles are distinct from intracellular compartments found in the clathrin pathway, are pH neutral, and devoid of usual clathrin internalized ligands such as transferrin [71]. Caveolae-mediated transcytosis has been implicated in brain delivery of a number of virus derived peptides [72,73], toxins [74] and NPs [75] and has been suggested to be involved in the trafficking of the LDL receptor [76] and the Aβ peptide via the receptor for advanced glycation end-products (RAGE) [77]. Considerable research has been performed to identify BBB-resident clathrin- or caveolae-mediated transcytosis systems and peptide or antibody vectors capable of selectively targeting them [78]. For example, a recent proteomic evaluation revealed the highly expressed CD98 heavy chain (CD98hc)

as a new target for BBB delivery, and this receptor exhibited colocalization with caveolin-1 [23].

2.3 Engineering BBB-targeting vectors

Key to the efficient implementation of BBB targeting vectors are protein engineering approaches that improve trans-BBB transport. Binding properties of targeting vectors have been engineered for enhanced trans-BBB trafficking and the decoration of NPs with targeting vectors has also been explored for improved targeting and trans-BBB transport (Figure 2.2).

2.3.1 Engineering targeting vectors for enhanced trans-BBB trafficking

The amount of peptide- or antibody-targeted therapeutic that not only endoctyoses, but also transcytoses the BBB, can be limited by the intrinsic vesicle trafficking process. Binding on the blood side, endocytosis, sorting, exocytosis and brain side release are all key components in regulating the fraction of the blood-borne dose that transits the BBB and enters the parenchyma [14] (Figure 2.2). Recent efforts have leveraged antibody engineering strategies to increase trans-BBB transport and have highlighted the importance of the vector binding and trafficking issues. The most well-developed set of examples deals with engineering the binding properties of anti-TfR antibodies and exploring their effects on trafficking and delivery *in vitro* and *in vivo*.

First, antibody affinity and avidity for TfR was evaluated, and it was demonstrated that higher brain uptake of anti-TfR antibodies can be accomplished by lowering antibody affinity [46]. Intravenous administration of antibodies having a range of affinity to TfR (Kd = 6.9 – 111 nM) indicated that at trace doses, mouse brain uptake directly correlated with affinity suggesting that receptor engagement at the blood side of the BBB was the key parameter governing uptake (Figure 2). However, at therapeutic dosing (20 mg/kg), an

inverse correlation was observed where the lowered affinity antibody demonstrated greater brain accumulation (up to 0.6 % ID/g). In addition, immunohistochemistry revealed more substantial colocalization of low affinity anti-TfR antibodies with neuronal markers as opposed to high affinity antibody clones that showed predominantly vascular localization. These data were posited to demonstrate that lowered affinity allows for antibody release from the TfR at the abluminal membrane while higher affinity variants remain bound to the TfR. Further, reduction of cortical TfR levels after administration of high affinity anti-TfR antibody was observed and mechanistic studies suggested it to be a result of increased lysosomal sorting and degradation of the high affinity variant within BMECs [79]. Thus, productive trans-BBB anti-TfR antibody trafficking could be increased by lowering antibody affinity. In addition to studies of TfR antibody binding affinity, the role of avidity has also been explored with similar conclusions. In order to investigate avidity effects on trans-BBB transport, an Fab fragment targeting the TfR was fused to the carboxy-terminus of an anti-BACE1 antibody in a bivalent (dFab) or monovalent (sFab) format [80]. The dFab exhibited a higher degree of colocalization with lysosomes compared to the sFab in the murine b.End3 BBB cell line (Figure 2.2). Moreover, dFab transcytosis was not detected across the human hCMEC/D3 BBB cell line whereas the sFab was found to transcytose. In an *in vivo* setting, the dFab was unable to substantially cross the mouse BBB and could be found colocalized with LAMP2, a lysosomal marker. In a mouse model of Alzheimer's disease, decreases in amyloid plaques were only observed after sFab administration, with the dFab remaining largely sequestered in the microvessels [80]. Receptor crosslinking has been associated with altered TfR trafficking [81,82], and this phenomenon likely plays an important role in BBB sequestration and

degradation of high affinity and bivalent anti-TfR antibodies and their coordinate decreases in brain uptake.

In addition to modulating targeting vector binding affinity or avidity, one could also envision regulating vector-receptor trafficking dynamics by engineering binding properties

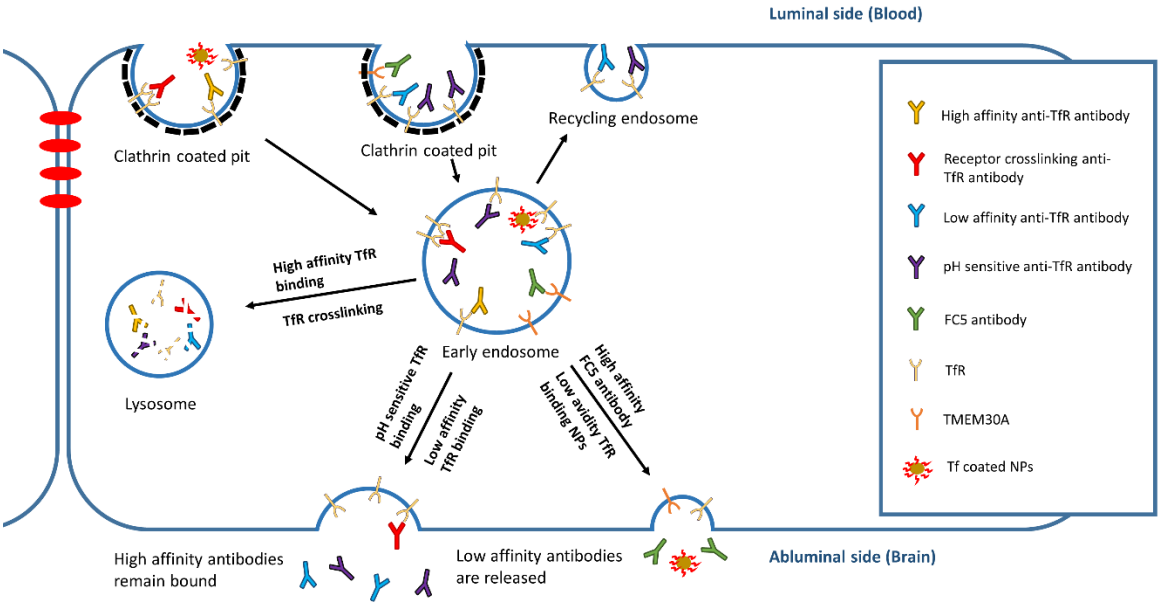

Figure 2.2 Transcytosis optimization. A schematic depiction of the various engineering optimization strategies for increased transcytosis of antibodies and NPs. High affinity monovalent and bivalent anti-TfR antibodies internalize readily into the EE, but then direct the antibody-receptor complex towards lysosomal degradation, possibly by crosslinking the TfR and altering its intracellular trafficking. While high affinity monovalent anti-TfR antibodies can transcytose the BBB, they remain bound to the receptor on the abluminal side, limiting the dose to the brain. In contrast, low affinity anti-TfR antibodies decrease antibody-TfR sorting to the lysosome and can either be recycled back to the luminal side, or are transcytosed to the abluminal side where they dissociate from TfR, leading to increased brain accumulation. Similarly, Tf coated nanoparticles show a higher transcytosis capability when lowering the Tf coating content, resulting in reduced avidity. Further, pH-sensitive TfR binding antibodies that can dissociate from TfR in the acidic EE lead to increased transcytosis compared to pH-insensitive antibodies. In the case of the single domain antibody FC5, increased affinity towards the receptor leads to an increase in the amount of transcytosed antibody, highlighting the fact that vectors utilizing different trafficking machinery may require customized optimization.

that are responsive to the trafficking environment. For instance, during CMT, acidification is a key step in the vesicle maturation and sorting process [67] (Figure 2.1), and this pH

gradient has been exploited in protein engineering involving FcRn binding, as well as in natural ligands including transferrin [83]. Along these lines, early work has investigated whether or not pH-sensitive binding could be an additional engineering handle for regulating anti-TfR antibody trafficking and increasing trans-BBB transport [34]. Using *in vitro* BBB models, differential intracellular trafficking was observed for a pH-insensitive anti-TfR antibody, 128.1, compared to a pH-sensitive anti-TfR antibody, MEM-189. Antibody 128.1 colocalized with the late endosomal/lysosomal marker CD63 while MEM-189 was instead found in vesicular structures distinct from late endosomes. Transcytosis of pH-sensitive MEM-189 across the hCMEC/D3 cell line increased; and in contrast, the lysosomal degradation of 128.1 was increased (Figure 2.2). These data are suggestive of pH-sensitive binding being a candidate for increasing trans-BBB transport, although the epitopes for these two antibodies may not be identical. In other recent studies, pH-sensitivity has been engineered into an anti-TfR antibody using histidine scanning mutagenesis methods, such that the resultant antibodies presumably recognize the same epitope as the pH-insensitive wild-type antibody [84]. As in the study with 128.1 and MEM-189, antibody trafficking in SK-BR-3 cells was also substantially affected by pH-sensitivity, with increased intracellular accumulation in distinct vesicular structures that did not appear endosomal or lysosomal in origin. These combined data are suggestive that engineered pH-sensitive binding to the TfR is a viable target for altering intracellular trafficking and ultimately enhancing trans-BBB transport.

It is important to note that not all trafficking pathways will likely respond to antibody binding properties in the same fashion as the TfR pathway. For example, in a recent publication, antibodies having different affinity against basigin and CD98hc were

evaluated regarding their transcytosis capability following trace and therapeutic dosing in mice [23]. While the high affinity basigin antibody exhibited increased uptake upon trace dosing like that observed with the high affinity anti-TfR antibody [23], both basigin antibodies (13.5 – 102nM affinity range) showed similar brain penetration at therapeutic dosing, which contrasts with anti-TfR antibody affinity results [46,79,85]. When produced as bispecific antibody constructs with an anti-BACE1 arm, anti-CD98hc/BACE1 bispecific antibodies exhibited a similar inverse relation between antibody affinity and brain exposure to that previously observed with anti-TfR/BACE1 antibodies [85]. However, unlike anti-TfR antibodies, the high and low affinity anti-CD98hc/BACE1 antibodies did not perturb trafficking or exhibit differential lysosomal uptake [23]. As another example, the effects of avidity on the trans-BBB passage of the FC5 sdAb mentioned above were investigated. FC5 was fused either in monovalent or bivalent format to human Fc region. In contrast to the TfR system, increased transcytosis of the bivalent construct (80% increase) was observed using an *in vitro* BBB model [86] (Figure 2.2). Despite the differences observed *in vitro*, levels of the monovalent and bivalent FC5 in the cerebrospinal fluid were not statistically different. Taken together, these results indicate that optimization of antibody properties needs to be tailored to each targeted trafficking receptor, and that antibodies targeting different receptors or even different epitopes of the same receptor may have different optimal binding properties.

Finally, in addition to engineering antibodies to enhance trans-BBB passage, factors such as immunogenicity, clearance, peripheral uptake, off-target toxicity and safety are also important for translation of these methods [85]. As an interesting example, a murine anti-human insulin receptor antibody 83-14 has been used to deliver

pharmaceutical payloads to rhesus monkey brain after intravenous administration [15]. A humanized version of the antibody was developed (HIRMAB) to lower immunogenicity and despite a 27% reduction in affinity, the antibody still bound to primate and human insulin receptor and accumulated in rhesus monkey brain [87]. Finally, the HIRMAB was further engineered as a fusion protein to a single-chain antibody that binds amyloid beta-amyloid as a potential treatment for Alzheimer's disease, with the fusion antibody accumulating in primate brain after intravenous administration [88].

2.3.2 Engineering NPs for increased brain penetration

NPs have been employed to deliver pharmaceutical payloads to the CNS [45]. *In vitro* studies regarding the transcytosis mechanism of non-functionalized NPs have found that NPs cross brain endothelial cells by a combination of fluid phase transcytosis [89], clathrin-mediated transcytosis and caveolae-mediated transcytosis [90], albeit at rather low efficiency. Therefore, coating NPs with vectors capable of targeting specific endocytosis pathways has been shown to influence their intracellular fate, as well as their transcytosing capacity (Figure 2.2). For example, NP trafficking *in vitro* was altered by coating NPs with polyethyleneimine (PEI) or prion protein. PEI-coated NPs entered the cell via macropinocytosis and exhibited diminished transcytosis while prion-coated NPs targeted receptor-mediated systems and exhibited enhanced transcytosis compared with uncoated NPs [91]. Multiple forms of NP functionalization can synergize to further increase cellular uptake, and transcytosis capability by leveraging multiple entry mechanisms. For instance NPs synthesized from AMT-targeting cationic PAMAM polymer and decorated with CMT-targeting lactoferrin (Lf) exhibited increased brain endothelial cell uptake than non-targeted PAMAM NPs by employing both AMT and CMT mechanisms [92]. Finally,

similar to antibody-based vectors, engineering the binding properties of the NP can influence transcytosis. For example, tuning the avidity of transferrin-decorated gold NPs regulated their brain accumulation in mice [93]. NPs with the highest avidity to the TfR were sequestered at the brain vasculature and exhibited reduced accumulation in the brain relative to NPs with low avidity, similar to observations of anti-TfR affinity and avidity described above. Although not directly related to engineering the targeting moiety, NP shape and size can also influence BBB trafficking. For instance, a study employing the hCMEC/D3 cell line and electron microscopy found that SiO_2 NPs of sizes ranging from 50-200 nm all internalized into the endo-lysosomal pathway, with the smaller NPs accumulating to a greater extent [89]. Moreover, for anti-transferrin receptor-targeted polystyrene NPs having either rod or spherical geometries, rod-shaped NPs were found to better accumulate in all murine tissues including brain after intravenous administration, likely as a combination of flow and binding effects [94].

2.4 Conclusions

Despite the obstacle presented by the BBB, the delivery of therapeutics employing endogenous BBB transcytosis mechanisms is moving forward. Targeting vector engineering has been successfully deployed to increase the amount of trans-BBB transport. Moving forward, it is anticipated that the simultaneous targeting of multiple pathways will be used to enhance uptake and specificity. In addition, one could envision employing sequential targeting of multiple pathways or environment-dependent binding to more substantially influence transcellular trafficking (e.g. cell surface targeting followed by intracellular redirection). Finally, it is our opinion that the mechanistic aspects of transcellular BBB trafficking should be an expanding research focus to better inform BBB targeting vector design and optimization.

Chapter 3 - Discovery of New Antibodies that Target and Transport the Blood-Brain Barrier

Here, we describe the screening of a phage display antibody library on an *in vitro* human Blood-Brain barrier model to identify brain penetrating antibodies with human relevance. Then, we proceed to characterize lead antibodies for *in vitro* and *in vivo* transcytosis capacity. The work presented in this Chapter leads to novel antibodies able to potentially serve as drug delivery vectors across the blood-brain barrier with exciting applications for brain disease treatment.

I would like to acknowledge Dr. Julia V. Georgieva, who contributed equally to the body of work presented in this Chapter, adapted from a co-first author manuscript in preparation. I specifically conceived and performed the phage display antibody discovery, performed production and characterization of antibodies for *in vitro* and *in vivo* assays, performed *in vitro* cell based assays, differentiated hBMECs, and contributed to image acquisition and analysis. I would also like to acknowledge Dr. Scott Canfield and Dr. Hannah Wilson for providing the hBMECs for the initial phage screening.

3.1 Introduction:

The blood-brain barrier (BBB) prevents access of biotherapeutics to their central nervous system (CNS) targets and therefore prohibits the effective treatment of neurological disorders. In the brain vasculature adjacent endothelial cells are connected by tight junctions that redirect molecular trafficking from the paracellular route towards transcellular trafficking [95]. This leads to the barrier's selectivity that maintains brain homeostasis allowing the selective passage of nutrients, but limits crossing of antibodies to the brain to only ~0.1% of circulating antibody levels [96]. A promising delivery method

lies in the utilization of existing active transport systems expressed on the luminal side of the brain endothelial cells such as receptor mediated transport mechanisms to mediate non-invasive delivery to the brain [11]. Two prominent examples are antibodies against the transferrin (TfR) [97] and insulin (IR) [15] receptors. Nevertheless, these systems, while mediating transport across the BBB, are relatively inefficient and non-specific resulting in deleterious off-target effects [80,85]. While it is possible to mitigate these effects by antibody engineering strategies [21], there remains a significant need for the discovery of novel BBB receptor targeting antibodies.

Currently, multiple approaches have been implemented to deliver novel antibody-target pairs [78]. Genomic and proteomic profiling of BBB endothelial cells has identified new BBB transport systems [23], however, it is difficult to determine a priori what BBB receptors are actually capable of transport from omics data. Phenotypic screening of large libraries *in vivo* [98] and *in vitro* [33] for new reagent identification has shown limited success, with only a handful of new antibodies isolated. *In vivo* screens of phage antibody libraries are plagued by high background recoveries masking relevant clones [99] while antibodies identified from *in vitro* biopanning often do no not cross-react with *in vivo* antigens [100] due to potential alteration of protein expression profiles in culture. Further, current human *in vitro* BBB models are inherently leaky, prohibiting functional transcytosis screens of antibody libraries.

Here, we identified new BBB targeting antibodies by panning a phage displayed human single chain antibody fragment (scFv) library against an *in vitro* human BBB model. This model, derived from induced pluripotent stem cells, has well-developed tight junctions and expresses a collection of markers unique to the BBB thereby enabling

transcytosis screening approaches [35,37]. Importantly, this model allows us to recover antibodies that can have human relevance. Using this approach, we identified a cohort of antibodies able to target brain vasculature *in vivo* and also react with human antigens. Two lead antibodies demonstrated increased transport across the *in vivo* BBB and were found associated with post vascular cells. Importantly, neither antibody appeared to interact with established RMT transferrin and insulin receptors, thus serving as potential candidates for novel methods for transporting therapeutic payload to the brain.

3.2 Materials and Methods:

3.2.1 Cell culture:

hBMEC differentiation was performed as previously described [101]. At day 8 of differentiation cells were plated on coated tissue culture plates or 1μm pore size poly-ester transwells (Corning #CLS3462), or on collagen/fibronectin coated tissue culture plates. The primary human lung and heart microvascular endothelial cells (hLECs and hCECs, CC-2527 and CC-7030) were obtained from LONZA (Walkersville, MD), and cultured as per manufacturer's instructions.

3.2.2 Phage selection:

All the screening methods preceding transcytosis are adapted from protocols outlined in Zhou and Marks, with a human naïve fd-tet based scFv library employed [44,102,103]. Initially, the human scFv library was pre-subtracted by serial application on hLECs and hCECs grown on T-75 flasks. All screening rounds were performed in appropriate culture media for each cell type. In each round 10^{11} colony forming units (CFU) were applied to a confluent cell monolayer. Pre-subtraction rounds were performed by incubating the library on monolayers for 1hr on ice, while internalization rounds on hBMECs were performed by incubating the phage library on hBMECs for 1h at 37 ^{o}C. Following phage internalization, media was aspirated and cells were washed 1X with stripping buffer I (150mM NaCl, 100mM Glycine pH 2.5) and 2X with stripping buffer II (500mM NaCl, 50mM Glycine, 0.2M Urea, pH 2.8) for 5min at RT to remove membrane bound phage. hBMECs were detached by trypsin treatment and spun down at 300g at 4 ^{o}C for 5min. The cell pallet was then resuspended in ice-cold lysis buffer (triethanolamine 100mM), incubated on ice for 15min, and neutralized (Tris-HCl pH 7.4). Phage eluted from each selection round were used to infect log phage E. coli TG1 cells. Phage particles

were rescued from the cells, amplified and used for subsequent rounds of antigen selection as described [22]. A total of 1 subtraction and 3 internalization rounds were performed.

For transcytosis selection 10^{11} CFU from the third internalization rounds were dosed on top of hBMECs purified onto 1µm pore size transwells and allowed to transcytose for 3 hrs at 37 ^{o}C before harvesting phage containing media from the bottom chamber and TG1 infection.

For the competition transcytosis screen selection 10^{11} CFU from the third internalization rounds were dosed onto hBMECs purified on 1µm pore size transwells along with 1µM of soluble scFv 3 and 22Ch and allowed to transcytose for 3 hrs at 37 ^{o}C before harvesting phage containing media from the bottom chamber and TG1 infection.

Individual TG1 colonies infected with phage particles were grown O/N, and DNA was heat-extracted, and PCR amplified using primers that flank the scFv gene. The primer sequences were 5′-TTTTTGGAGATTTTCAACGTGA-3′, and 5′-GAATTTTCTGTATGAGGTTTTGCTAAA-3′ for the forward and reverse primers, respectively. PCR fragments were then Sanger sequenced (UW Madison Sequencing facility).

3.2.3 Phage immunochemistry:

hBMECs were purified on 96-well tissue culture plates as described above. The day of the assay, each well of BMECs was blocked with 250 µL of PBS with calcium and magnesium (PBSCM; PBS with 1 mM of calcium chloride and 0.5 mM of magnesium sulfate) supplemented with 40% goat serum (PBSCMG) (Sigma– Aldrich, #G6767). The wells were washed three times with 250 µL of PBSCM. Next, cells were fixed with

paraformaldehyde (PFA, 4% w/v in PBS) for 10 min at RT. Overnight cultures of phage harboring bacteria were centrifuged, and 50 µL of the phage containing supernatant from each sample was incubated directly on the BMECs in the presence of 100 µL of fresh PBSCMG. The plate was incubated for 1 hr at 4°C and then washed once. An anti-M13 antibody (GE healthcare #27942001) diluted 1:500 in PBSCMG was incubated in each well for 1 hr at 4°C. Cells were washed with PBSCM, and incubated with secondary goat anti-mouse Alexa488 for 30 min at 4°C. Following this, the cells were washed three times in PBSCM and post-fixed for 8 min at room temperature with PFA. The plate was then imaged on an Olympus epifluorescence microscope (Center Valley, PA).

3.2.4 Soluble scFv and scFv-Fc preparation:

The following method for production of soluble scFv-His6 fusions is based on a protocol described in Zhou and Marks [104]. An overnight bacterial culture transformed with the scFv secretion plasmid was used to inoculate 2xYT medium containing 100 µg/mL ampicillin and 0.1% glucose, which was then grown at 37°C until an OD600 nm of 0.9 was reached. Expression was induced by addition of 1 mM isopropyl-β-D-thiogalactopyranoside (IPTG, Fisher Scientific, # 50213380) and bacteria allowed to grow for 4 h at 30°C. The bacteria was harvested and the scFv recovered by serial incubation with a periplasmic extraction buffer (PPB, 200 g/L sucrose, 1 mM EDTA, 30 mM tris–HCl, pH 8.0) supplemented with DNAse I (Roche Applied Sciences, # 10104159001) to 100 µg/mL, and complete Mini protease inhibitor cocktail tablets (Roche Applied Sciences, # 11836153001) followed by an osmotic shock buffer (OSB, 5 mM magnesium sulfate in ddH2O) supplemented with DNAse I and complete, Mini protease inhibitor cocktail. The resulting solution was syringe filter sterilized and dialyzed against PBS + 10 mM

imidazole. The scFv were purified from the crude extract with Qiagen Ni-Nta Spin Columns (Qiagen #31014) using manufacturer recommended protocol for purification. The purified scFvs were eluted and subsequently dialyzed against PBS, and the purity of the scFv was verified by sodium dodecyl sulfate–polyacrylamide gel electrophoresis (SDS–PAGE) and Coomassie blue staining. Soluble scFvs were pre-dimerized with rabbit polyclonal anti c-myc antibody (Thermo fisher #PA1-981) in 4:1 molar ratio for 2 hrs in PBSG (10 % goat serum in PBS) and used as dimers for all downstream assays.

For scFv-Fc fusion production, scFv genes were subcloned to a custom pIRES-rabbitFc vector using NheI and AgeI restriction sites via standard PCR amplification, restriction digestion, and ligation procedures. Large scale DNA purification for HEK 293F transfection was done with ZymoPURE II plasmid kit (Zymo Research # D4200), and PEI transfection performed as described [105]. 2 Total protein concentration was quantified using UV 280 absorbance and extinction coefficients generated by ExPASy (http://web.expasy.org/protparam/).

3.2.5 Cell based assays:

Membrane binding and endocytosis assay: hBMECs were purified on Lab Tek II chamber slides (Nunc #154917). Cells were washed once with PBS and incubated with blocking buffer PBSG (10 % goat serum in PBS) for 30 min on ice. Pre-dimerized scFvs (13 µg/ml) or scFv-Fc (5 µg/ml) were added to cells and incubated for additional 30 min on ice to allow binding. The chamber slides were then transferred at 37°C for 45 min to allow internalization. Afterwards cells were washed with cold PBS and incubated with anti-rabbit AlexaFluor555, 1:1000 in PBSG for 30 min on ice to label the membrane-bound fraction of scFv-Fcs. Cells were washed once more on ice, fixed with 4% PFA on

ice for 10 min and permeabilized with 0.2% Triton X for 2 min. At this stage cells were additionally incubated with mouse anti-human ZO-1 (Invitrogen #339100) or mouse anti-human PECAM1/CD31 (Cell Sciences #MON6002-1), diluted 1:50 in PBSG for 45 min at RT. Anti-rabbit AlexaFluor488, 1:1000 in PBSG was used to label the internalized fraction for 30 min at RT or in combination with 1:1000 diluted anti-mouse AlexaFluor647. Finally, cells were washed and mounted with ProLong Gold antifade reagent with DAPI (Invitrogen, P36935). Images were acquired on Zeiss Axio Imager Z2 Upright microscope or Leica SP8 3X STED Super-resolution microscope in confocal mode.

Internalization assay: hBMECs were purified on 96-well flat-bottomed plates (Corning #3539948). Cells were serum starved for 1 hr at 37^{o} C in serum free endothelial cell media. 1μM purified scFv-Fc diluted in serum media were added to cells. For temperature dependent internalization experiments one group of cells was incubated at 37^{o} C and one group with the same concentration of scFv-Fc at 4^{o} C for 1 hr. After scFv-Fc incubation membrane bound antibodies were stripped by 5X acid washing (100mM Citric Acid pH 3) on ice. Cells were fixed with 4% paraformaldehyde for 8 min and blocked and permeabilized with 0.1% Triton X diluted in odyssey blocking buffer (LICOR #927-40000) for 15 min. Internalized scFv-Fcs were detected by incubation for 1 hr at 4^{o} C with IRdye800CW goat-anti-rabbit IgG pAb (LICOR #925-32211) and cell number in each well measured with CellTag (LICOR # 926-041090), both diluted in odyssey blocking buffer. After primary antibody incubation hBMECs were washed on ice 7X with PBS 0.05 % Tween-20, and signal from each well measured with a LICOR Odyssey Imager with a focus offset of 3mm and resolution of 169μm. scFv-Fc signal in each well was normalized to total cell number by dividing with the equivalent CellTag signal.

Equilibrium binding measurements: hBMECs were purified on 96-well flat-bottomed plates, washed 2X with PBS, and fixed with 2% PFA for 8 min. Fixed cells were blocked and permeabilized as described above for LICOR imaging. Apparent equilibrium affinity titration measurements were performed by incubating fixed cells with a range of scFv-Fc concentrations ranging from 1nM to 1μM at room temperature for 2 hr, depending on the antibody used. After extensive washing with PBS 0.05 % Tween-20 at 4^{o} C cells were labeled for scFv-Fc detection and for total cell number evaluation with IRdye reagents and CellTag as described above. Fraction of cellular antigens bound by scFv-Fc was quantified using background subtracted, - total cell number normalized - binding signal and the data was fit to a bimolecular equilibrium binding model to determine the dissociation constant (K_D).

Competition assay: scFv-Fcs were incubated with 10X K_D concentrations of recombinant receptor ecto-domain proteins rIR (R&D Systems #1444-IR, rhTfR (R&D Systems # 2474-TR) in PBS 1 % BSA for 30 min at room temperature and then applied to serum starved hBMECs in 96 well plats to allow scFv-Fcs to bind to membrane antigens. Plates were incubated at 4^{o} C for 2 hrs, and extensively washed, fixed and labeled with IRdye reagents for detection as described above. Total signal of the receptor competed scFv-Fcs was compared to un-competed scFv-Fc signal intensity.

3.2.6 SDS-PAGE and western blot:

scFvs and scFv-Fcs were mixed with SDS containing sample buffer either with or without reducing reagent and boiled for 10 min prior to loading onto a 4-12 % Bis-Tris gel (ThermoFisher #NP0321). Gels were stained with Coomassie blue or transferred to a nitrocellulose membrane for Western blotting. Membranes were blocked with 5% fat free

dry milk in PBST, probed with primary antibody 9E10 (1:3000 dilution) followed by anti-species horseradish peroxidase (HRP) - conjugated antibodies (1:2000 dilution). For scFv-Fc detection, a one-step Western blot with a goat-anti-rabbit-HRP antibody was performed. Clarity Western ECL Substrate (Bio-Rad) was used to develop the membranes and imaging was performed with the ChemieDoc XRS+ system (Bio-Rad). Protein band quantification was performed with the Image Lab Software (Bio-Rad).

3.2.7 Flow cytometry:

hBMECs were cultured in 6 well plates as described above. The cells (~$2x10^6$ cells/sample) were washed in PBS and detached from the culture plate with versene treatment for 1 hr at 37° C. The cells were transferred to 1.5 mL tubes and blocked for 1 hr at 4 ° C with PBS 1% BSA while rotating. 10^{11} CFU of phage (either from each round of panning, or negative control anti-botulinum toxin phage ABN) were incubated with blocked hBMECs for 1 hr at 4 ° C. Following, cells were washed 3X with PBS 1% BSA to remove weakly bound phage and labeled with anti-M13 antibody as described above. The cells were washed two times and resuspended in flow buffer (PBS + 0.1% BSA + 5 mM EDTA) and analyzed on a flow cytometer (Becton Dickinson FACSCalibur).

3.2.8 Immunofluorescence labeling of human and mouse brain cryosections *ex vivo*

Health human tissue was obtained from an epileptic human patient. A mouse was anesthetized with isoflurane and sacrificed by cervical dislocation, the brain removed and snap frozen in liquid nitrogen. Human and mouse tissue were cryosectioned in 8 and 30 µm sections on Thermo Scientific Microm HM 525. Due to the unknown structure of the corresponding antigens multiple modes of fixation were used. Prior to immunolabeling

sections were fixed with either 4% PFA for 20 min at RT or in cold acetone at -20°C for 20 min. In some instances, sections were post-fixed after incubation with scFvs or scFv-Fcs. Sections fixed with PFA were, additionally, permeabilized with 0.2% Tx-100 in PBS. Sections were blocked with 10% goat serum in PBS (PBSG) for 30 min at room temperature. Dimerized form of soluble scFvs (13 µg/ml) or scFv-Fcs 5µg/ml for human brain sections or 50 µg/ml for mouse brain sections were incubated onto sections for 24 hrs at 4°C. In human sections the blood vessels were labeled with mouse anti-human PECAM1/CD31 (Cell Sciences #MON6002-1), diluted 1:50 in PBSG for 2 hrs at RT. The blood vessels in mouse brain sections were directly labeled with LelDyLight488 (Vector laboratories Lel Dylight488) added to the secondary antibodies, which were goat anti-mouse AlexaFluor555 (1:1000) or goat anti-rabbit AlexaFluor555 (1:1000) in PBSG. Sections were mounted with ProLong Gold antifade reagent with DAPI (Invitrogen, P36935) and analyzed on Zeiss Axio Imager Z2 Upright microscope.

3.2.9 Immunofluorescence labeling of mouse brain cryosections after IV administration of antibodies

Mice C57BL6, 5-6 weeks old, were obtained from Envigo. Mice were injected intravenously with scFv-Fcs in a dose 5 mg/kg. After 1 hr, mice were anesthetized with ketamine/xylazine 100mg/kg/10mg/kg, and whole-body perfusion was performed in a regimen 5 ml/min for 5 min with a physiological solution, supplemented with 100 U/ml heparin, 4 µg/ml fluorescently labeled lectin (LEL Dylight488 Vector laboratories) and 0.1% BSA, followed by additional 5 min perfusion with 4% PFA. Organs, brain, heart, lung, liver, kidney and spinal cord were collected and snap frozen in liquid nitrogen and stored at -80°C. Sections 8 or 30 µm were made on Thermo Scientific Microm HM 525.

Before immunolabeling sections were air dried for 1 hr, permeabilized with 0.05% saponin for 30 min, and blocked with PBSG for 30 min at RT. To visualize bound scFv-Fcs, sections were incubated with anti-rabbit AlexaFluor555-conjugated secondary antibody (Invitrogen #A21428), diluted 1:1000 in PBSG with 0.05% saponin, overnight at 4°C. Washing steps were with 0.05% saponin in PBS. Sections were mounted with ProLong Gold antifade reagent with DAPI (Invitrogen, P36935) and analyzed on Zeiss Axio Imager Z2 Upright microscope.

IV injected mouse brain 30 µm thick sections were additionally labeled for glial fibrillary acidic protein (GFAP) and collagen IV. After blocking with 10% goat or donkey serum, respectively and permeabilization as described previously, sections were incubated with either mouse anti-GFAP (BD Pharmingen #556329) or goat anti-collagen IV (Milipore Sigma #AB769) in the corresponding blocking buffer plus 0.05% saponin for 2 hrs at room temperature. Sections were washed with 0.05% saponin in PBS and incubated with secondary antibodies: anti-rabbit AlexaFluor555 (Invitrogen #A21428) and anti-mouse AlexaFluor647 (Invitrogen #A-21235) or anti-rabbit AlexaFluor555 (Invitrogen #A31572) and anti-goat AlexaFluor647 (Invitrogen #A-21447).

3.2.10 Quantification of antibodies in mouse brains with ELISA

Mice C57B6, 5-6 weeks old were injected intravenously with scFv-Fcs at a dose 20 mg/kg. After 1 hr, blood was sampled, briefly spun down and the plasma was frozen at -80°C until analysis. Mice were anesthetized with ketamine/xylazine 100mg/kg/10mg/kg, and whole body perfused at rate 5 ml/min for 10 min with a physiological solution, supplemented with 100 U/ml heparin and 0.1% BSA. Brains were removed and homogenized in 1% NP-40 in PBS with Complete Mini EDTA-free protease

inhibitor cocktail tablets (Roche Diagnostics) as described previously [23]. To allow extraction of antibodies from the tissue, brains were rotated at 4°C for 24 hrs. Supernatant was collected after centrifugation at 14,000 rpm for 20 min at 4°C. Brain extracts were either analyzed immediately or frozen at -80°C. No differences in the antibodies brain concentration was observed in fresh or frozen samples.

Nunc Maxisorp 96-wells plates were coated with anti-HA tag antibody 1µg/ml (Thermo Fisher Scientific #MA1-12429) diluted in 0.2 M $NaCO_3$/$NaHCO_3$. at 4°C overnight. Plates were washed three times 5 min each with 0,05% Tween-20 in PBS and blocked with 2% BSA in washing buffer. Brain extracts were added undiluted to the plate, blood plasma samples were diluted in blocking buffer. Antibodies with known concentration were diluted in brain extracts prepared from untreated mice or blocking buffer and added in serial dilutions to construct the standard curve for calculation of brain or terminal plasma concentration. After 2 hrs incubation at RT the samples were aspirated, the plate was washed three times 5 min each and anti-rabbit HRP antibody was added for 1 hr at RT. The unbound detection antibody was washed six times 5 min each and 1-Step Ultra TMB-ELISA Substrate Solution (ThermoFisher Scientific #34028) was added. Absorbance was measured at 450 nm on Infinite M200 (Tecan) plate reader. The lower limit of detection was 1.03 nM, 0.02 nM and 0.44 nM for clone 46.1, 17 and CTRL-Fc, respectively. The standard curve, used to calculate the concentrations, was based on four-parametric logistic fit. Statistical analysis was performed with two-tailed unpaired Students *t* test, p values<0.05 were considered statistically significant.

The plasma concentration for clone 17 was determined using Western Blot. Blood plasma samples and serial dilutions of clone 17 antibody were separated on 4-12 % Bis-

Tris gel (ThermoFisher #NP0321). The proteins were transferred onto a PVDF membrane, the membrane blocked with Odyssey blocking buffer (LICOR #927-40000) and probed with goat-anti-rabbit IR800CW antibody (LICOR #925-32211). The membrane was scanned on Odyssey Imager (LICOR). ImageJ was used to measure the intensities of the bands and the plasma concentration was calculated from the corresponding standard curve.

3.3 Results:

3.3.1 Phage display screening for transcytosing antibodies

A major challenge in selecting antibodies able to transcytose the human BBB is the inherent leakiness of most current BBB models, resulting in significant background phage recovery masking potentially valuable clones. In this study we employ an iPSC-derived hBMEC BBB model that combines the advantages of human sourced material with robust BBB properties, particularly the ability to form a very tight barrier [37]. These hBMECs express a collection of markers unique to the BBB and express a host of transporter proteins including nutrient transporters, drug efflux transporter, and large molecule RMT systems [35,37]. Importantly, the permeability of the model for large particle such as phage decreases significantly with increased model fitness as assessed by TEER values, leading to low flux of phage at high TEER thereby allowing us to perform transcytosis screens (Supplementary table 3.1)

A library of $5x10^8$ human-derived scFvs displayed on the surface of fd-tet phage [102] was used in panning as multivalent display helps bias the screen towards antibodies capable of internalization [106] – a requirement for transcytosis. Within the screen, a presubtraction step was performed on human lung and heart endothelial cells (Figure 3.1a, step 1) to de-enrich phage binding to common endothelial antigens, as transcriptomics studies have shown a close relation between lung and heart cells to the BBB [107]. As it was previously determined that a minimum of 10^5 copies/clone are necessary in order to observe transcytosis through hBMECs (data not shown), panning rounds were performed in order to increase clonal oversampling. The pre-subtracted phage pool was incubated on hBMECs grown on tissue culture flasks first on ice as a binding step and then at 37^{o}C to allow for phage internalization (Figure 3.1a, step 2). The

surface of hBMECs was subsequently stripped of phage particles with low pH washes, cells were lysed, and internalized phage recovered in TG1 E. coli and tittered to calculate enrichment factors (Supplementary table 3.4). Significant phage binding to hBMECs was observed after the third panning round (Figure 3.1b). In order to identify scFv-bearing phage able to transcytose across the *in vitro* BBB, hBMECs were purified on collagen/fibronectin coated 1μm pore size transwells to form a tight (TEER value >1000 Ω cm^2) barrier. Phage pools from step 2 were then added to the upper chamber and allowed to transcytose for 3 hrs before harvesting phage containing media from the bottom chamber and TG1 infection (Figure 3.1a, step 3). At this point, scFv-bearing phage were sequenced at a clonal basis. Phage immunochemistry on hBMEC monolayers was performed to separate ‘’true’’ binders from non-specific phage able to leak through the monolayer (Figure 3.1c). It was observed that clones 3 and 22Ch represented >50% of the transcytosing phage pool (142/220 sequences, supplementary table 3.5). Hence, we theorized that it is possible those phages saturate the transcytosis capacity of hBMECs. In order to expand the recovered repertoire, we produced clones 3 and 22Ch as soluble protein and performed a competitive transcytosis screen by adding soluble scFvs at saturating conditions along with phage pools to the upper chamber (Figure 3.1d). Soluble scFvs outcompeted respective phage particles from binding to the cell monolayer and transcytosing across. Individual clones from the bottom chamber were isolated and sequenced. Interestingly, neither clone 3 nor 22Ch was found in the transcytosed fraction following soluble scFv competition, contrary to a control, non-competitive screen where scFv 3 and 22Ch again comprised the majority of output sequences (supplementary tables 3.5 & 3.6 &3.7). Further, no clone dominated the output of competitive transcytosis,

allowing us to identify more unique sequences.

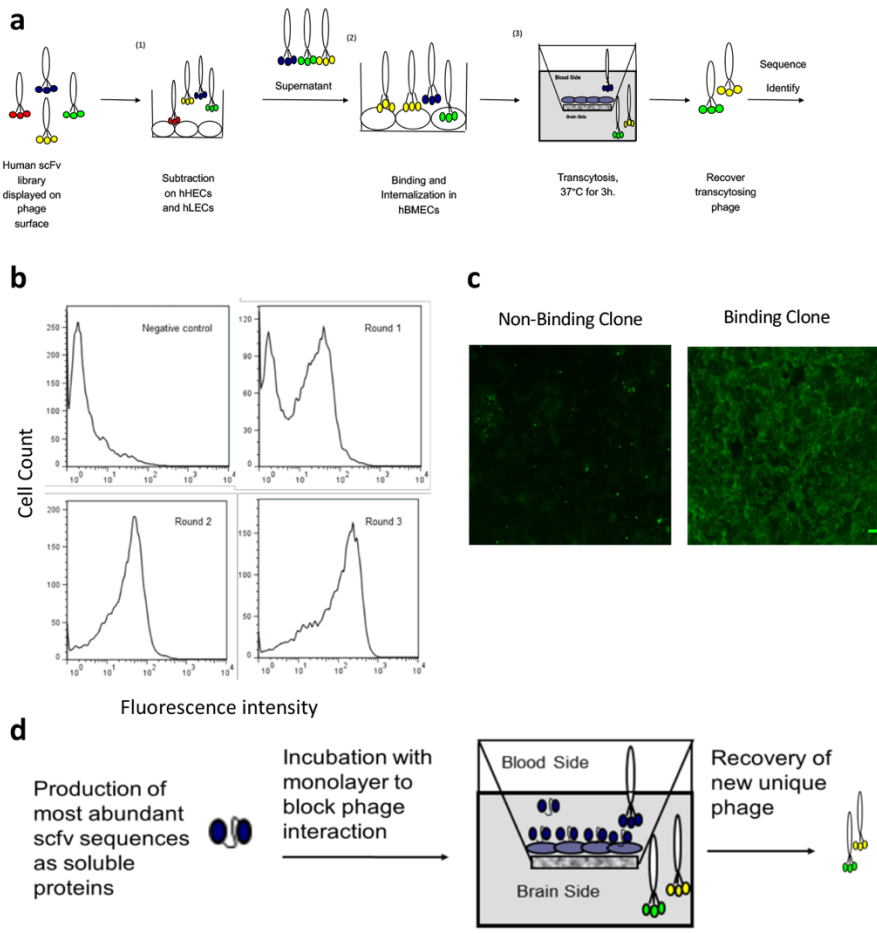

Figure 3.1 Antibody library screening on in vitro BBB model a) Step 1: pre-subtraction of phage library on human HEL and LEC to promote brain specificity. Step 2: Library incubation with hBMECs to allow for binding and internalization of the antibody bearing phage. Step 3: phage were dosed onto hBMECs in a transwell format for 3h to allow for transcytosis. Recovered phage particles were subjected to further analysis. b) Enrichment of hBMEC binding phage antibodies as seen by FACS-analysis of phage antibody pools during selection step 2. Shown are representative histograms of hBMECS stained with phage antibodies after respective panning rounds. The number of cells (counts: Y-axis) is given as function of the fluorescence intensity of phage antibody staining of the cells (X-axis). In all experiments, cells were incubated with phage antibody pools, and cell-binding was detected by anti-M13 antibody and FITC-conjugated anti-rabbit antibody c) Sample images from clonal phage immunochemistry using hBMECs to determine which clones display a binding phenotype. Image on the left is a non-binding clone, image on the right is a binding scFv in phage format. Scale bar, 50µm. d) Expanding the repertoire by screening using scFv competition. Soluble scFv 3 and 22Ch were incubated along with library pools at the upper chamber blocking interaction of phage with the monolayer. Individual clones recovered from the transcytosis round were subjected to further analysis.

3.3.2 ScFv-Fcs endocytose into *in vitro* human BBB model and bind to human brain microvessels *ex vivo*

Individual scFvs identified from both non-competitive and competitive transcytosis rounds that bound hBMECs in phage format were expressed in bacteria and purified via a hexahistidine tag. A total of 12 lead scFvs show a binding signal to hBMECs and a subset interacts with endothelial cells on mouse brain cryosections *ex vivo* as pre-dimerized soluble scFvs (Table 3.1 and examples shown in Supplementary Figure 3.7). For further evaluation, scFvs were reformatted as scFv-Fc fusions with a rabbit IgG Fc region and expressed in HEK293F expression system (Figure 3.2a). ScFv-Fc antibodies migrated as monomers of approximately 55kDa under reducing conditions (Figure 3.2b). Apparent affinity was determined by measuring the binding signal intensity to hBMECs monolayers at increasing concentrations of scFv-Fc and fitting the data to a bimolecular equilibrium binding model to calculate the dissociation constants (K_D) (Figure 3.2c). Six out of twelve clones were produced in sufficient amounts for downstream applications and it was decided that further evaluation will proceed with these clones. Reformatting scFvs from phage particles into full-size antibodies might influence their binding to the respective antigen [108], hence we sought to assay scFv-Fc fusions' binding and internalization in hBMECs next to measuring antibodies apparent affinity. Antibodies were incubated onto hBMECs on ice to allow binding the surface antigens. Cells were then transferred at 37°C to allow endocytosis. Cellular uptake was terminated with cold wash and cells returned back on ice for incubation with fluorescently labeled anti-rabbit Fc antibody to visualize the surface bound fraction. To access the internalized antibody fraction cells were further fixed, permeabilized and incubated with different fluorophore-

conjugated anti-rabbit Fc antibody. All of the assayed scFv-Fcs preserve their capacity to bind and to endocytose in hBMECs. Five of six antibodies show similar appearance, namely clones 3, 9, 17, 22Ch, and 26. The surface bound antibodies have distinct dotted-pattern (Figure 3.2e, red pseudocolored), whereas the internalized antibodies appear as larger in size perinuclear punctae (Figure 3.2e, green pseudocolored), reminiscent of intracellular vesicles. In striking contrast, only minor fraction of the internalized 46.1-scFv-Fc seems to be confined within vesicles proximal to the cell-cell contacts. The major fraction localizes at cellular junctions upon uptake.

Quantitative internalization assays were carried on hBMEC monolayers and all clones (with the exception of clone 26) exhibited a temperature dependent internalization (Figure 3.2d). Comparison of ligand internalization in cells incubated at 37^{o}C versus cells kept at 4^{o}C where receptor mediated endocytosis is inhibited points towards an active, temperature dependent endocytosis mechanism.

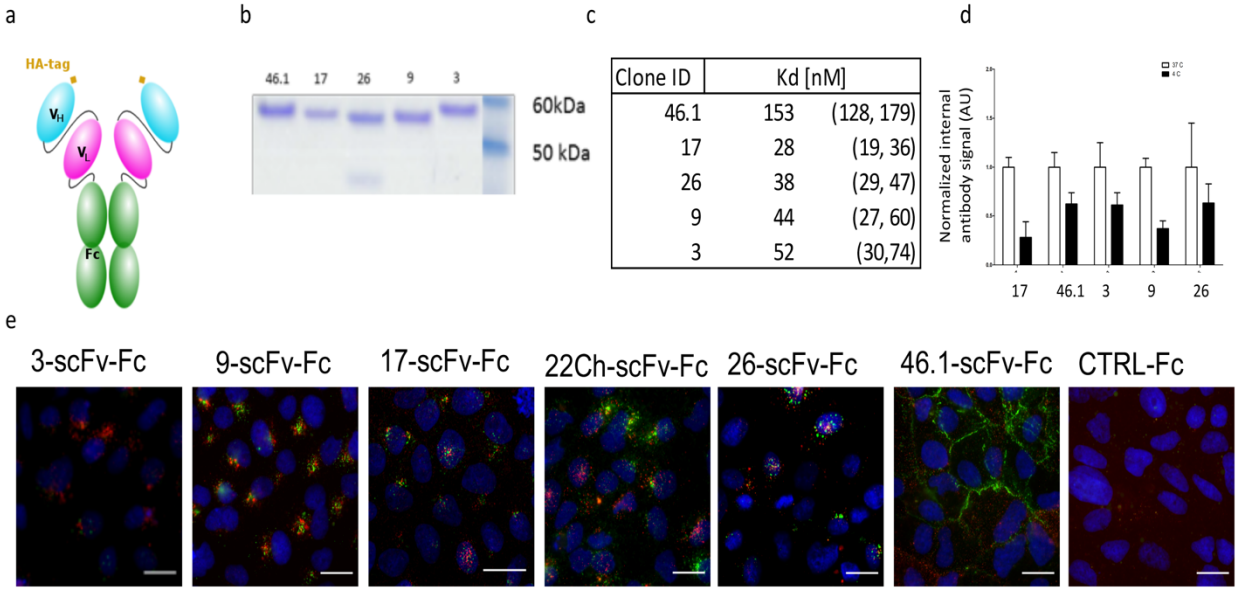

Figure 3.2 Antibody binding to BBB in vitro. a) scheme of the antibody constructs. b) SDS-PAGE analysis of scFv-Fc antibodies following expression in HEK293F cells and protein A/G purification. Proteins were separated on a 4-12% Bis-Tris SDS-polyacrylamide gel in reducing conditions and stained with Coomassie blue for molecular weight detection. Typical purification results of 5 clones are shown with MW in the range of 55 kDa. c) Apparent equilibrium binding affinity of selected clones. Mean data from N>3 independent experiments. The table shows numeric values for the best-fit equilibrium binding affinity (K_d) and associated 95% CI. d) Temperature-dependent internalization of antibodies in 96-wells assay. Internalized fraction fluorescent signal values are normalized to the total signal per cell at 37°C, with N=3. e) Binding and internalization of example lead antibodies into hBMECs. Live cells were incubated with antibodies (5 µg/ml) at 4°C and subsequently at 37°C for 30 min. The cell membrane was washed with cold buffer and the membrane bound fraction (red) labeled with anti-rabbit Fc AlexaFluor555 antibody. After fixation and permeabilization the internalized antibodies (green) were labeled with anti-rabbit Fc AlexaFluor488 antibody. Four of five clones appear confined within intracellular vesicles, whereas clone 46.1 is localized mainly at cell-cell contacts. Scale bar, 20 µm.

BBB endothelial cells form a polarized monolayer with two distinct domains – apical and basolateral plasma membrane – separated by tight junctions [109]. Given the unexpected intracellular distribution of clone 46.1, we next sought to determine its precise localization with respect to the tight junction protein ZO-1 (Supplementary Figure 3.8a) and the basolateral protein CD31. hBMECs were incubated with 5 µg/ml 46.1-scFv-Fc as described in Supplementary Figure 3.8a. After the fixation and permeabilization step, cells were additionally labeled for ZO-1 or CD31. The spatial distribution of clone 46.1 (internalized fraction, pseudocolored in red), ZO-1 or CD31 (pseudocolored in green) and

clone 46.1 (surface bound fraction, pseudocolored in blue) was resolved in a series of confocal images spanning the cell monolayer in basolateral to apical direction. Clearly, the internalized fraction of clone 46.1 localizes downstream from ZO-1, i.e. the basolateral membrane, whereas the surface bound fraction is upstream from ZO-1, i.e. the apical membrane (Supplementary Figure 3.8b). The endocytosed fraction of 46.1-scFv-Fc occasionally colocalizes with CD31, nonetheless it completely repeats the staining pattern of CD31 (Supplementary Figure 3.8b). Collectively, clone 46.1 seems to traffic intracellularly from the apical to the basolateral membrane in hBMECs.

Clone ID	BMECs binding	BMECs internalization	human BBB binding	mouse BBB binding	IV BBB target
	12/12	9/12	10/12	9/12	5/12
3	√	√	√	√	√
9	√	√	√	√	x
17	√	√	√	√	√
26	√	√	√	√	√
46.1	√	√	√	√	√
22Ch	√	√	√	x	ND
6i	√	x	x	ND	ND
5A	√	√	x	ND	ND
2F-scFv	√	√	√	√	ND
4B-scFv	√	√	√	√	ND
5E-0.4	√	x	√	√	ND
B3-R3	√	x	√	√	ND

Table 3-1 Clonal evaluation for BBB interaction. X denotes no interaction, ND denotes interaction not determined. The red color coded scFvs were produced in sufficient amounts as scFv-Fc fusions to allow for downstream *in vivo* work and were further evaluated. scFvs color coded in black showed initial BBB interaction *in vitro* and *ex vivo*.

In vitro modeling of the BBB often results in altered expression of surface receptors [29]. Hence, next to binding to human BMECs, we analyzed the binding of scFv-Fc to human brain sections *ex vivo* (Figure 3.3a). Sections were obtained from resection of epileptic human brain, only juxtapose healthy tissue was used. All of the antibodies (pseudocolored in red) recognize and bind to their cognitive antigens on human brain microvessels (visualized with CD31, pseudocolored in green). In parallel, using the same

immunofluorescence assay, we assessed the binding of clones to mouse brain tissue sections (Figure 3.3b). Only clones that show both binding to human and mouse brain section were used in downstream applications. Clone 22Ch was scored as negative for binding to mouse brain sections and was excluded from further analysis.

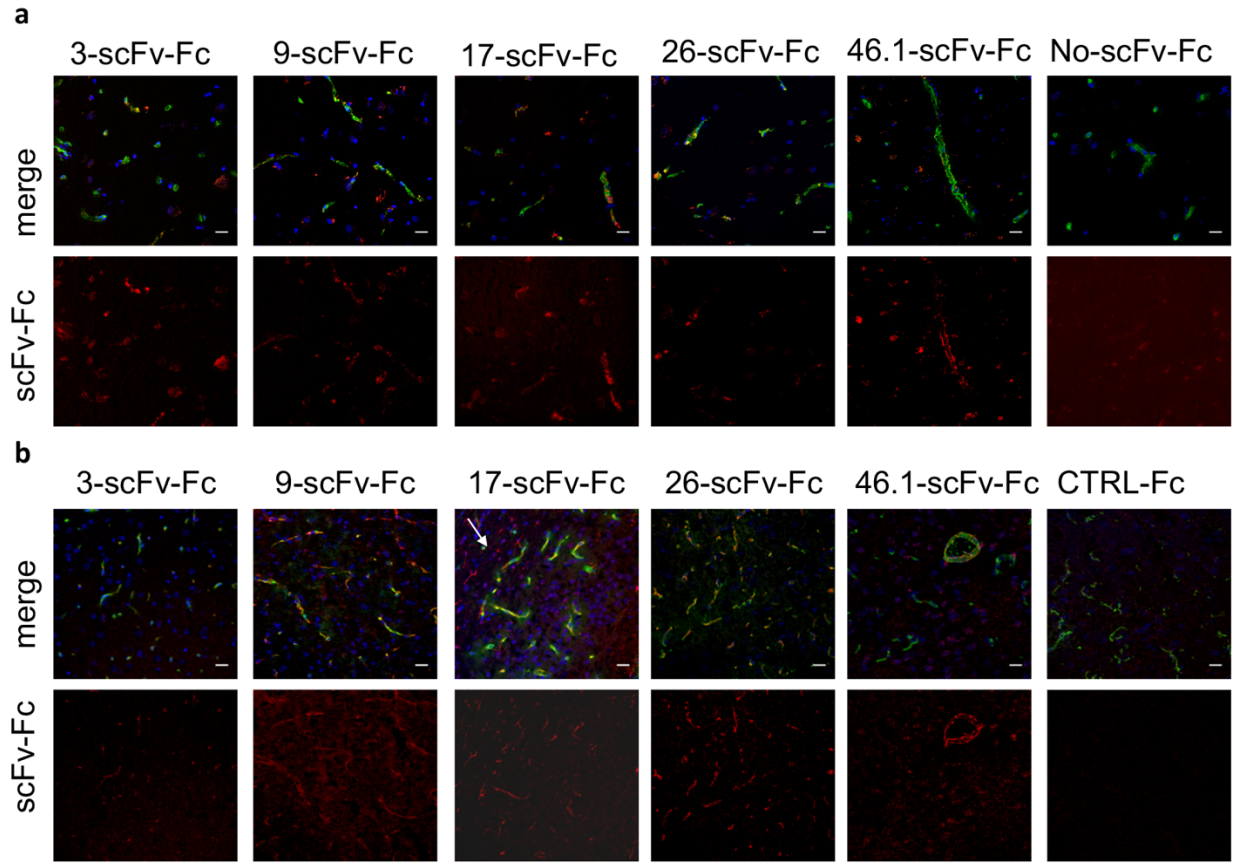

Figure 3.3 ScFv-Fcs bind to human brain microvasculature *ex vivo*. a) Cryosections of human brain were immunolabeled for CD31 (green) to visualize the blood vessels and incubated with 5 µg/ml scFv-Fcs (red), nuclei are in blue. Scale bar, 20µm. b) ScFv-Fcs bind to mouse brain microvasculature *ex vivo*. Cryosections of mouse brain were immunolabeled for lectin (green) to visualize the blood vessels and incubated with 50 µg/ml scFv-Fcs (red), nuclei are in blue. Next to brain endothelium, the antigen of clone 17 appears to be expressed on brain cells of non-vascular origin (white arrow). Scale bar, 20µm.

3.3.3 ScFv-Fcs show accumulation in brain microvessels after intravenous administration in mice

The *in vivo* relevance of scFv-Fcs that showed binding to brain microvessels in

human and mouse brain sections *ex vivo* was investigated further after intravenous administration in mice (Figure 3.4). Mice were injected in a dose 5 mg/kg. The antibodies were allowed to circulate for 1 hr. The unbound fraction of antibodies was cleared from the blood vessels with whole body perfusion with a physiological solution containing fluorescently labeled lectin (pseudocolored in green in Figure 3.4a and 3.4b) to visualize the lumen of the blood vessels and as an indirect control of the integrity of the BBB. Finally, the mice were perfused with 4% PFA to fix tissues and organs. Immunohistochemical analysis of brain sections reveals four of five injected antibodies, visualized with fluorescent anti-rabbit Fc antibody (pseudocolored in red), recognize antigens exposed on the apical surface of the brain endothelium. Interestingly, binding clones 3-, 17-, 26- and 46.1-scFv-Fcs appear to have distinct intracellular distribution. While clone 17 showed homogeneous staining pattern, clones 3, 26 and 46.1 are visible as punctate structures (Figure 3.4a, white arrows). Occasionally, post-vascular fluorescent signal was detected in brain sections from clone 46.1 injected mice (Figure 3.4a, yellow arrow).

Clone ID	brain	heart	lung	liver	kidney	spinal cord
3-scFv-Fc	positive	negative	intravascular localization	positive	positive	positive
9-scFv-Fc	negative	negative	negative	Positive low accumulation	negative	positive
17-scFv-Fc	positive	positive	Positive high accumulation endothelium	Positive high accumulation	positive	positive
26-scFv-Fc	positive large vesicles	negative	negative	Positive low accumulation	negative	positive
46.1-scFv-Fc	Positive post-vascular	negative	dose dependent cell-specific	Positive high accumulation cell-specific	positive cell-specific	positive
CTRL-Fc	negative	negative	negative	negative	negative	negative

Table 3-2 Qualitative analysis of biodistribution of antibodies after i.v. application in mice. ND denotes interaction not determined. X denotes no interaction.

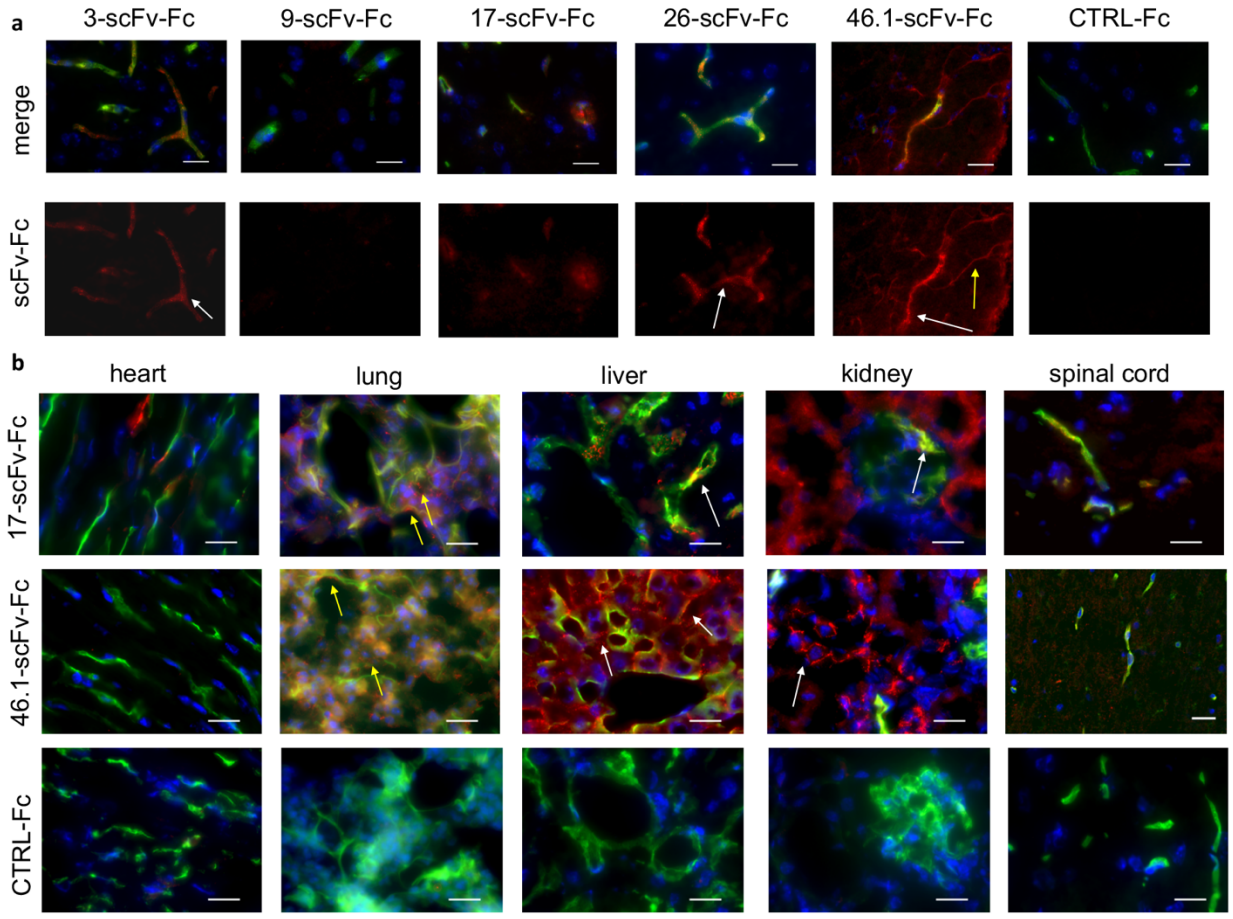

Figure 3.4 Antibodies bind to mouse brain microvessels *in vivo*. Antibodies (5mg/kg) were injected intravenously in mice. 1 hr post-injection mice were whole body perfused, brains and organs collected and snap frozen. ScFv-Fcs (red) were labeled with fluorescent anti-rabbit Fc antibody in 8 µm or 30 µm (lung) thick tissue sections. Blood vessels (green) were visualized with DyLight488 lectin diluted in the perfusion buffer. a) Four of five analyzed antibodies accumulate in brain vasculature. The white arrows indicate punctate structures in brain endothelial cells. Post vascular immunoreactivity was observed in the brain sections from mice injected with clone 46.1 (yellow arrow). Scale bar, 20µm. b) Qualitative analysis of antibodies biodistribution *in vivo*. Clone 17 was the only one found in heart tissue (Table 3.2). Both clones shown, 17 and 46.1 localize intracellularly and along alveolar lumen in mice lung tissue (yellow arrows). 17-scFv-Fc colocalizes with the perfused lectin in the liver, whereas 46.1-scFv-Fc localizes at the basolateral membrane of hepatocytes (white arrows). In mice kidney tissue sections clone 17 is confined within the glomerular network (white arrow), clone 46.1 localizes at cell-cell contacts in renal epithelial cells (white arrow). Both clones are detectable in the blood vessels of the spinal cord. Scale bar, 20µm.

To assess the brain selectivity of candidate antibodies heart and lung as highly vascularized organs, and liver and kidney as major clearance organs were additionally collected and immunolabeled. The qualitative analysis of organ biodistribution is

summarized in Table 3.2. Representative images for clones 17, 46.1 and the negative control are shown in Figure 3.4b. The antigen of clone 17 is expressed in heart coronary vessels, as only clone 17 was detectable in heart tissue. Clone 9 and clone 26 were not present in the lung tissue, contrary to clones 3, 17 and 46.1. Interestingly, the three antibodies that show binding to lung tissue have distinct subcellular localization. Clone 3 was found in the lumen of blood vessels (not shown). Clone 17 and 46.1 line the lumen of alveolae and were found, occasionally, as vesicular structures in lung epithelial cells (Figure 3.4b, yellow arrows). Of note, the perfused lectin (pseudocolored in green) diffused throughout the lung tissue. The liver tissue of mice injected intravenously with antibodies was positive for the presence of all analyzed clones. Likewise, we observed differences in the subcellular distribution of scFv-Fcs. Hepatocytes, like BBB endothelial cells, are polarized, with apical and basolateral membrane, segregated by tight junctions [110]. Clearly, clone 46.1 localizes at the cell-cell interface of hepatocytes, with at least two instances where we were able to point exactly the basolateral membrane of contacting hepatocytes (Figure 3.4b, white arrows). The rest of the antibodies were found either intracellular in hepatocytes or, as shown for clone 17, within the hepatic sinusoids.

The cutoff size of molecules filtered by the tubular cells of the kidneys is 60kDa. The average size of ScFv-Fcs is 100 kDa. Hence, reformatting the scFvs into full-size IgGs will limit their kidney clearance and allow longer system circulation. Indeed, we did not detect clone 9 and 26 in any kidney structure. Clones 3 and 17 occupied the glomerular vasculature. Yet again, clone 46.1 localized at the cell-cell contacts of tubular epithelial cells, suggesting its active secretion through the glomerular endothelial cells and active uptake in downstream tubular cells. The blood vessels in the spinal cord were

positive for all clones, even for clone 9 that was scored as negative for binding brain endothelial cells *in vivo* (Figure 3.4b).

The control-Fc antibody does not seem to accumulate in any of the analyzed organs in amounts sufficient to be detected with the immunofluorescence assay (Figure 3.4b). Overall, the variable organ and tissue distribution of candidate antibodies points to different receptors engaged it their uptake and transport on organ and cellular level.

3.3.4 Transcytosis across the blood-brain barrier and parenchymal accumulation of scFv-Fcs *in vivo*

The abluminal site of the brain endothelial cells is surrounded by the basal lamina, with its major component collagen IV [109]. Hence, we next examined the localization of i.v. injected scFv-Fcs relevant to collagen IV as a determinant of transcytosis across the BBB. At least three consecutive frozen brain sections – 30 µm thick – from mice injected with scFv-Fcs as described in Figure 3.4 were additionally labeled for collagen IV (Figure 3.5a). It is beyond the scope of this study to quantify the colocalization events in the whole mouse brain, hence we show representative images from a 3D volume acquired with a confocal microscope. Three of the analyzed antibodies 3, 26 and 46.1 (pesudocolored in red) show colocalization with collagen IV (pseudocolored in blue) Figure 3.5a.

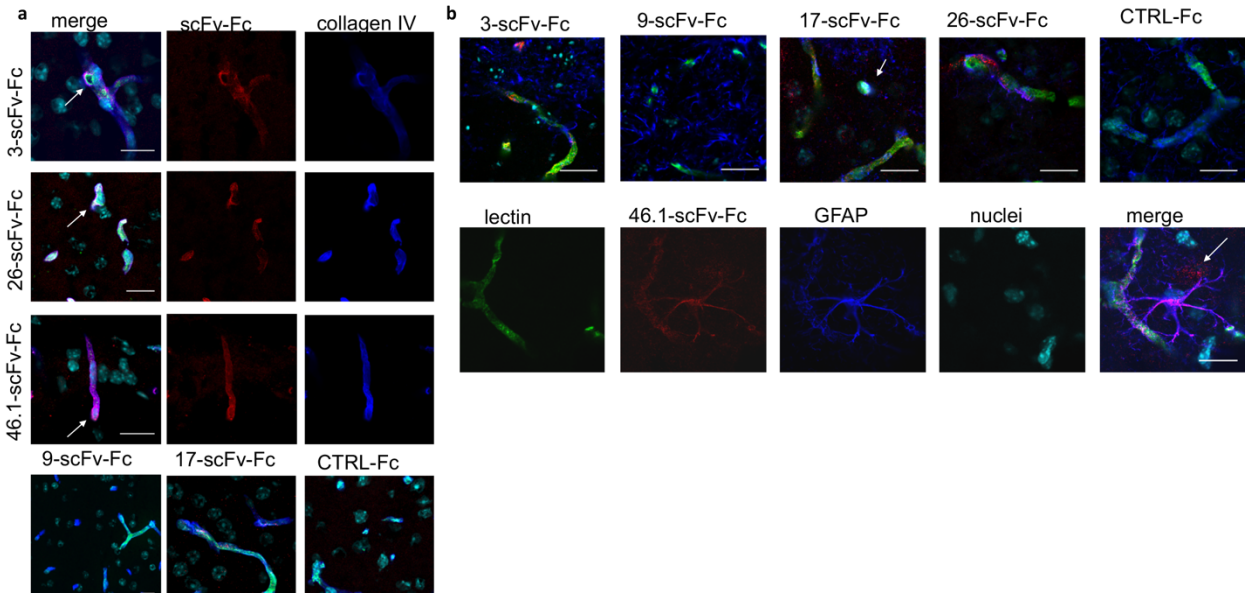

Figure 3.5 Post-vascular localization of i.v. injected antibodies in mice. Brains sections - 30 µm thick - from mice injected with antibodies as described in Figure 3.3. were post-labeled with the basal membrane component collagen IV (blue) and the astrocytic marker GFAP (blue). a) Confocal images from a z-stack showing the localization of scFv-Fcs (red) with respect to collagen IV. Clones 3, 26, and 46.1 colocalize with collagen IV (white arrows). Note, the luminal lectin (green) is fainting at the abluminal site of the blood vessel and is barely detectable in the image showing 46.1-scFv-Fc. Clone 17 shows no colocalization with collagen IV, nevertheless diffuse parenchymal staining is detectable. b) 46.1-scFv-Fc colocalizes with astrocytic end-feet and projections. For clarity the separated channels are shown for clone 46.1. The white arrows in clone 17 and clone 46.1 images indicate accumulation of antibodies in unclassified types of brain cells. Scale bar, 20 µm.

Astrocytic end-feet cover almost entirely the abluminal face of the capillary endothelial cells in the CNS [111]. Likewise, a macromolecule transported from the blood to the brain will eventually encounter the astrocytic membrane. Once endocytosed in astrocytes it could be further transported along the processes in a retrograde mode to reach the cell body [112]. Indeed, we frequently observed clone 46.1 in elongated structures emanating from the capillaries in mouse brain sections *in vivo* (Figure 3.4a, white arrow). To determine the cellular origin of these processes, we next labeled mice brain sections, obtained as described in Figure 3.3, with the astrocytic specific marker glial fibrillary acidic protein - GFAP (Figure 3.5b). As hypothesized, clone 46.1 (pseudocolored in red) colocalizes with GFAP (pseudocolored in blue) within the length of astrocytic processes

(Figure 3.5b, lower panel). Astrocytes, positive for 46.1-scFv-Fc, were unevenly spread throughout the 3x 30 µm consecutive sagittal sections analyzed, with a tendency to primarily occupy the hippocampal area. Other, unidentified CNS cells of non-vascular origin, likely accumulate i.v. injected antibodies, namely clone 17 and 46.1 (Figure 3.5b, white arrows). Thus far, we show at least three antibodies to transcytose the BBB endothelial cells *in vivo*, clone 3, 26 and 46.1 and two to reach the post-vascular CNS space, clone 17 and clone 46.1, respectively.

3.3.5 Quantification of scFv-Fcs accumulation in mice brain after i.v. application

Based on our immunofluorescence analysis, we further quantify the accumulation of clone 17 and 46.1 in whole mouse brain after intravenous administration. Antibodies, 20 mg/kg, were injected in mice and allowed to circulate for 1hr. Mice were whole body perfused to remove the vascular portion of antibodies (as described in Materials and Methods), brains isolated, homogenized and antibodies extracted in 1% NP-40 buffer. The concentration of antibodies in brain extracts (vascular and parenchymal fraction) was determined with ELISA and values adjusted to the brain volume extracted (Figure 3.6a). The measured concentration of clone 46.1 (8.1± 1.2 nM) was significantly higher ($p<0.005$) and shows 26-fold increase over the control-Fc clone (0.31 ± 0.11 nM). Similarly, to a lower extent with a 9-fold increase, the concentration of clone 17 (2.79 ± 0.63 nM) in mice brains was significantly higher than control-Fc antibody. Additionally, the terminal plasma concentration of antibodies, i.e. blood withdrawn at 60 min after injection, was measured and the brain concentration expressed as a ratio of the plasma concentration (Figure 3.6b and the adjacent table). As evident, clones 46.1 and 17 show significantly higher plasma to brain ratio than control-Fc, suggesting their active

sequestration into the brain.

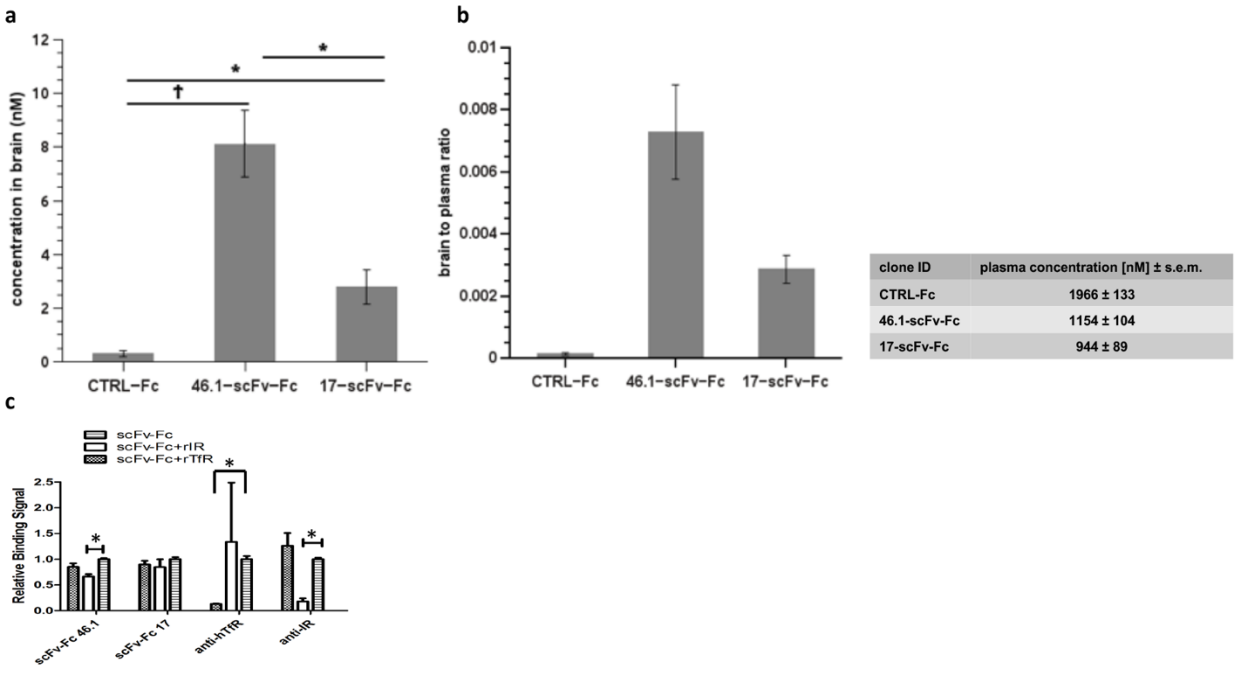

clone ID	plasma concentration [nM] ± s.e.m.
CTRL-Fc	1966 ± 133
46.1-scFv-Fc	1154 ± 104
17-scFv-Fc	944 ± 89

Figure 3.6 Quantification of brain accumulation of scFv-Fcs. Antibodies, clone 17, 46.1 and a control, were injected i.v. in mice (n=4). After 1 hr the mice were whole body perfused, brains collected, and antibodies extracted. a) The concentration of antibodies in brain extracts was determined with ELISA b) Brain to plasma ratio and table showing the terminal plasma concentration of antibodies c) Competitive binding assay on hBMECs used to determine scFv-Fc binding to major targets for brain drug delivery. Binding signal of each scFv-Fc following competition with soluble receptor ectodomains was normalized to binding in the absence of competition. Data are the means and error bars standard deviation calculated from independent experiment with n=3.

3.3.6 Known receptors engaged in BBB transcellular transport are not antigens for clone 17 and 46.1

To investigate if scFvs recognize known BBB transcytosis capable receptors, a competitive binding assay was used to determine if scFv-Fcs interact with major targets for brain delivery, transferrin receptor (TfR), and insulin receptor (IR). scFv-Fcs were pre-incubated with excess recombinant receptor ectodomains before a cell surface binding assay on live hBMECs. Cell surface binding of both clones 46.1 and 17 was not altered by any of the competing ligands (Figure 3.6c). Clone 46.1 when competed with soluble

IR ectodomain showed statistically significant signal intensity reduction, but not to the extent that would indicate interaction of antibody-receptor. In contrast, the binding signal of an anti-human TfR and anti-IR antibody was reduced to ≈15% of the non-competition signal when competed with the respective antigen.

3.4 Discussion:

In this study we developed an original selection strategy to identify antibodies that transcytose the *in vivo* BBB and also target human relevant antigens. Our functional screening strategy employed iPSC derived hBMECs as positive selection substrate and human lung and heart microvascular endothelial cells for subtraction in an effort to provide brain specificity. scFvs were selected from a fd-tet phage display scFv library to gear towards recovery of internalization and transcytosis capable clones. The scFv library was 1) presubtracted against peripheral endothelial cells; 2) positively selected for internalization on hBMECs; 3) selected from transcytosis against hBMEC monolayers. Pilot experiments in our laboratory established a reverse relationship between monolayer TEER and paracellular, nonspecific, phage leakage as well as necessary clonal oversampling parameters that allowed for successful phage transcytosis *in vitro*. Following three rounds of enrichment aimed towards recovery of endocytosing antibodies a transcytosis screen resulted in a limited transcellular phage flux and a collapse of the library's diversity with a concurrent increase in phage hBMEC specificity (~75% of output phage positive for hBMEC binding). We observed two clones dominating the output's sequence space, potentially masking transcytosis of other interesting phage clones. We performed a transcytosis screen where dominant phage were outcompeted from binding to the hBMEC monolayer following competitive addition of soluble scFv protein alongside the library. Following the transcytosis rounds phage were evaluated in individual basis via phage immunochemistry and DNA sequencing, and the overall diversity was reduced to twelve scFvs capable of binding and/or internalizing in hBMECs as soluble protein or full IgGs.

ScFv-Fcs interact with *in vitro* BBB model cells in a temperature dependent mode

and target different intracellular loci, suggesting RMT as a predominant route of cellular uptake. The morphology and cellular localization particularly of a few 46.1-scFv-Fc containing intracellular structures, namely vesicles proximal to the cell-cell contacts, seems to be distinct from recycling or degradative compartments [113]. In contrast, the major fraction of endocytosed 46.1-scFv-Fc is localized at the brain-facing site of BBB endothelial cells *in vitro*. Hence, the antigen of clone 46.1 functions as a transcytosing molecular shuttle in brain endothelial cells via a potentially unexplored transcytosis mechanism.

Brain endothelial cells phenotype, when cultured *in vitro*, might differ from the *in vivo* BBB endothelial cells [29]. Hence, we next sought to establish that our antibodies recognize antigens expressed *in vivo. Ex vivo* immunostaining of human and mouse brain cryosections with scFv-Fcs highlighted the interaction of antibodies with *ex vivo* present antigens and offered the necessary cross-reactivity to allow further *in vivo* evaluation. Four of five scFv-Fcs accumulated in brain endothelium after intravenous injection in mice. Clones 3, 26 and 46.1 seem to engage in RMT as evident by their intracellular vesicular localization along the brain microvessels. Moreover, we found clone 46.1 in post-vascular cellular processes, which supports the notion of successful transport of clone 46.1 across the BBB and its distribution in the brain parenchyma.

Unlike conventional small molecule drugs, therapeutic antibodies benefit from having high binding specificity to their corresponding antigen. Hence, off-target effects are minimized and adverse effects are usually associated with the downstream antigen (effector) function [114]. Likewise, a brain targeting antibody should have a specificity towards brain endothelium. However, receptor-mediated transcytosis is a common

process in polarized cells, and brain specificity is desirable. Here, we addressed this issue by qualitatively characterizing our hit antibodies in context of body biodistribution after intravenous administration. In at least one instance we show a moderate success of our phage library presubtraction strategy. Namely, clone 26 was not found to bind antigen in heart or lung tissue. In contrast, clone 17 is the single one detected in coronary vessels. Interestingly, clone 46.1 was found in kidney and liver cells. Unlike the other clones, the presence of clone 46.1 in these tissues is associated with distinct cellular localization. Similarly, to hBMECs *in vitro*, 46.1-scFv-Fc localizes at the cell-cell contacts in kidney tubular epithelium and hepatocytes, suggesting its common entry route and trafficking in polarized cells.

Ultimately, a brain targeting antibody should deliver therapeutic payload to the brain parenchyma, i.e. after exocytosis at the abluminal site of brain microvascular cells, the antibody-drug conjugate should diffuse through the basal lamina and will eventually encounter the plasma membrane of astrocytic end-feet. We used collagen IV and GFAP as markers to characterize the transport of hit antibodies beyond the BBB endothelial cells. In addition to its colocalization with collagen IV, 46.1-scFv-Fc is taken up by astrocytes and traffics retrogradely along the astrocytic processes to the cell body. Interestingly, clone 46.1 was detected as punctae in not yet characterized brain cells in the vicinity of positive astrocytes. These results illustrate the significant capacity of scFv-Fc 46.1 for transport across the BBB.

To obtain stronger evidence for the accumulation of clone 17 and 46.1, we next quantify the amount of antibodies in the brain. After intravenous administration in mice the concentration of clone 46.1 in brain extracts was 26-fold higher than control,

comparable to brain concentration previously reported for anti-transferrin receptor antibodies [115]. The brain extracts were prepared from the whole tissue, i.e. brain parenchyma plus blood vessels. Our immunofluorescence data, however, suggests at least a fraction of the amount measured being isolated from cells of non-vascular origin. In addition, the concentration of clone 17 in brain extracts was measured to be ~3 nM, significantly higher than control antibody.

Until now, the antigens of clone 46.1 and 17 remain unclear, the work on their characterization is ongoing. However, we demonstrated the potential novelty of these RMT pairs in a competitive assay, providing evidence pointing that highly expressed at the BBB transferrin and insulin receptors are likely not the binding partners for antibody 46.1-scFv-Fc and 17-scFv-Fc.

In summary, we have identified new promising antibodies that show enhanced brain uptake. These novel antibodies were discovered via a functional transcytosis screen of phage display libraries. Importantly for translational considerations, our antibodies demonstrated cross-reactivity to mouse and human antigens. In particular, antibody 46.1 had robust brain uptake as well as accumulation in astrocytic end-feet and astrocytes following BBB transcytosis. This work broadens the possibilities for employing new antibodies as platforms to deliver therapeutics to the brain.

Supplementary Figures:

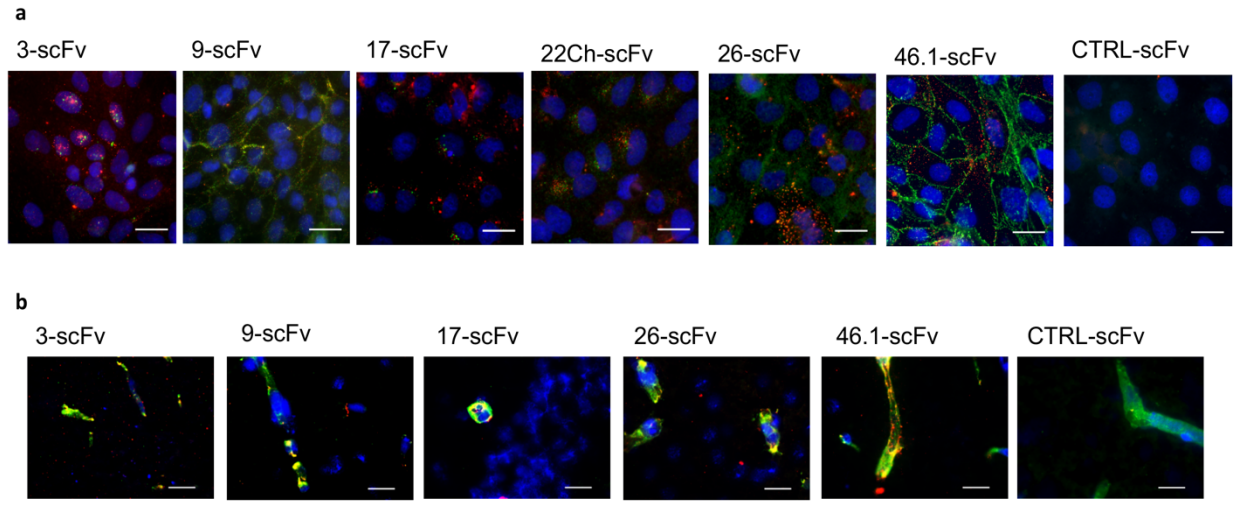

Figure 3.7 ScFvs-dimers bind to hBMECS and frozen mouse brain sections. a) ScFvs (13 µg/ml) were pre-dimerized with mouse anti-c-myc antibody in 4:1 molar ratio. hBMECs were incubated with scFv-dimers at 4°C and subsequently at 37°C for 30 min. The cell membrane was washed with cold buffer and the membrane bound fraction (red) labeled with anti-mouse AlexaFluor555 antibody on ice. After fixation and permeabilization the internalized scFv-dimers (green) were labeled with anti-mouse AlexaFluor488 antibody. b) ScFvs in pre-dimerized form (red) bind to brain vasculature, visualized with lectin (green), on mouse cryosections *ex vivo*. scFvs shown are clones. Example scFvs are shown. Scale bar, 20 µm.

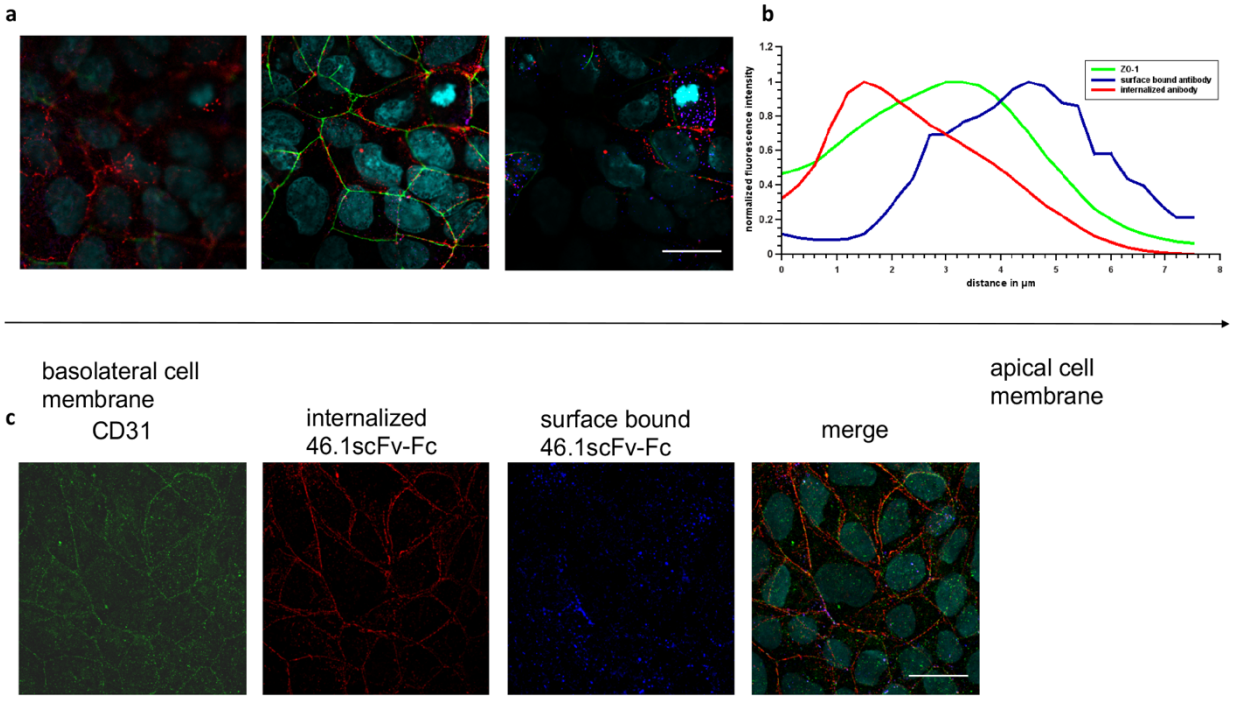

Figure 3.8 46.1 trafficking in vitro a) 46.1-scFv-Fc traffics to the basolateral membrane in hBMECs. 46.1scFv-Fc (5 µg/ml) was allowed to internalize in hBMECs. The localization of surface-associated antibody (blue) and endocytosed antibody (red) was determined with respect to the tight junction marker ZO-1 (green) and adherence junction marker CD31 (green). Upper left panel, confocal images from a z-stack spanning the hBMECs monolayer in basolateral to apical direction. The internalized antibody appears at the basolateral cell-cell contacts and diminishes in apical direction, where the cell surface bound antibody is visible. b) Upper right panel, normalized fluorescence intensity per channel plotted as a distance from the beginning (basal membrane) to the end (apical membrane) of the z-stack. Note, the shift of the peak intensity of internalized antibody to the left and of surface bound antibody to right with respect to ZO-1. 46.1-scFv-Fc traffics to the basolateral membrane in hBMECs. c) Lower panel, confocal images showing the internalized 46.1-scFv-Fc with respect to CD31. 46.1 scFv-Fc appears to repeat the CD31 expression pattern, with occasional colocalization. Scale bar, 20 µm.

Supplementary tables:

TEER (ohm-cm^2)	Total CFU (Brain Side)
182	3.8 x 10^7
201	4.2 x x10^7
482	3.9 x 10^5
712	1.24 x 10^3
1302	812
1905	205

Table 3-3. Nonspecific phage particle passage through the hBMEC monolayer as a function of model tightness as measured by TEER values. At high TEER the non-specific crossing of phage is minimal,

allowing the researcher to screen out nonspecific phage by low throughput techniques such as colony picking.

Selection round	Phage titer (cfu)*	Enrichment ratio
Round 1	3×10^7	3.75
Round 2	1×10^6	5
Round 3	2.5×10^7	12.5
Transcytosis round	220	-

Table 3-4 Phage titers in outputs and enrichment ratios after each panning round. Input in each round was 10^{11} CFU. * Phage titers represent outputs.

scFv sequences [a]	scFv sequence frequency [b]	scFv sequence count [c]	scFv sequence occurrence [%] [d]
1	84	84	38.2
1	58	58	26.4
1	15	15	6.8
1	6	6	2.7
1	3	3	1.4
3	2	6	2.7
48	1	48	21.8
56		**220**	**100%**

Table 3-5 Frequency of diverse scFv antibody sequences among 220 clones from transcytosis round. [a] Frequency of unique scFv antibody sequences [b] Numbers of different scFv sequences [c] Number of scFv sequences with respective sequence diversity [d] Sequence occurrence was calculated as percentage of sequence count. Here individual phage from the transcytosis round were sequenced and the unique sequences of displayed scFvs evaluated.

scFv sequences [a]	scFv sequence frequency [b]	scFv sequence count [c]	scFv sequence occurrence [%] [d]
1	17	17	17.7
1	9	9	9.4
2	4	8	8.3
2	2	4	4.2
59	1	59	61.4
65		**96**	**100**

Table 3-6 Frequency of diverse scFv antibody sequences among 96 clones following addition of soluble scFv clones 3 & 22Ch. [a] Frequency of unique scFv antibody sequences [b] Numbers of different scFv sequences [c] Number of scFv sequences with respective sequence diversity [d] Sequence occurrence was calculated as percentage of sequence count. Here individual phage from the transcytosis round with competition were sequenced and the unique sequences of displayed scFvs evaluated.

scFv sequences [a]	scFv sequence frequency [b]	scFv sequence count [c]	scFv sequence occurrence [%] [d]
1 (clone 3)	24	24	25
1 (clone 22Ch)	20	20	20.8
1	18	18	18.8
1	10	10	10.4
1	2	2	2.1
22	1	22	22.9
27		**96**	**100**

Table 3-7 Frequency of diverse scFv antibody sequences among 96 clones in control transcytosis screen. In bold are clones 3 and 22Ch. [a] Frequency of unique scFv antibody sequences [b] Numbers of different scFv sequences [c] Number of scFv sequences with respective sequence diversity [d] Sequence occurrence was calculated as percentage of sequence count. Here individual phage from the control transcytosis round without competition were sequenced and the unique sequences of displayed scFvs evaluated. This table can be directly compared to table 3.6 to highlight the lack of recovery of clones 3 and 22Ch in the competition screen's output.

Chapter 4 - Impacts of the -1 Amino Acid on Yeast Production of Protein-Intein Fusions

This chapter was adapted from: L. I. Goulatis, R. Ramanathan, and E.V. Shusta, "Impacts of the -1 Amino Acid on Yeast Production of Protein-Intein Fusions", Biotechnol. Prog, 2018. Optimization of a semi-synthetic site-specific antibody functionalization platform in yeast is described to serve as a first step in functionalizing our brain penetrating antibodies for further downstream *in vivo* evaluation and brain drug delivery.

4.1 INTRODUCTION

Custom chemical functionalization of antibodies can enable a variety of therapeutic and biochemical applications. For example, such modifications can facilitate protein immobilization[116,117], small molecule drug conjugation[118], conjugation to nanoparticles[119], and conjugation of imaging probes[120]. Site-specific modifications are often preferred in order to provide uniformly modified proteins and limit deleterious effects that can accompany non-specific conjugation approaches[121,122]. One approach for site-specific functionalization of proteins is expressed protein ligation (EPL)[123], where target proteins are fused to a non-self-cleaving intein such as Mxe GyrA[124–126]. Subsequently, intein-mediated protein splicing is activated by the addition of a thiol nucleophile that releases the target protein from the intein moiety while appending a reactive C-terminal thioester intermediate[127]. The thioester can subsequently react with an N-terminal cysteine derivative to form a native amine bond enabling the addition of numerous chemical functionalities[53]. Recently, we described using this approach to functionalize proteins produced in yeast[53]; however, protein fusion to the wild-type Mxe GyrA intein decreased production levels. To remedy the deleterious effects of the intein fusion, an evolved Mxe

GyrA intein named 202-08 was developed that enhanced the secretion levels of scFv-intein fusions to those of the unfused protein, and the resultant protein could be functionalized for downstream applications[51].

Since large quantities of functionalized protein are often desirable for a variety of applications, we sought to identify approaches to further elevate the yield of EPL-compatible proteins employing the 202-08 intein. One approach is to increase the intein cleavage efficiency as previous work indicated incomplete cleavage of Mxe GyrA fusion proteins[51]. Studies using bacterial production platforms have demonstrated that Mxe GyrA intein cleavage can be modulated by altering conditions such as pH and temperature[128–130]. Further, for EPL applications, a number of nucleophiles (such as thiophenol, DTT, or 2-mercaptoethansulfronic acid (MESNA)) have been evaluated for reactive thioester formation and protein splicing, with MESNA being one of the most efficient for EPL applications[127,131]. As an alternative approach, the identity of the last amino acid residue of the protein that is fused to the intein N-terminus (-1 residue) has also been shown to influence cleavage kinetics[127,132–135]. Various inteins have their own preference at this position, with certain residues associated with increased levels of off target cleavage *in vivo*, and other residues associated with total lack of cleavage[128,130,135]. Thus, in the current study, we explored the impact of the -1 residue in the cleavage and production properties of scFv-intein fusions. Substitution of -1 residue with each of the 20 naturally occurring amino acids was performed, and nucleophile-induced cleavage efficiency and scFv-intein secretion levels were evaluated for a number of proteins. We identified two amino acids at the -1 position that offer the most robust scFv cleavage upon addition of MESNA while also resulting in the highest scFv-intein titers, thereby facilitating

applications requiring protein functionalization.

4.2 MATERIALS AND METHODS

4.2.1 Yeast Strains, and Plasmids

Saccharomyces cerevisiae strain YVH10[136] (MATα PDI1::GAPDHPDI1::LEU2 ura3−52 trp1 leu2Δ1 his3Δ200 pep4::HIS3 prb1Δ1.6R can1 GAL) was used for protein secretion. The engineered Mxe GyrA intein-fused pRS316-FLAG-202-08 vector[51] was used as a backbone for protein secretion and plasmid mutagenesis, with the original vecotor having Gly preceding the intein (at the -1 position). Gly (-1) was mutated to 19 other amino acids by site directed mutagenesis (Q5 site directed mutagenesis kit, NEB) and primers designed by the Q5 NEB software. scFv2224, scFvH7, scFv4-4-20, and GFP were subcloned to appropriate pRS316-FLAG-202-08 vectors from pCT4Re plasmids generated in a previous study[53].

4.2.2 Yeast Growth and Induction

Yeast were transformed using the LiAc/ssDNA/PEG method[137]. YVH10 transformants were selected on leucine and uracil deficient SD-2XSCAA + Trp agar plates (20 g/L dextrose, 6.7 g/L yeast nitrogen base, 10.19 g/L Na2HPO4·7H2O, 8.56 g/L NaH2HPO4·H2O, 15 g/L agar 190 mg/L Arg, 108 mg/L Met, 52 mg/L Tyr, 290 mg/L Ile, 440 mg/L Lys, 200 mg/L Phe, 1260 mg/L Glu, 400 mg/L Asp, 480 mg/L Val, 220 mg/L Thr, 130 mg/L Gly, and 40 mg/L Trp, lacking leucine and uracil). YHV10 was grown in SD-2XSCAA + Trp (20 g/L dextrose, 6.7 g/L yeast nitrogenous base, 10.19 g/L Na2HPO4·7H2O, 8.56 g/L NaH2HPO4·H2O, 190 mg/L Arg, 108 mg/L Met, 52 mg/L Tyr, 290 mg/L Ile, 440 mg/L Lys, 200 mg/L Phe, 1260 mg/L Glu, 400 mg/L Asp, 480 mg/L Val, 220 mg/L Thr, 130 mg/L Gly, and 40 mg/L Trp, lacking leucine and uracil) at 30 ^{o}C,260 rpm overnight. The following day, cultures were reset to OD_{600} =0.1, and grown for 72 h at 30 ^{o}C,260 rpm. Yeast were induced by replacing the media with an equivalent volume

of SG-2XSCAA + Trp (20g/L galactose replacing dextrose) containing 0.1% w/v bovine serum albumin (BSA) and culturing the cells for 72 h at 20 ^{o}C, 260 rpm. Where noted, after induction yeast were refed at 24 h and 48 h with 0.1X of respective culture volume of 10X solution of yeast nitrogen base and amino acids (67 g/L yeast nitrogenous base, 1900 mg/L Arg, 1080 mg/L Met, 520 mg/L Tyr, 2900 mg/L Ile, 4400 mg/L Lys, 2000 mg/L Phe, 12600 mg/L Glu, 4000 mg/L Asp, 4800 mg/L Val, 2200 mg/L Thr, 1300 mg/L Gly, and 400 mg/L Trp, lacking leucine and uracil).

4.2.4 SDS-PAGE and Western Blotting

Yeast culture supernatants were collected and denatured by boiling in LDS sample buffer (Life Technologies) containing 1mM 2-mercaptoethanol for 10 min prior to resolution on a 4-12% Bis-Tris gel (Life Technologies). Under these reducing conditions, no intein cleavage reaction is observed (e.g Figure 4.2B with Gly and Ala as -1 residues and Figure 4.5B with Phe and Gln as -1 residues). Proteins were then transferred to a nitrocellulose membrane for western blot analysis. Detection of FLAG tagged proteins was performed with an anti-FLAG M2 mouse monoclonal antibody (Sigma-Aldrich, 1:3000 dilution), followed by an anti-mouse HRP conjugate (Sigma-Aldrich, 1:2000 dilution). Detection of biotinylated proteins was performed with an anti-biotin mouse monoclonal antibody Ab-2 clone BTN.4 (Lab Vision Corporation, 1:500 dilution) followed by an anti-mouse HRP conjugate. Clarity Western ECL Substrate (Bio-Rad) was used to develop the membranes and imaging was performed with the ChemieDoc XRS+ system (Bio-Rad). Protein band quantification was performed with the Image Lab Software (Bio-Rad). Intein cleavage efficiency was calculated as the ratio of cleaved protein to total protein (cleaved plus uncleaved fusions) following western blot densitometry. Per cell

protein-intein fusion secretion levels were determined by western blot quantification and normalization to sample culture density, OD_{600nm}.

4.2.5 Intein-Mediated Release and EPL

The ability to release the scFv and GFP from secreted intein fusions was performed as described previously[51]. Briefly, 1M mercaptoethanesulfonic acid (MESNA, Sigma-Aldrich) was added to scFv- or GFP- containing supernatants or purified protein to a final concentration of 100mM and the reaction was allowed to proceed for 20 h at RT prior to anti-FLAG western blot analysis. For glutathione (GSH) induced cleavage, 30μM or 10mM of reduced GSH was used for 20 h at room temperature at pH 6 in order to keep glutathione reduced and pH conditions similar to that of culture supernatants. To generate biotin functionalized proteins through expressed protein ligation (EPL) 1mM of a biotinylated cysteine peptide (BioP1 synthesized by the University of Wisconsin Biotechnology Center, Sequence: NH2-CDPEK(Bt)DS-CONH2)[53] was added along with MESNA and the reaction was allowed to proceed for 20 h prior to anti-biotin Western Blot.

4.2.6 Protein Purification

After 72 h of growth in SG-2XSCAA + Trp at 20 ^{o}C, the yeast supernatant containing the secreted proteins (Phe and Gln fusions at 24 hours and 4-4-20, H7, 2224, and GFP fusions at 72 hours for EPL reactions) were collected by centrifugation and dialyzed against Tris-buffered saline (TBS, 25 mM Tris, 150 mM NaCl, 2 mM KCl, pH 7.9). Ni-NTA Superflow resin (Qiagen) was equilibrated with 10 mL of bind buffer (TBS with 5mM imidazole) prior to loading the dialyzed yeast supernatant. The column was subsequently washed with 5X resin volume of bind buffer, followed by 5X wash with wash buffer (TBS with 20mM imidazole). Proteins were eluted with 1X resin volume of elution

buffer (TBS with 250mM imidazole).

4.2.7 Total Glutathione assay

Supernatant total glutathione (GSH + 2XGSSG) levels were measured with a glutathione colorimetric detection kit (ThermoFisher Scientific). Briefly, standard curves are generated by combination of glutathione standards, NADPH, and detection reagent concentrate followed by incubation with glutathione reductase. The assay was linear in the range of 0.5 – 12.5 μM GSH / GSSG. Supernatant samples were diluted to fall in the assay's linear range, and total glutathione levels were calculated by comparison to standard curves. Assays were performed in triplicate on each time point and triplicate cultures of each condition were studied.

4.2.8 Intracellular Protein Assay

For the preparation of protein extracts, a modified glass bead lysis protocol was used[138]. Briefly, cells were collected, washed once with phosphate buffered saline (PBS), and resuspended in disruption buffer (20mM TRIS-CL (pH 9), 0.02mM EDTA, complete EDTA free protease inhibitors (Roche), and 50mM ammonium sulfate) with equal volume of 20% trichloroacetic acid (TCA). Cells were lysed by agitation with 200 μL of zirconium oxide beads in two 50 sec pulses separated by centrifugation, and washed twice with 1:1 TCA buffer:TCA mix. The precipitate was then collected and boiled in resuspension buffer (2% sodium dodecyl sulfate (SDS), 20mM TRIS – CL) for 5 min. The resuspended supernatant was then resolved in SDS-PAGE and assayed via anti-FLAG western blot.

4.3 RESULTS

4.3.1 Effects of the -1 residue on intein cleavage

The protein-intein fusion expression vector has been previously described[51]. In this system, an anti-fluorescein scFv (4-4-20) was employed as the fusion partner to the engineered 202-08 intein. The scFv is flanked by a synthetic PrePro leader sequence, N-terminal FLAG and C-terminal c-*myc* tags that allow for detection and a hexahistidine tag used for nickel affinity purification (Figure 4.1A). In the present study, each of the 20 naturally occurring amino acids were cloned immediately preceding the 202-08 intein at the -1 position to determine preferred -1 residues for production and thiol-induced cleavage (Figure 4.1A). The 202-08 intein undergoes an N- to S-acyl shift at its N-terminal cysteine forming a thioester intermediate susceptible to nucleophilic attach. Upon reaction with the sulfur nucleophile MESNA, the protein, scFv 4-4-20, is cleaved from the intein and a reactive thioester is formed at the C-terminus of the released protein (Figure 4.1B)[51,53]. The secreted product can then be assayed with an anti-FLAG tag western blot to identify the fraction of produced protein that has undergone successful cleavage. Since intein cleavage efficiency and specificity is often difficult to predict[139–141], and mutations to the Mxe GyrA intein can potentially affect intein cleavage activity[139,142,143], the effects of -1 residue substitution were also screened for the presence of undesirable cleavage events that occur in the absence of MESNA (termed autocleavage). These could occur within the yeast secretory pathway or in the culture medium. To this end, many amino acids at the -1 position resulted in significant (>40%) levels of autocleavage (Figure 4.2A). Of those residues leading to measurable autocleavage, addition of MESNA yielded increased cleaved product for only Val and Phe at the -1 position (Figure 4.2A and 4.2B). Of those -1 residues without appreciable autocleavage, Pro also resulted in inhibition of

MESNA induced cleavage, as previously observed[127] and Thr also exhibited no MESNA induced cleavage. Met, Cys and Ser, while not resulting in autocleavage, had limited (<20%) MESNA cleavage, and were not pursued further. By contrast, when Ala and Gly were used at the -1 position, MESNA-induced cleavage was about 65%, with no detectable autocleavage product, representing the best -1 residues from the initial screen. Importantly autocleaved product for the -1 residues teste (Phe, Gln, and Leu), while lacking the intein, was not endowed with the desirable thioester generated by MESNA reaction, and therefore could not be subsequently functionalized (supplementary Figure 4.7). Given the deleterious autocleavage behavior of certain -1 residues, we sought to identify whether the observed autocleavage starts within the cell during secretory processing or once exported to the culture supernatant. Analysis of a representative subset of -1 residues indicated that autocleavage of Gln, Leu and Phe was observed in intracellular samples; whereas Ser, Ala and Gly did not yield intracellular cleavage product (Figure 4.2C). Finally, for -1 residues Ile or Asn, no target protein, fused or cleaved, was detected in the secreted supernatant. Examination of the intracellular content indicated that 4-4-20 intein fusions with Ile at the -1 position were trapped intracellularly with a considerable portion of the protein running as higher molecular weight aggregates; whereas, fusions with Asn in the -1 position were not detected (Figure 4.1C).

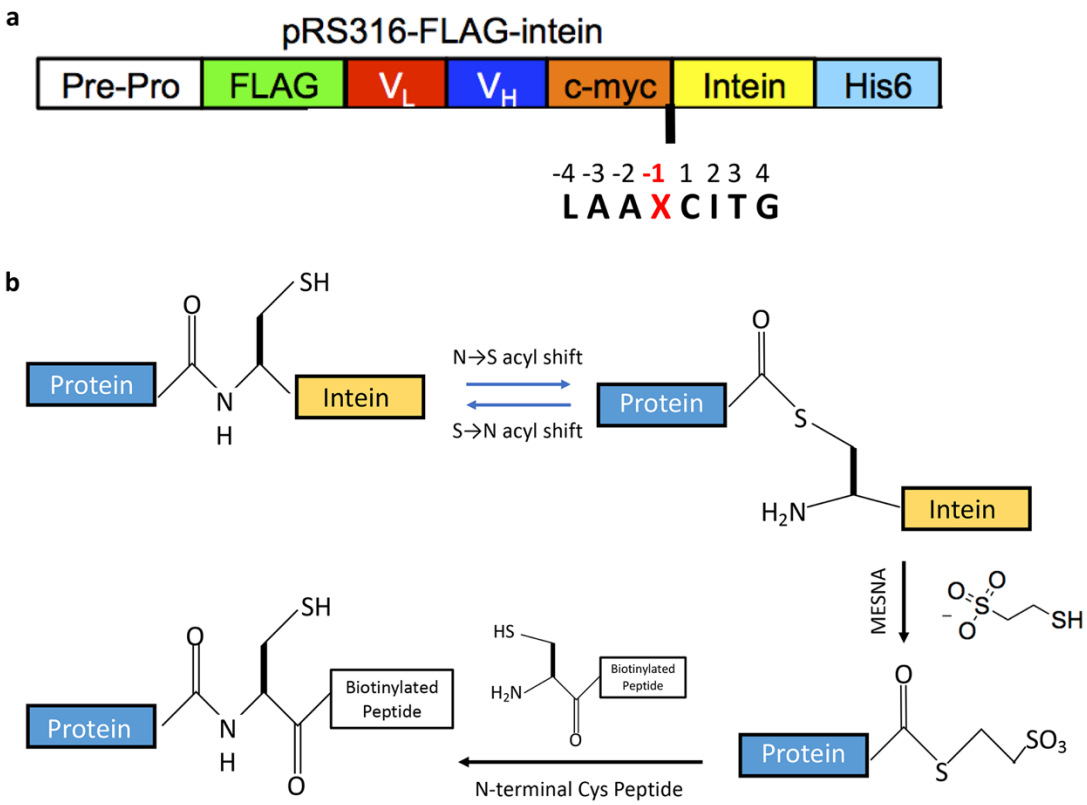

Figure 4.1 Protein-intein fusion secretion construct (a) pRS316-FLAG-intein contains a synthetic PrePro leader sequence directing secretion of an scFv (VL-VH) or GFP. The amino acid sequence upstream of the N-terminal cleavage site of the evolved 202-08 intein, as well as the first intein amino acids are shown. The -1 residue (X) was substituted for all 20 naturally occurring amino acids. (b) EPL can be used to install chemical entities onto the carboxy-terminus of intein fused proteins. The intein catalyzes a reversible N- to S- acyl shift between the target protein and the intein. This exposes a thioester at the carboxy-terminus of the target protein that is susceptible to attack by a nucleophile. Commonly used nucleophiles, such as thiol-based reagents then react to release the intein and install a carboxy-terminal thioester on the target protein.

4.3.2 Engineering of 202-08 responsible for autocleavage

While certain amino acids at the -1 position preceding the wild-type Mxe GyrA intein are known to either abolish cleavage altogether (Pro), or autocleave (Asp) in bacterial systems, as well as in native chemical ligation[127], the significant autocleavage observed for many amino acids at the -1 positon was somewhat unexpected. Thus, the autocleavage of the evolved 202-08 intein was compared with the wild-type Mxe GyrA intein. Gly, Phe, and Gln were chosen as -1 residues since they spanned the range from

no autocleavage (Gly), to high autocleavage (Gln). The wild-type intein demonstrated significantly less autocleavage than the 202-08 intein for these -1 residues, with no autocleavage for Phe as -1 residue, while the autocleavage for Gln was 3-fold lower than that for 202-08 intein (Figure 4.3A). However, despite the lack of autocleavage when using the wild-type intein, secretion levels were 10-30-fold lower for the three -1 aa tested compared to the evolved 202-08 intein having Gly as the -1 residue (Figure 4.3B and Ref. [51]). As engineering Mxe GyrA inteins can lead to altered cleavage function[143], we sought to establish that the self-splicing function of the intein itself was responsible for the observed autocleavage behavior. Mutation of the Cys residue residing at the N-terminus of the 202-08 intein (Figure 4.1A), a critical residue for catalytic function[144], to alanine (C1A), resulted in a complete elimination of either MESNA-induced cleavage or autocleavage as no cleaved product was observed even after MESNA treatment (Figure 4.3C). These combined results indicate that the evolution of the 202-08 intein exacerbates the autocleavage effects endowed by the -1 residue. However, expression levels are substantially enhanced by the 202-08 intein compared to the wild-type intein, and when put in combination with a residue like Gly, which has no autocleavage, the 202-08 intein is preferable.

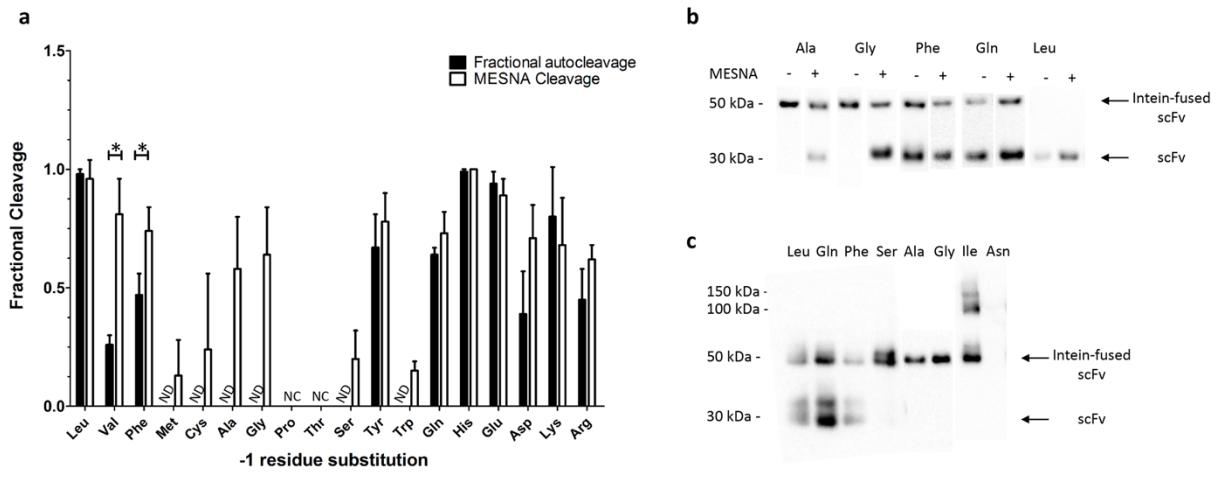

Figure 4.2 Effect of the -1 amino acid on fusion protein cleavage. (a) Autocleavage and MESNA-induced cleavage of secreted 4-4-20-intein fusions in supernatants after 72 h of induction was evaluated with quantitative anti-FLAG Western blot. 4-4-20-intein fusions were not detected in the supernatant when Ile and Asn were used as -1 residues and thus, these were not included on the plot. Plotted on the graph are the mean ±SD for n=3 independent yeast transformants. Statistical significance was determined by an unpaired Student's t-test (*$p<0.05$). ND=autocleavage not detected, NC=No autocleavage or MESNA cleavage detected. (b) Sample Western blots of supernatants with or without MESNA treatment, probed with an anti-FLAG antibody. Such data were quantified to produce the bar graph in panel (a). (c) Yeast expressing 4-4-20-intein fusions were lysed to evaluate intracellular intein fused and autocleaved scFv. Ile as -1 residue also displayed high molecular weight aggregates in addition to full size intein fusion protein, while Asn resulted in very little, if any, detectable protein production.

4.3.4 Refeeding limits autocleavage and increases yield

To further examine the autocleavage timecourse and explore potential remedies, we examined the autocleavage of proteins spanning 24-72 hours of induction. While secreted proteins with Phe and Gln as the -1 residues did not have appreciable autocleavage at less than 24 h of induction (Supplemental Figure 4.7), autocleavage increased at 48 and 72 h (Figure 5.4A). By contrast, Leu as the -1 residue was found autocleaved at each time point (Supplemental Figure 4.8 and Figure 4.4A). Since the autocleavage events were linked to the catalytic activity of the intein, we explored the possibility that an endogenous thiol nucleophile could be impacting the autocleavage process. In particular, it has been shown that yeast excrete small thiols such as glutathione upon heterologous expression of proteins[145]. In principle, it could be possible

for reduced glutathione to act as a nucleophile to cleave the intein, appending a short-lived thioester that is not compatible with EPL functionalization. Thus, the excretion of glutathione during scFv-intein fusion expression was explored. Indeed, total glutathione excretion was enhanced as a function of secretion time (Figure 4.5A). However, similar total glutathione levels were produced for constructs having -1 residues with low (Gly), intermediate (Phe) and high autocleavage levels (Gln, Leu) (Figure 4.5A). Addition of reduced glutathione (GSH) to purified scFv-intein fusions with Glu or Phe at the -1 positions, at concentrations similar to those found for total glutathione in the yeast supernatants (30 μM) did not lead to any detectable intein cleavage (Figure 4.5B). However, in the yeast secretion machinery where intracellular autocleavage occurs, total glutathione levels are in the millimolar range with GSH:GSSG ratios of 3:1[146]. When fusion proteins with autocleavage susceptible -1 residues were incubated in a 10 mM GSH, Gln but not Phe exhibited detectable autocleavage (Figure 4.5B). By comparison, MESNA drove much more substantial intein cleavage (Figure 4.5B). Thus, extracellular glutathione does not appear to be driving the autocleavage process, but intracellular GSH may play a role in promoting the observed autocleavage.

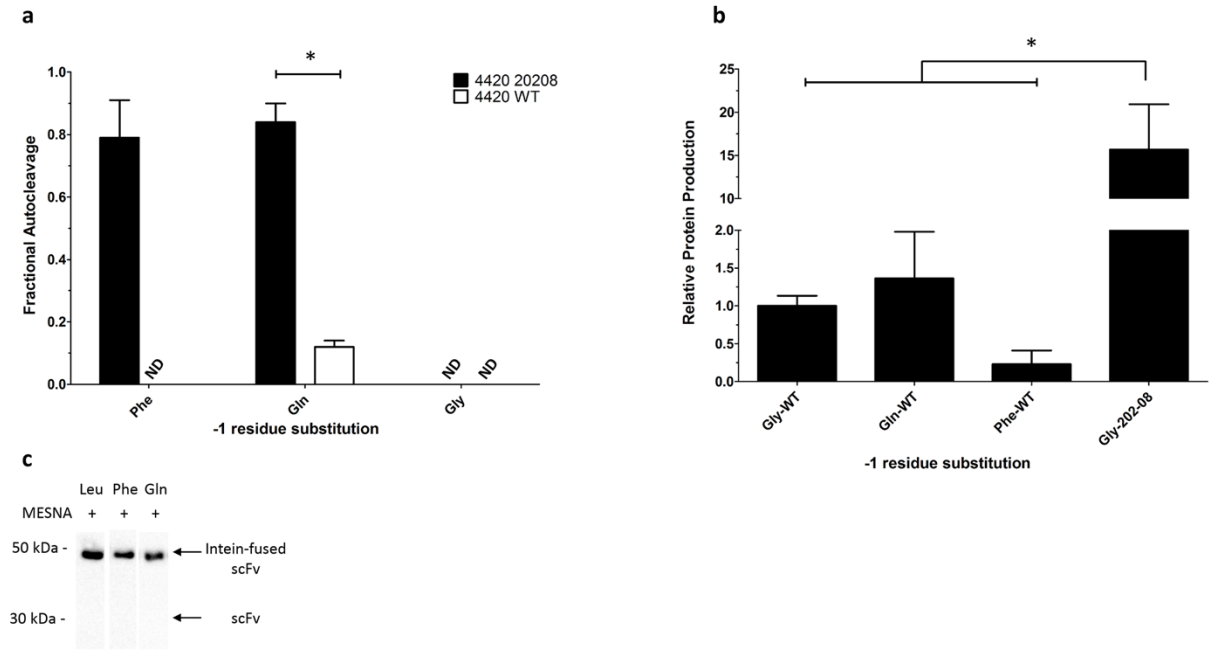

Figure 4.3 Effects of intein evolution on cleavage behavior and protein production. (a) Autocleavage for 202-08 and wild-type (WT) Mxe GyrA intein with Phe, Gly and Gln as -1 residues was evaluated in culture supernatant at 72 h with quantitative anti-FLAG Western blot. Plotted on the graph are the mean ±SD of n=3 independent yeast transformants. Statistical significance was determined by an unpaired Student's t-test (*p<0.05). ND= autocleavage not detected. (b) Protein secretion levels of selected -1 residues of wild-type Mxe GyrA and 202-08 intein. Supernatants at 72 h were quantified using anti-FLAG Western blotting and normalized to the Gly-WT secretion level. Plotted are the total relative per cell secretion levels that combine both the intact and cleaved fusions. Plotted on the graph are the mean ±SD of n=3 independent yeast transformants. Statistical significance was determined by an unpaired Student's t-test (*p<0.05). (c) Lack of cleavage of C1A 202-08 intein mutants upon addition of MESNA in 72 h supernatant was evaluated through an anti-FLAG tag Western blot.

Depletion of nitrogen base and amino acids has been linked to post-secretory protein loss in yeast protein secretion studies, and refeeding of yeast nitrogen base and casamino acids both restored culture pH values and limited protein loss[147–149]. Thus, we sought to investigate the effects of refeeding on intein autocleavage, glutathione production and total protein yield. Refeeding with fresh nitrogen base and casamino acids at 24 and 48 h post-induction reduced autocleavage when Phe and Gln were the -1 residues, while refeeding did not affect autocleavage when Leu was the -1 residue where complete autocleavage was observed with or without refeeding (Figure 4.4A). In addition, although total glutathione levels were generally lowered by refeeding, this did not limit the

complete autocleavage of Leu containing fusions (Figure 4.4A). While refeeding had modest effects on limiting autocleavage, it did increase total protein production across all -1 residues tested from 1.5-4-fold (Figure 4.4B) with Gly fusions producing at ~2.5 mg/L titers.

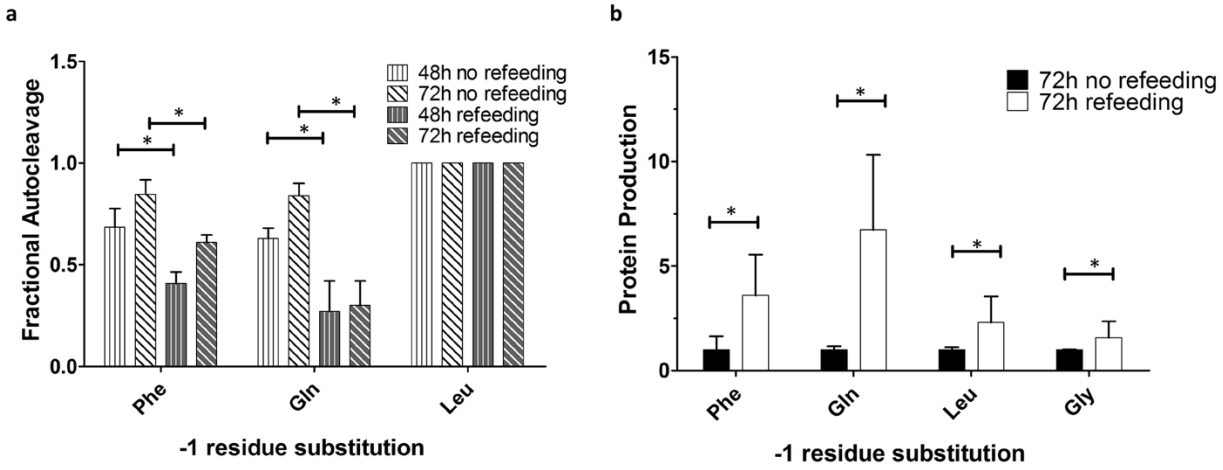

Figure 4.4 Effects of refeeding on intein autocleavage (a) Intein autocleavage at 48 and 72 h post induction with or without refeeding for selected -1 residues was evaluated in culture supernatants. Plotted are the mean ±SD of n=3 independent yeast transformants. Statistical significance was determined by an unpaired Student's t-test (*p<0.05). (b) Protein secretion levels of selected -1 residues with or without refeeding at 72 h post induction. Plotted are the relative per cell secretion levels that combine both the intact and cleaved fusions. Levels are also normalized to no refeeding conditions for each -1 residue. Plotted on the graph are the mean ±SD of n=3 independent yeast transformants. Statistical significance was determined by an unpaired Student's t-test (*p<0.05).

4.3.5 Alanine and Glycine are the preferred -1 residues

Since Gly and Ala performed the best as -1 residues in terms of having undetectable autocleavage and high MESNA cleavage yield, they were tested on multiple protein fusion partners using the refeeding production strategy to test generalizability. Three scFvs (anti-transferrin receptor scFvH7, anti-epidermal growth factor receptor scFv 2224, and 4-4-20) and green fluorescent protein (GFP) were produced as fusions to the 202-08 intein and secretion levels quantified. Secretion of 4-4-20 and GFP intein fusions exhibiting modest but statistically significant increases in secretion when Ala was used as

the -1 residue (Figure 4.6A). For H7 and 2224 fusions, the use of Gly and Ala as -1 residues yielded indistinguishable secretion levels. None of the assayed protein-intein fusions showed measurable autocleavage. Finally, protein fusions with the 202-08 intein and Gly as the -1 residue have been assessed for cleavage efficiency and EPL compatibility since the initial evolved 202-08 fusion construct fortuitously possessed Gly as the -1 residue[51].

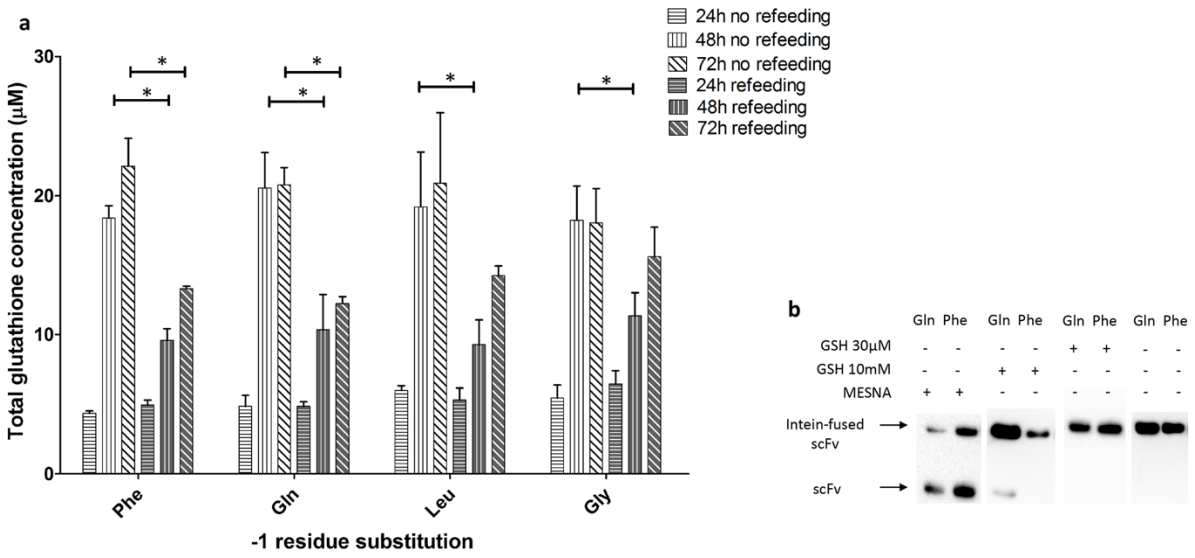

Figure 4.5 Excreted glutathione and effects on intein cleavage. (a) Total supernatant glutathione concentration (GSH + 2×GSSG) for selected -1 residues from 24-72 h post induction were measured with and without refeeding. Plotted on the graph are the mean ±SD of n=3 independent yeast transformants. Statistical significance was determined by an unpaired Student's t-test (*p<0.05). (b) The ability of glutathione to induce intein cleavage for Phe and Gln -1 residues was assessed by reacting purified 4-4-20-intein fusions with reduced glutathione at either 30 μM or 10 mM concentrations. It is worth noting that less than 24 h post induction both Phe and Gln -1 residue constructs do not exhibit substantial autocleavage but are secreted in low amounts necessitating purification and concentration steps before use. To verify that secreted fusion proteins were responsive to thiol-induced cleavage, they were also reacted with MESNA.

Thus, we similarly evaluated -1 Ala fusions in a full EPL setting. Upon addition of MESNA (Figure 4.6B), cleavage efficiencies were 0.60±0.24, 0.69±0.24, 0.34±0.15 and 0.35±0.06 for 4-4-20, H7, GFP, and 2224 fusion partners, respectively. Finally, protein-intein fusions with Ala at the -1 position were functionalized to demonstrate compatibility with all steps of EPL. The secreted and purified scFv- and GFP- 202-08 intein fusion proteins were reacted with MESNA in the presence of a biotinylated peptide bearing an N-terminal

cysteine[51]; thereby, releasing the scFv or GFP from the intein and installing a C-terminal biotin onto the protein (Figure 4.1B). Each of the scFvs and GFP were successfully modified with biotin (Figure 4.6C). Taken together, Gly and Ala constitute the optimal candidates as -1 residues for maximizing protein secretion of EPL-compatible fusions.

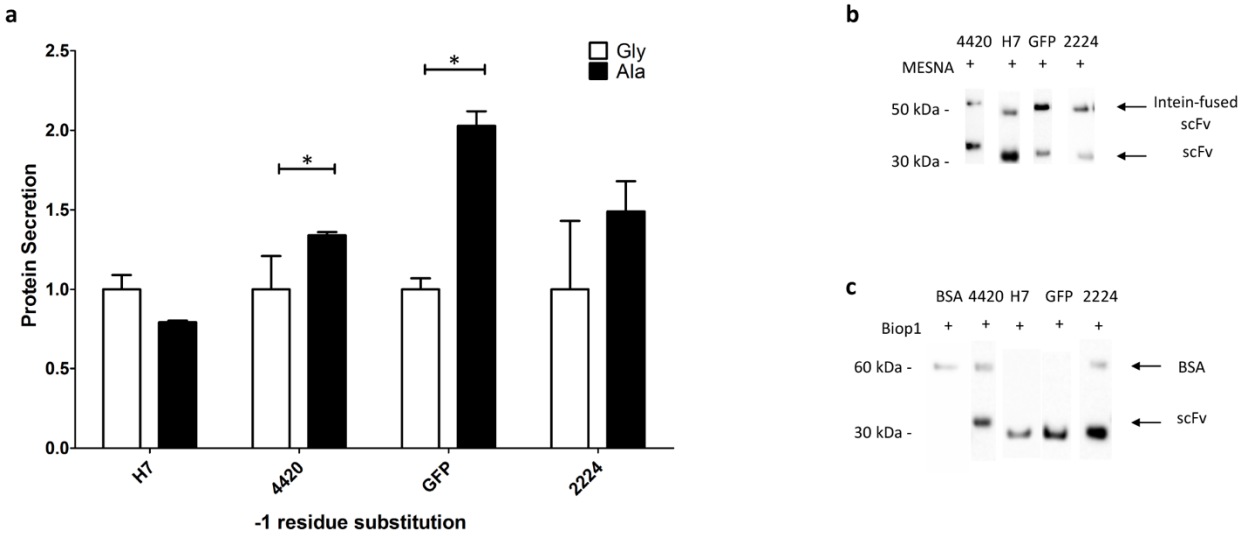

Figure 4.6 Production of protein-intein fusions with Gly and Ala as the -1 residue. (a) Comparison of the protein secretion levels of three scFvs (4-4-20, H7, 2224) and GFP with Gly or Ala as -1 residues in supernatants at 72 h. Amount of secreted full-length intein fusion were normalized to the Gly construct for each fusion partner. Plotted are the mean $\pm$SD of n$\geq$3 independent yeast transformants. Statistical significance was determined by an unpaired Student's t-test (*p<0.05). (b) MESNA induced cleavage for protein-intein fusions with Ala in the -1 position was evaluated with anti-FLAG Western blot in supernatants at 72 h. Quantitative cleavage percentages ± SD from 3 independent yeast transformants can be found in the text. (c) Purified fusions were subjected to a complete EPL reaction with Biop1 peptide and evaluated with anti-biotin Western blot to examine biotinylation of the target protein. There exists a background band in some lanes at ~60kDa due to the presence of BSA, included in the reaction to prevent adsorption and loss of the target protein.

4.4 Discussion

The -1 amino acid at the N-terminus of an intein has been shown to be critical in

regulating intein cleavage and splicing efficiencies[127]. In this study, we evaluated the effects of the -1 residue on the cleavage efficiency and protein yields of the evolved 202-08 Mxe GyrA intein. The importance of the -1 residue was clearly demonstrated as this single amino acid change could lead to either significant autocleavage effects, or low thiol-induced cleavage efficiency abolishing the ability to perform EPL. In addition, amino acid changes at the -1 position could also substantially affect protein production levels by eliminating fusion production. Two candidate amino acids, Gly and Ala, performed the best with no detectable autocleavage, effective thiol-induced cleavage, and elevated protein expression yields across multiple protein-intein fusion constructs.

When using the evolved 202-08 intein that was optimized for yeast surface display and secretion[51], the effects of the -1 residue on autocleavage differed substantially from those seen using the wild-type Mxe GyrA intein in bacteria[135] or Npu^N mammalian production systems[150]. For instance, Leu had high (>70%) autocleavage, contrary to bacterial expression where limited (<10%) autocleavage was observed. Moreover, in the case of -1 residues that are known to lead to increased autocleavage such as Tyr and Glu[151], the evolved 202-08 intein had even higher autocleavage. Asn is associated with high autocleavage in bacteria (Mxe GyrA intein) and in HEK cells (Npu intein) but fusion protein was not detected in the yeast secretion system, likely indicating a production defect. The autocleavage products evaluated in this study were not capable of EPL, likely because they lacked an appropriate C-terminal thioester. Given the observed autocleavage behavior of 202-08 intein, the impacts of two -1 residues that drove autocleavage, Phe and Gln, were also investigated in the context of the wild-type Mxe GyrA intein. Interestingly, no autocleavage was observed when the -1 residue was

mutated to Phe and more limited autocleavage was observed for Gln. It has previously been reported that engineering inteins for a particular property can lead to unexpected changes in cleavage efficiency and behavior[139,143], therefore it is possible that the engineering of 202-08 for increased secretion led to a more promiscuous cleavage behavior. Although autocleavage was limited when using the wild-type intein compared with the 202-08 intein, total secretion levels of the protein-intein fusion were considerably lower for the wild-type intein, similar to values reported previously[51]. Importantly, Gly and Ala at the -1 position did not exhibit autocleavage and combined with the elevated expression levels driven by the 202-08 intein, represent the optimal approach for protein-intein fusion expression in yeast. Indeed, Gly or Ala as the -1 residue were shown to be compatible with a number of scFvs and GFP, having undetectable autocleavage, reasonably high (~50%) thiol-induced cleavage yields and EPL reaction compatibility.

Substitution of the critical Cys residue that allows the N-S acyl shift required for thiol-based cleavage completely abolished both autocleavage and thiol-induced cleavage, indicating that the intein function was critical for the autocleavage behavior. In addition, autocleavage clearly started in the yeast secretory pathway. These findings suggested the possibility of thiol-induced cleavage by an endogenous yeast substrate. In addition, millimolar concentrations of glutathione are present in the yeast secretory pathway, and during protein secretion from yeast, it has been observed that levels of glutathione are also elevated in the culture supernatant[145]. We also observed that total glutathione was elevated as a function of protein secretion time. While reduced glutathione concentrations relevant to supernatant glutathione levels (GSH at 30μM) were not sufficient to drive cleavage of intein fusions, fusions treated with concentrations more

relevant to secretory pathway conditions (GSH at 10mM), resulted in limited intein cleavage, suggesting that the thiols in the secretory pathway may play a role in autocleavage.

In an effort to limit detrimental autocleavage and increase secretion titer, we investigated the effects of nutrient refeeding. Depletion of nitrogen base and amino acids has previously shown to lead to protein loss[147,152], and change in culture pH[148], and supplementation reversed these effects leading to gains in secretion titer. Supplemental addition of nitrogen base and casamino acids reduced but did not eliminate autocleavage for a number of -1 residues. In addition, we observed a drop in excreted total glutathione levels; and thus, refeeding may reduce the chemical species, glutathione and others, that are responsible for intein autocleavage. While the entire compliment of yeast factors that drive autocleavage effects is unclear, Gly and Ala can circumvent these issues and facilitate the intended downstream EPL applications. Finally, refeeding also resulted in increased absolute protein-intein fusion yields from 1.5 to 5-fold, for the -1 residues tested. In conclusion, when employing the yeast protein-intein fusion system described here, the 202-08 intein requires a -1 residue of Gly or Ala to minimize autocleavage and maximize production of EPL functionalizable protein for downstream applications.

Supplementary Figures:

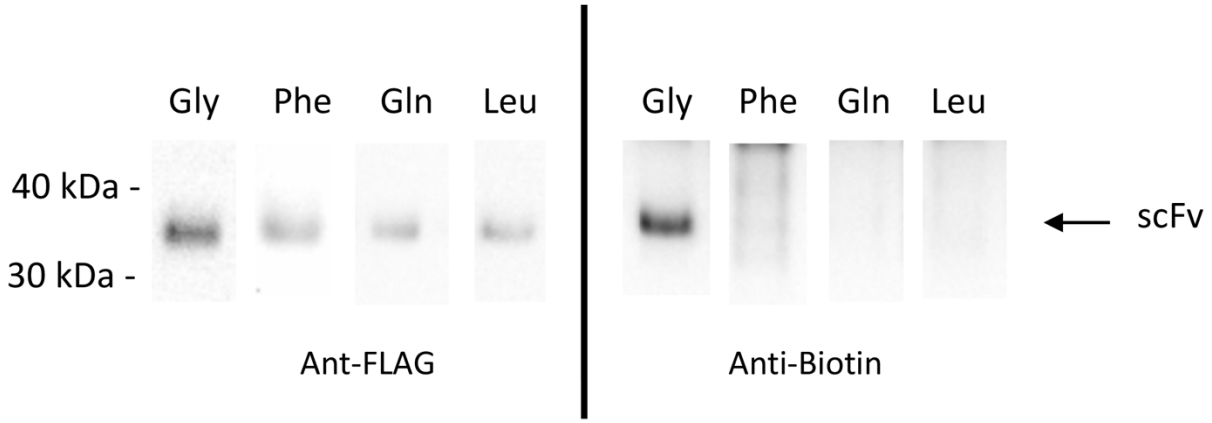

Figure 4.7 Autocleaved protein EPL capacity. The capacity to functionalize autocleaved scFvs was assayed by anti-Flag and anti-Biotin Western blots of 4-4-20–202-08 fusions that were subject to the EPL reaction with a N-terminal cysteine biotinylated peptide. The presence of autocleaved protein is shown in an anti-FLAG tag Western blot. No biotinylated product was detected.

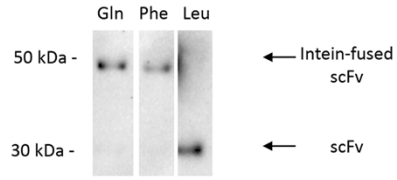

Figure 4.8 Supernatant autocleavage evaluated with anti-FLAG Western blot at 24 h of induction for selected -1 residues. The absence of cleaved 30 kDa 4-4-20 scFv for Gln and Phe, indicates that at this

time point, minimal autocleavage is observed. Leu is included as a comparison where autocleavage is observed at 24 h of induction.

Supplementary table:

Supplemental Table 1 - Data plotted in Figure 2a		
-1 residue substitution	**Fractional Autocleavage**	**MESNA Cleavage**
	Average ± S.D	Average ± S.D
Leu	0.98 ± 0.02	0.96 ± 0.08
Val	0.26 ± 0.04	0.81 ± 0.15
Phe	0.47 ± 0.09	0.74 ± 0.10
Met	0.00	0.13 ± 0.15
Cys	0.00	0.24 ± 0.32
Ala	0.00	0.58 ± 0.22
Gly	0.00	0.64 ± 0.20
Pro	0.00	0.00
Thr	0.00	0.00
Ser	0.00	0.20 ± 0.12
Tyr	0.67 ± 0.14	0.78 ± 0.12
Trp	0.00	0.15 ± 0.04
Gln	0.64 ± 0.03	0.73 ± 0.09
His	0.99 ± 0.01	1.00
Glu	0.94 ± 0.05	0.89 ± 0.07
Asp	0.39 ± 0.18	0.71 ± 0.14
Lys	0.80 ± 0.21	0.68 ± 0.20
Arg	0.45 ± 0.13	0.62 ± 0.06

Table 4-1 Cleavage of -1 residues

Chapter 5 - Brain penetrating antibody functionalization

As described in Chapter 3, a cohort of brain penetrating antibodies was discovered through panning naïve antibody libraries on a human model of the blood-brain barrier. Chapter 4 contained an investigation aimed to optimize semi-synthetic antibody functionalization through an antibody-intein fusion secreted in yeast. As introduced in Chapter 2, the state-of-the-art methods of drug delivery to the brain involve functionalization of antibodies, or conjugation to particles that contain the therapeutic payload. This brief communication will focus on our first efforts to integrate our brain penetrating antibodies with the intein-mediated functionalization platform and discuss future uses as drug delivery vectors.

I would like to acknowledge Dr. Benjamin Umlauf for providing the initial vectors for the mammalian antibody-intein fusion secretion.

5.1 Introduction

Antibody mediated drug delivery across the BBB has long been researched in academic and industrial settings [21]. Antibodies aimed to penetrate the BBB are used as either fusions to enzymes [153,154], bispecifics [155], or as targeting ligands coating nanoparticles [94,156]. In the case of potent active pharmaceutical ingredients it is possible to employ current antibody-based delivery methods to achieve sufficient brain drug concentrations to observe a pharmacological effect [157]. However, if the active molecule has high toxicity, high cost, or low potency, a higher flux brain penetrating vector is necessary. To this end, we advanced our brain penetrating antibodies into a functionalization platform to take advantage of the apparent high capacity of these

molecules for brain transport.

In order to combine antibodies with functional molecules such as drugs [158], polymers [159], other proteins [160], and nanoparticles [161] it is necessary to employ chemical conjugation approaches. Antibody-drug conjugates (ADCs) are a novel therapeutic paradigm and are comprised of a monoclonal antibody conjugated through a chemical linker with a small molecule. The possibilities that nanoparticles in particular offer is linked to their ability to be functionalized with a diverse set of targeting reagents that serve to increase their capacity for BBB crossing [20]. In a great advantage, the selection of payload that can be ferried to the brain is expanded via the use of NPs since potentially toxic drugs are now safely transported inside the nanoparticles to the site where they can excise their therapeutic effect [162]. Moreover, transcytosis properties are solely dependent on nanoparticles' properties and not on the nature of the payload further increasing their utility – and their tunability - as trans-BBB delivery vectors. NPs' biological stability, feasibility to incorporate both hydrophobic and hydrophilic pharmaceuticals, and ability to tune the degree of coating with a variety of targeting ligands is invaluable [162]. There are numerous classes of NPs, with NPs commonly utilized for medical purposes such as liposomes, and polymer based NPs [162].

During chemical conjugation reactions accessible amino acid residues on the surface of the antibody undergo a controlled reaction with an appropriate chemical handle. There is a wide literature for antibody functionalization methods, and the reader is directed to an excellent review in the field [47]. Non-specific conjugation results in a mixture of ADC species with variable Drug-Antibody Ratios (DAR), and non-controlled

location of conjugation. In general, broad distribution of DAR results in decreased potency, increased risk of aggregation and clearance rate, as well as instability of the release profile of the payload [158]. Further, nonspecific reaction of protein residues often results in loss or alteration of antibody binding with detrimental effects for the activity [157]. To ameliorate this problem, it is possible to employ site-specific conjugation methodologies to construct a homogeneous population of ADCs. We have previously employed EPL to append an azide as a reactive handle for copper catalyzed azide-alkyne cycloaddition (CuAAC) [53]. In EPL reactions, addition of a thiol reagent results in cleavage of the intein moiety and simultaneous addition of a reactive thioester at the point of the previous protein-intein interface [51]. This thioester can be further reacted with a chemical handle with an N-terminal cysteine molecule to append the desired functionality in a site-specific fashion that results in the formation of a stable, covalent linkage. CuAAC reaction is suitable for use in *in vitro* applications due to the high rate of reaction, nevertheless in *in vivo* applications the oxidative stress caused by the Cu(I) and the need for complex optimization of each step and reagent participating in the reaction is a hindrance [54]. As an alternative to copper catalyzed reactions it is possible to resort in strained cyclooctynes such as DBCO that react with azides in copper free conditions [163] by appending an azide handle to the protein of interest that subsequently reacts with the DBCO modified entity.

In order to enable many downstream laboratory and preclinical applications, we aimed to provide a proof of concept study showing the ability to functionalize our brain penetrating antibodies through a strain promoted reaction with a biotinylated probe.

5.2 Materials and Methods

5.2.1 Cells, media, and plasmids

Saccharomyces cerevisiae strain YVH10 [136] (MATα PDI1::GAPDHPDI1::LEU2 ura3−52 trp1 leu2Δ1 his3Δ200 pep4::HIS3 prb1Δ1.6R can1 GAL) was used for all yeast protein secretion. The engineered Mxe GyrA intein-fused pRS316-FLAG-202-08 [136] vector was used as a backbone for protein secretion. HEK293 Freestyle (HEK 293F) cells were used for mammalian antibody secretion. The engineered Mxe GyrA intein was cloned from pRS316-FLAG-202-08 vector into the pIRES based vector described previously in Chapter 3.

5.2.2 Cell growth, and protein production

Large scale DNA purification for HEK 293F transfection was done with ZymoPURE II plasmid kit (Zymo Research # D4200), and PEI transfection performed as described [105]. Transfected cultures were then incubated for 5-7 days at 37^{o} C, 8% CO_2, 135 rpm in a humidified incubator and the supernatant containing scFv-Fc-intein fusions was separated from the cell mass via centrifugation and filtration. scFv-Fc-intein fusions were purified from the cleared supernatant via protein A chromatography (ThermoFisher #20333). After elution with 100mM Citric Acid pH 3 the solution was neutralized with 1M Tris-base pH 9 and dialyzed against PBS before 4^{o} C storage. Soluble single chain antibody fragments (scFv) – intein fusions in yeast were prepared as described [51].

5.2.3 Intein-mediated release and EPL

The ability to release the scFv and scFv-Fc from secreted intein fusions was performed as described previously [51]. Briefly, 1M mercaptoethanesulfonic acid (MESNA,

Sigma-Aldrich) was added to scFv- or scFv-Fc- purified protein to a final concentration of 100mM and the reaction was allowed to proceed for 20 h at RT prior to anti tag western blot analysis. A cysteine reagent was used in this study to perform the EPL reactions, cysteine azide (Anaspec), and Bio-P1, an N-terminal cysteine peptide containing a biotin (synthesized by the University of Wisconsin Biotechnology Center based upon the Bio-P1 peptide from New England Biolabs. Sequence: NH_2-CDPEK(Bt)DS-$CONH_2$). To generate azide proteins, 5 µl of 50 mM cysteine azide in PBS was added directly to 50 µl of the released protein products and the reactions were allowed to proceed for 20 h at room temperature. The reactions were subsequently dialyzed against PBS with a Slide-A-Lyzer dialysis cassette to remove unreacted cysteines. The reactions were subsequently dialyzed against 100mM MESNA with a Slide-A-Lyzer dialysis cassette to remove unreacted cysteines under reducing conditions, and then further dialyzed against PBS to remove the reducing agent.

5.2.4 SDS-PAGE and Western blot

Samples were collected and denatured by boiling in LDS sample buffer (Life Technologies) containing 1mM 2-mercaptoethanol for 10 min prior to resolution on a 4-12% Bis-Tris gel (Life Technologies). Under these reducing conditions, no intein cleavage reaction is observed. Proteins were then transferred to a nitrocellulose membrane for western blot analysis. Detection of FLAG tagged proteins was performed with an anti-FLAG M2 mouse monoclonal antibody (Sigma-Aldrich, 1:3000 dilution), followed by an anti-mouse HRP conjugate (Sigma-Aldrich, 1:2000 dilution). Detection of HA tagged proteins was performed with an anti-HA tag rat monoclonal antibody (Roche, 1:1000

dilution) followed by an anti-rat HRP conjugate (Sigma-Aldrich, 1:2000 dilution).

5.3 Results

5.3.1 Production of antibody-intein fusion and thiol induced cleavage

As a first step lead antibodies showing an increased brain penetration 46.1 and 17 (Chapter 3) were produced as soluble scFv-intein fusions employing 202-08 intein as a fusion partner (Figure 5.1a). scFv 17 was also cloned into a modified pIRES vector were scFv is inserted in tandem with 202-08 intein and a rabbit Fc region (Figure 5.1b). Clones 46.1 and 17 were solubly produced as intein fusions in a yeast secretion platform, and scFv 17 was also successfully produced as a rabbitFc-intein fusion, with the intein retaining its activity as evident by cleavage upon addition of MESNA (Figure 5.2a and 5.2b). Critically, scFv17-rabbitFc-202-08 fusions did not exhibit significant autocleavage in the mammalian secretion system (Figure 5.2b). As of note, upon reduction with MESNA that results in intein cleavage, the scFv-rabbitFc-202-08 intein fusion is reduced to a mixture of scFv-Fc, and scFv-Fc-intein monomers due to incomplete intein mediated cleavage (Figure 5.2b). Removal of the reducing agent and incubation under oxidizing conditions results in a partial reformation of interchain disulfide bonds and the generation of a mixture of products that complicate further downstream evaluation (Figure 5.2c). Typically, after verifying intein mediated cleavage, the nest step would be to perform an EPL reaction and show the feasibility of antibody functionalization.

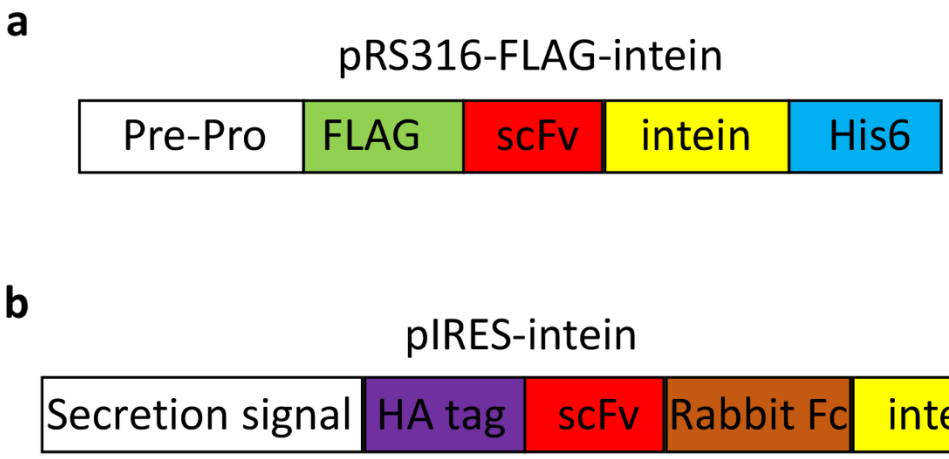

Figure 5.1 Constructs used for EPL. a) pRS316-FLAG-intein contains a synthetic PrePro leader sequence directing secretion of an scFv. b) pIRES-intein contains a secretion signal directing scFv- Fc intein fusions secretion. FLAG and HA tags are used for detection and His6 tag and Fc regions are used for purification of constructs from protein containing supernatants.

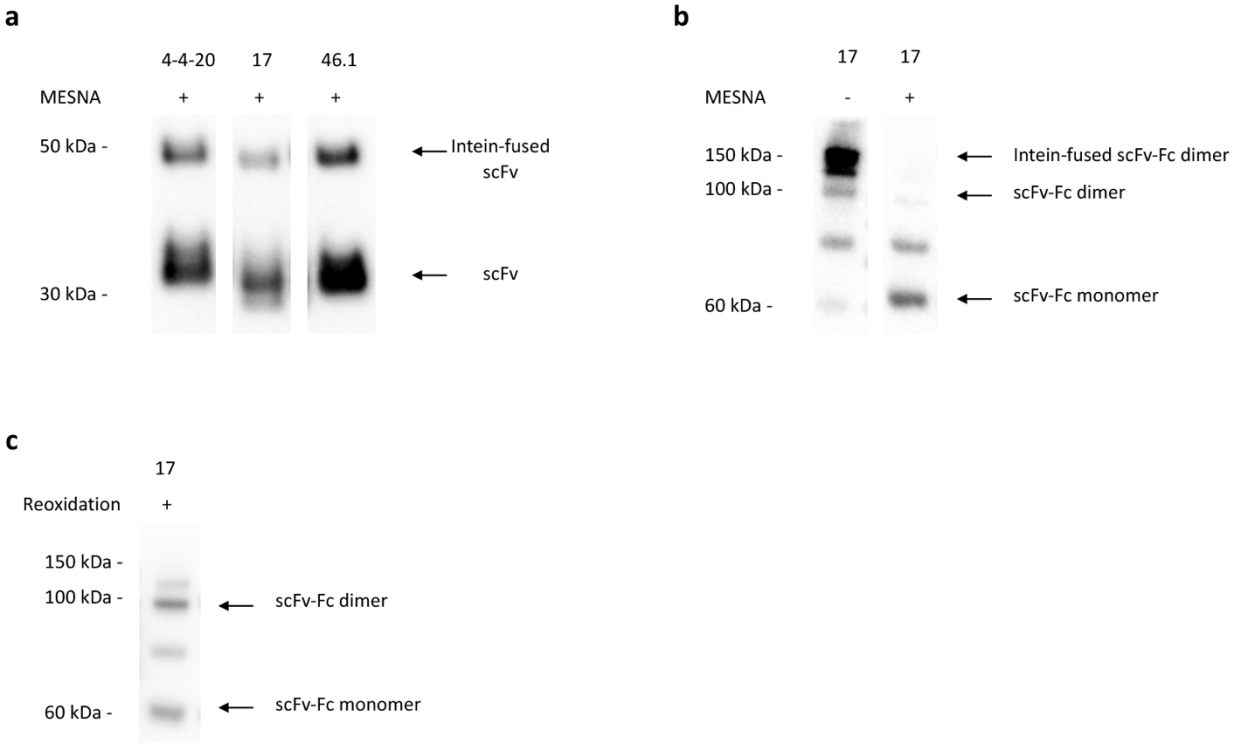

Figure 5.2 MESNA induced cleavage of antibodies. a) scFvs expressed in yeast are cleaved from the intein molecule upon addition of MESNA and cleavage is assayed through an anti-FLAG Western blot. The cleaved product is evident at 30kDa. b) scFv-rabbitFc intein fusions are successfully produced in HEK cells. Upon addition of MESNA a mixture of cleaved and uncleaved scFv-rabbitFc intein fusions results as assayed by an anti-HA Western blot. c) Removal of reducing agents results in partial re-oxidation of

disulfide bonds and reformation of dimeric scFv-rabbitFc. A number of byproducts such as scFv-rabbitFc-intein/scFv-rabbitFc dimers and unrefolded scFv-rabbitFc arms are also evident.

5.3.2 EPL functionalization of antibodies

Given the availability of biotinylation reagents, we chose to functionalize our antibodies through click chemistry by attaching a biotin entity at the C-terminus of the protein. While we opted to use an azide-DBCO chemistry to attach the biotin to yeast produced scFvs to closer mimic a reaction with potential for nanoparticle conjugation of antibodies, the use of DBCO-azide click chemistry proved complicated in scFv-Fc functionalization and resulted in significant non-specific by-products hence a simple biotinylation strategy using the BioP1 peptide was preferred in this case. ScFvs 46.1, 17, and 4-4-20 were secreted as intein fusions in yeast and after intein cleavage cysteine-azide was added to attach a chemical handle at the C-terminus. Following removal of excess cysteine-azide reagent a DBCO-biotin was attached to the scFvs (Figure 5.3a). For scFv-Fc intein fusions, EPL reaction was possible by using a biotinylated cysteine peptide to append the desired functionality. The fusion protein was cleaved from the intein upon addition of MESNA along with the addition of BioP1. This resulted in a functionalization of the scFv-Fc fusion as evident by the 60kDa band indicating a functionalized scFv-Fc monomer (Figure 5.3b). As scFvs 46.1 and 17 are isolated from a phage display platform and the capacity of the yeast secretion machinery to produce them as soluble protein had not been tested, here we present the first data showing the ability to integrate identified brain penetrating antibodies into a yeast and mammalian based intein functionalization platform.

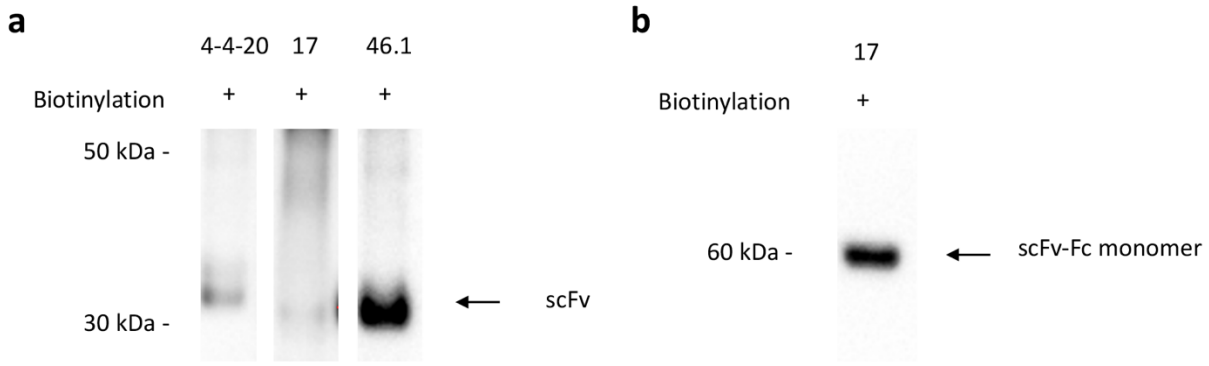

Figure 5.3 The capacity to functionalize antibodies was assayed. a) scFvs functionalized with a cysteine-azide chemical handle were reacted with DBCO-biotin and a biotin functionality was appended as evident by the corresponding band at 30kDa. b) 17-rabbitFc was functionalized through reaction with a N-terminal cysteine biotinylated peptide. In this reducing gel the scFv-Fc monomer is detected through an anti-Biotin blot showing successful biotinylation of the construct.

5.4 Discussion and future directions

These are the first attempts to functionalize the isolated brain penetrating antibodies through EPL functionalization. Here we functionalize antibodies after secretion in both yeast, and mammalian secretion platforms. Antibodies 46.1 and 17 are very promising as drug delivery vectors, and 4-4-20 is an excellent negative control vector. Antibodies as scFvs can be readily integrated in a yeast scFv-intein secretion platform that enables C-terminal functionalization. Further, antibodies can be produced as rabbitFc-intein fusions and secreted in mammalian cells providing an alternative platform for site-specific functionalization. Mammalian secretion results in minimal intein autocleavage, but the analysis of post-cleavage products is complicated due to the dimeric nature of scFv-Fc fusions and incomplete intein cleavage that leads to a mixture of scFv-Fc and scFv-Fc-intein products that are difficult to separate. Antibodies are readily functionalized through DBCO-azide chemistry that can serve to potentially functionalize nanoparticles [161]. Site-specific functionalization allows for attachment of chemical handles away from the scFv reactive site minimizing deleterious effects on protein function.

Binding parameters and antibody format have been shown to influence transcytosis capacity [21]. Engineering antibody binding properties is a laborious process that is complicated in the lack of a clear antigen. In lieu of antibody engineering campaigns, it is possible to alter nanoparticles coating to accomplish similar effects. The degree of functionalization of nanoparticles can be controlled by varying the number of scFvs per particle allowing the tuning of avidity, which in the case of nanoparticles coated with transferrin altered the transcytosis capacity of the vector [93]. This enables elucidation of avidity and affinity effects on the transcytosis capacity of brain penetrating antibodies without a precise knowledge of the target or implementation of antibody engineering approaches to alter antibody binding properties.

In summary, this preliminary work paves the way for functionalization of brain penetrating antibodies that in turn enables delivery of therapeutics or targeted nanoparticles delivery to the brain, as well as elucidation of parameters affecting the transcytosis capacity of these antibodies.

REFERENCES

1. Cuny GD. Neurodegenerative diseases: challenges and opportunities. *Future Med Chem*. 2012;4(13):1647-1649. doi:10.4155/fmc.12.123
2. Pardridge WM. The Blood-Brain Barrier : Bottleneck in Brain Drug Development. *NeuroRx*. 2005;2(January):3-14.
3. Bergers G, Song S. The role of pericytes in blood-vessel formation and maintenance. *Neuro Oncol*. 2005. doi:10.1215/S1152851705000232
4. Abbot N. Astrocyte–endothelial interactions and blood–brain barrier permeability. *J Ant*. 2002;200:629-638.
5. Stollg G, Jander S. The role of microglia and macrophages in the pathophysiology of the CNS. *Prog Neurobiol*. 1999;58(3):233-247. doi:10.1016/S0301-0082(98)00083-5
6. Hawkins BT, Davis TP. The Blood-Brain Barrier / Neurovascular Unit in Health and Disease. 2005;57(2):173-185. doi:10.1124/pr.57.2.4.173
7. Leslie EM, Deeley RG, Cole SPC. Multidrug resistance proteins: role of P-glycoprotein, MRP1, MRP2, and BCRP (ABCG2) in tissue defense. *Toxicol Appl Pharmacol*. 2005;204(3):216-237. doi:10.1016/j.taap.2004.10.012
8. Mitic LL, Van Itallie CM, Anderson JM. Molecular Physiology and Pathophysiology of Tight Junctions I. Tight junction structure and function: lessons from mutant animals and proteins. *Am J Physiol Gastrointest Liver Physiol*. 2000;(26):250-254.
9. Stamatovic SM, Johnson AM, Keep RF, Andjelkovic A V. Junctional proteins of the blood-brain barrier : New insights into function and dysfunction. 2016;(March):1-12.
10. Jr RSB, Reynolds JJ, Bearden SE, Hhcy H. Hyperhomocysteinemia increases permeability of the blood-brain barrier by NMDA receptor-dependent regulation of adherens and tight junctions. *Vasc Biol*. 2011;118(7):2007-2015. doi:10.1182/blood-2011-02-338269.The
11. Jones AR, Shusta E V. Blood-brain barrier transport of therapeutics via receptor-mediation. *Pharm Res*. 2007;24(9):1759-1771. doi:10.1007/s11095-007-9379-0
12. Villegas JC, Broadwell RD. Transcytosis of protein through the mammalian cerebral epithelium and endothelium. II. Adsorptive transcytosis of WGA-HRP and the blood-brain and brain-blood barriers. *J Neurocytol*. 1993;22(2):67-80. doi:10.1007/BF01181571
13. Tsuji A, Tamai I. Carrier-mediated or specialized transport of drugs across the blood–brain barrier. *Adv Drug Deliv Rev*. 1999;36(2-3):277-290. doi:10.1016/S0169-409X(98)00084-2
14. Lajoie JM, Shusta E V. Targeting Receptor-Mediated Transport for Delivery of Biologics Across the Blood-Brain Barrier. *Annu Rev Pharmacol Toxicol*. 2015;55(1):613-631. doi:10.1146/annurev-pharmtox-010814-124852
15. Pardridge WM, Kang YS, Buciak JL, Yang J. Human Insulin Receptor Monoclonal Antibody Undergoes High Affinity Binding to Human Brain Capillaries in Vitro and Rapid Transcytosis Through the Blood–Brain Barrier in Vivo in the Primate. *Pharm Res*. 1995;12(6):807-816.
16. Golden PL, Maccagnan TJ, Pardridge WM. Human Blood-Brain Barrier Leptin Receptor Binding and Endocytosis in Isolated Human Brain Microvessels. *J Clin Invest*. 1997;99(1):14-18.
17. Fenart L, Dehouck M, Pierce A. A New Function for the LDL Receptor: Transcytosis

of LDL across the Blood–Brain Barrier. 1997;138(4):877-889.
18. Paterson J, Webster CI. Drug discovery and the BBB Exploiting transferrin receptor for delivering drugs across the blood-brain barrier. *Drug Discov Today Technol*. 2016;20:49-52. doi:10.1016/j.ddtec.2016.07.009
19. Müller SK, Wilhelm I, Schubert T, et al. Gb3-binding lectins as potential carriers for transcellular drug delivery. *Expert Opin Drug Deliv*. 2017;14(2):141-153. doi:10.1080/17425247.2017.1266327
20. Saraiva C, Praça C, Ferreira R, Santos T, Ferreira L, Bernardino L. Nanoparticle-mediated brain drug delivery : Overcoming blood – brain barrier to treat neurodegenerative diseases. *J Control Release*. 2016;235:34-47. doi:10.1016/j.jconrel.2016.05.044
21. Goulatis LI, Shusta E V. Protein engineering approaches for regulating blood–brain barrier transcytosis. *Curr Opin Struct Biol*. 2017;45:109-115. doi:10.1016/j.sbi.2016.12.005
22. Jones AR, Stutz CC, Zhou Y, Marks JD, Shusta E V. Identifying blood-brain-barrier selective single-chain antibody fragments. *Biotechnol J*. 2014;9(5):664-674. doi:10.1002/biot.201300550
23. Zuchero YJY, Chen X, Bien-Ly N, et al. Discovery of Novel Blood-Brain Barrier Targets to Enhance Brain Uptake of Therapeutic Antibodies. *Neuron*. 2016;89(1):70-82. doi:10.1016/j.neuron.2015.11.024
24. Wilhelm I, Fazakas C, Krizbai IA. In vitro models of the blood-brain barrier. *Acta Neurobiol Exp*. 2011:113-128.
25. Perrière N, Yousif S, Cazaubon S. A functional in vitro model of rat blood – brain barrier for molecular analysis of efflux transporters. *Brain Res*. 2007;50:1-13. doi:10.1016/j.brainres.2007.02.091
26. Patabendige A, Skinner RA, Abbott NJ. Establishment of a simplified in vitro porcine blood – brain barrier model with high transendothelial electrical resistance. *Brain Res*. 2013;1521:1-15. doi:10.1016/j.brainres.2012.06.057
27. Coisne C, Dehouck L, Faveeuw C, et al. Mouse syngenic in vitro blood – brain barrier model : a new tool to examine inflammatory events in cerebral endothelium. *Lab Invest*. 2005;85(6):734-746. doi:10.1038/labinvest.3700281
28. Dehouck M, Méresse S, Delorme P, Fruchart J, Cecchelli R. An Easier, Reproducible, and Mass-Production Method to Study the Blood–Brain Barrier In Vitro. *J Neurochem*. 1990;54(5):1798-1801.
29. Helms HC, Abbott NJ, Burek M, et al. In vitro models of the blood – brain barrier : An overview of commonly used brain endothelial cell culture models and guidelines for their use. *J Cereb Blood Flow Metab*. 2016;36(5):862-890. doi:10.1177/0271678X16630991
30. Roux F. Regulation of Gamma-Clutamy l Transpeptidase and Alkaline Phosphatase Activities in Immortalized Rat Brain Microvessel Endothelial Cells. *J Cell Physiol*. 1994;159(1).
31. Williams FL, Risau W. Endothelioma Cells Expressing the Folyoma Middle T Oncogene Induce Hemangiomas by Host Cell Recruitment. *Cell*. 1989;57(6):1053-1063.
32. Weksler BB, Subileau EA, Holloway K, et al. Blood-brain barrier-specific properties of a human adult brain endothelial cell line. *FASEB J*. 2005;26:1-26.

33. Muruganandam A, Tanha J, Narang S, Stanimirovic D, Aims S. Selection of phage-displayed llama single-domain antibodies that transmigrate across human blood – brain barrier endothelium. *FASEB J*. 2002;16:240-242. doi:10.1096/fj.01
34. Sade H, Baumgartner C, Hugenmatter A, Moessner E, Freskgård P-O, Niewoehner J. A Human Blood-Brain Barrier Transcytosis Assay Reveals Antibody Transcytosis Influenced by pH-Dependent Receptor Binding. *PLoS One*. 2014;9(4):e96340. doi:10.1371/journal.pone.0096340
35. Lippmann ES, Azarin SM, Kay JE, et al. Derivation of blood-brain barrier endothelial cells from human pluripotent stem cells. *Nat Biotechnol*. 2012;30(8):783-791. doi:10.1038/nbt.2247
36. Ponio JB, El-ayoubi F, Glacial F, et al. Instruction of Circulating Endothelial Progenitors In Vitro towards Specialized Blood-Brain Barrier and Arterial Phenotypes. *PLoS One*. 2014;9(1). doi:10.1371/journal.pone.0084179
37. Lippmann ES, Al-Ahmad A, Azarin SM, Palecek SP, Shusta E V. A retinoic acid-enhanced, multicellular human blood-brain barrier model derived from stem cell sources. *Sci Rep*. 2014;4:4160. doi:10.1038/srep04160
38. Shusta E V, Boado RJ, Mathern GW, Pardridge WM. Vascular Genomics of the Human Brain. *J Cereb Blood Flow Metab*. 2002;22(3):245-252.
39. Enerson BE, Drewes LR. The rat blood – brain barrier transcriptome. *J Cereb blood flow Metab*. 2006;26(7):959-973. doi:10.1038/sj.jcbfm.9600249
40. Daneman R, Zhou L, Agalliu D, Cahoy JD, Kaushal A, Barres BA. The mouse blood-brain barrier transcriptome: a new resource for understanding the development and function of brain endothelial cells. *PLoS One*. 2010;5(10):e13741. doi:10.1371/journal.pone.0013741
41. Winter G, Griffiths AD, Hawkins RE, Hoogenboom HR. Making antibodies by phage display technology. *Annu Rev Immunol*. 1994;(12):433-455.
42. Smith GP. Filamentous Fusion Phage : Novel Expression Vectors that Display Cloned Antigens on the Virion Surface. *Science (80-)*. 1985;228(4705):1315-1317.
43. Smith GP, Petrenko VA. Phage Display. *Chem Rev*. 1997;2665(96):391-410. doi:10.1021/cr960065d
44. Yu Zhou, Lequn Zhao and JDM, Zhou Y, Zhao L, Marks JD. Selection and characterization of cell binding and internalizing phage antibodies. *Arch Biochem Biophys*. 2012;526(2):107-113. doi:10.1016/j.abb.2012.05.007
45. Kreuter J. Drug delivery to the central nervous system by polymeric nanoparticles: What do we know? *Adv Drug Deliv Rev*. 2014;71:2-14. doi:10.1016/j.addr.2013.08.008
46. Yu YJ, Zhang Y, Kenrick M, et al. Boosting brain uptake of a therapeutic antibody by reducing its affinity for a transcytosis target. *Sci Transl Med*. 2011;3(84):84ra44. doi:10.1126/scitranslmed.3002230
47. Dennler P, Fischer E, Schibli R. Antibody Conjugates: From Heterogeneous Populations to Defined Reagents. *Antibodies*. 2015;4(3):197-224. doi:10.3390/antib4030197
48. Kalkhof S, Sinz A. Chances and pitfalls of chemical cross-linking with amine-reactive N -hydroxysuccinimide esters. *Anal Bioanal Chem*. 2008:305-312. doi:10.1007/s00216-008-2231-5
49. Christopher J, Spencer J, Michael C, Peter G. A General Method for Site-Specific

Incorporation of Unnatural Amino Acids into Proteins. *Science (80-)*. 1989;244:182-188.
50. Xie J, Schultz PG. Adding amino acids to the genetic repertoire. *Curr Opin Chem Biol*. 2005;9:548-554. doi:10.1016/j.cbpa.2005.10.011
51. Marshall CJ, Grosskopf VA, Moehling TJ, et al. An evolved Mxe GyrA intein for enhanced production of fusion proteins. *ACS Chem Biol*. 2015;10(2):527-538. doi:10.1021/cb500689g
52. Muir TW. Semisynthesis of Proteins by Expressed Protein Ligation. *Annu Rev Biochem*. 2003;(72):249-289. doi:10.1146/annurev.biochem.72.121801.161900
53. Marshall CJ, Agarwal N, Kalia J, et al. Facile chemical functionalization of proteins through intein-linked yeast display. *Bioconjug Chem*. 2013;24(9):1634-1644. doi:10.1021/bc4002618
54. Umlauf BJ, Mix KA, Grosskopf VA, Raines RT, Shusta E V. Site-Specific Antibody Functionalization Using Tetrazine–Styrene Cycloaddition. *Bioconjug Chem*. 2018;29:1605-1613. doi:10.1021/acs.bioconjchem.8b00114
55. Pardridge WM. Blood-brain barrier delivery. *Drug Discov Today*. 2007;12(1-2):54-61. doi:10.1016/j.drudis.2006.10.013
56. Pardridge WM. Molecular Trojan horses for blood-brain barrier drug delivery. *Curr Opin Pharmacol*. 2006;6(5):494-500. doi:10.1016/j.coph.2006.06.001
57. Smith MW, Gumbleton M. Endocytosis at the blood-brain barrier: from basic understanding to drug delivery strategies. *J Drug Target*. 2006;14(4):191-214. doi:10.1080/10611860600650086
58. Lim JP, Gleeson PA. Macropinocytosis: an endocytic pathway for internalising large gulps. *Immunol Cell Biol*. 2011;89(8):836-843. doi:10.1038/icb.2011.20
59. Brightman MW, Reese TS. Junctions between intimately apposed cell membranes in the vertebrate brain. *J Cell Biol*. 1969;40(3):648-677. doi:10.1083/jcb.40.3.648
60. Hervé F, Ghinea N, Scherrmann J-M. CNS delivery via adsorptive transcytosis. *AAPS J*. 2008;10(3):455-472. doi:10.1208/s12248-008-9055-2
61. Broadwell RD, Balin BJ, Salcman M. Transcytotic pathway for blood-borne protein through the blood-brain barrier. *Proc Natl Acad Sci U S A*. 1988;85(2):632-636. doi:10.1073/pnas.85.2.632
62. Bickel U, Yoshikawa T, Pardridge WM. Delivery of peptides and proteins through the blood-brain barrier. *Adv Drug Deliv Rev*. 2001;46(1-3):247-279. doi:10.1016/S0169-409X(00)00139-3
63. Triguero D, Buciak J, Pardridge WM. Capillary depletion method for quantification of blood-brain barrier transport of circulating peptides and plasma proteins. *J Neurochem*. 1990;54(6):1882-1888. doi:2338547
64. Béduneau A, Saulnier P, Benoit JP. Active targeting of brain tumors using nanocarriers. *Biomaterials*. 2007;28(33):4947-4967. doi:10.1016/j.biomaterials.2007.06.011
65. Drin G, Rousselle C, Scherrmann J-M, Rees AR, Temsamani J. Peptide delivery to the brain via adsorptive-mediated endocytosis: advances with SynB vectors. *AAPS PharmSci*. 2002;4(4):E26. doi:10.1208/ps040426
66. Mayor S, Pagano RE. Pathways of clathrin-independent endocytosis. *Nat Rev Mol Cell Biol*. 2007;8(8):603-612. doi:10.1038/nrm2216
67. Huotari J, Helenius A. Endosome maturation. *EMBO J*. 2011;30(17):3481-3500.

doi:10.1038/emboj.2011.286
68. Wilfred A. Jefferies, Malcolm R. Brandon, Simon V. Hunt, Alan F. Williams, Kevin C. Gatter DYM. Transferrin receptor on endothelium of brain capillaries. *Nature*. 1984;312:162-163.
69. Duffy KR, Pardridge WM. Blood-brain barrier transcytosis of insulin in developing rabbits. *Brain Res*. 1987;420(1):32-38. doi:10.1016/0006-8993(87)90236-8
70. Haqqani AS, Delaney CE, Tremblay T-L, Sodja C, Sandhu JK, Stanimirovic DB. Method for isolation and molecular characterization of extracellular microvesicles released from brain endothelial cells. *Fluids Barriers CNS*. 2013;10(1):4. doi:10.1186/2045-8118-10-4
71. Pelkmans L, Helenius A. Endocytosis via caveolae. *Traffic*. 2002;3(5):311-320. doi:10.1034/j.1600-0854.2002.30501.x
72. Liu Y, Huang R, Han L, et al. Brain-targeting gene delivery and cellular internalization mechanisms for modified rabies virus glycoprotein RVG29 nanoparticles. *Biomaterials*. 2009;30(25):4195-4202. doi:10.1016/j.biomaterials.2009.02.051
73. Park T-E, Singh B, Li H, et al. Enhanced BBB permeability of osmotically active poly(mannitol-co-PEI) modified with rabies virus glycoprotein via selective stimulation of caveolar endocytosis for RNAi therapeutics in Alzheimer's disease. *Biomaterials*. 2015;38:61-71. doi:10.1016/j.biomaterials.2014.10.068
74. Wang P, Xue Y, Shang X, Liu Y. Diphtheria toxin mutant CRM197-mediated transcytosis across blood-brain barrier in vitro. *Cell Mol Neurobiol*. 2010;30(5):717-725. doi:10.1007/s10571-010-9496-x
75. Gao H, Yang Z, Zhang S, Pang Z, Jiang X. Internalization and subcellular fate of aptamer and peptide dual-functioned nanoparticles. *J Drug Target*. 2014;2330(5):1-10. doi:10.3109/1061186X.2014.886038
76. Candela P, Gosselet F, Miller F, et al. Physiological pathway for low-density lipoproteins across the blood-brain barrier: transcytosis through brain capillary endothelial cells in vitro. *Endothelium*. 2008;15(5-6):254-264. doi:10.1080/10623320802487759
77. Candela P, Gosselet F, Saint-Pol J, et al. Apical-to-basolateral transport of amyloid-β peptides through blood-brain barrier cells is mediated by the receptor for advanced glycation end-products and is restricted by p-glycoprotein. *J Alzheimer's Dis*. 2010;22(3):849-859. doi:10.3233/JAD-2010-100462
78. Stutz C, Zhang X, Shusta E. Combinatorial approaches for the identification of brain drug delivery targets. *Curr Pharm Des*. 2014;20:1564-1576.
79. Bien-Ly N, Yu YJ, Bumbaca D, et al. Transferrin receptor (TfR) trafficking determines brain uptake of TfR antibody affinity variants. *J Exp Med*. 2014;211(2):233-244. doi:10.1084/jem.20131660
80. Niewoehner J, Bohrmann B, Collin L, et al. Increased brain penetration and potency of a therapeutic antibody using a monovalent molecular shuttle. *Neuron*. 2014;81(1):49-60. doi:10.1016/j.neuron.2013.10.061
81. Weflen AW, Baier N, Tang Q-J, et al. Multivalent immune complexes divert FcRn to lysosomes by exclusion from recycling sorting tubules. *Mol Biol Cell*. 2013;24(15):2398-2405. doi:10.1091/mbc.E13-04-0174
82. Marsh EW, Leopold PL, Jones NL, Maxfield FR. Oligomerized transferrin receptors

are selectively retained by a lumenal sorting signal in a long-lived endocytic recycling compartment. *J Cell Biol*. 1995;129(6):1509-1522. doi:10.1083/jcb.129.6.1509

83. Lao BJ, Kamei DT. Improving therapeutic properties of protein drugs through alteration of intracellular trafficking pathways. *Biotechnol Prog*. 2008;24(1):2-7. doi:10.1021/bp070080b
84. Tillotson BJ, Goulatis LI, Parenti I, Duxbury E, Shusta E V. Engineering an anti-transferrin receptor ScFv for pH-sensitive binding leads to increased intracellular accumulation. *PLoS One*. 2015;10(12):1-21. doi:10.1371/journal.pone.0145820
85. Couch J a., Yu YJ, Zhang Y, et al. Addressing safety liabilities of TfR bispecific antibodies that cross the blood-brain barrier. *Sci Transl Med*. 2013;5(183):183ra57, 1-12. doi:10.1126/scitranslmed.3005338
86. Farrington GK, Caram-Salas N, Haqqani AS, et al. A novel platform for engineering blood-brain barrier-crossing bispecific biologics. *FASEB J*. 2014;28(11):4764-4778. doi:10.1096/fj.14-253369
87. Boado RJ, Zhang Y, Zhang Y, Pardridge WM. Humanization of anti-human insulin receptor antibody for drug targeting across the human blood-brain barrier. *Biotechnol Bioeng*. 2007;96(2):381-391. doi:10.1002/bit.21120
88. Boado RJ, Zhang Y, Zhang Y, Xia CF, Pardridge WM. Fusion antibody for Alzheimer's disease with bidirectional transport across the blood-brain barrier and A?? fibril disaggregation. *Bioconjug Chem*. 2007;18(2):447-455. doi:10.1021/bc060349x
89. Ye D, Raghnaill MN, Bramini M, et al. Nanoparticle accumulation and transcytosis in brain endothelial cell layers. *Nanoscale*. 2013;5(22):11153-11165. doi:10.1039/c3nr02905k
90. Ye D, Anguissola S, O'Neill T, Dawson K a. Immunogold labeling reveals subcellular localisation of silica nanoparticles in a human blood–brain barrier model. *Nanoscale*. 2015:10050-10058.
91. Georgieva J V, Kalicharan D, Couraud P-O, et al. Surface characteristics of nanoparticles determine their intracellular fate in and processing by human blood-brain barrier endothelial cells in vitro. *Mol Ther*. 2011;19(2):318-325. doi:10.1038/mt.2010.236
92. Huang R, Ke W, Han L, et al. Brain-targeting mechanisms of lactoferrin-modified DNA-loaded nanoparticles. *J Cereb Blood Flow Metab*. 2009;29(12):1914-1923. doi:10.1038/jcbfm.2009.104
93. Wiley DT, Webster P, Gale A, Davis ME. Transcytosis and brain uptake of transferrin-containing nanoparticles by tuning avidity to transferrin receptor. *Proc Natl Acad Sci U S A*. 2013;110(21):8662-8667. doi:10.1073/pnas.1307152110
94. Kolhar P, Anselmo AC, Gupta V, et al. Using shape effects to target antibody-coated nanoparticles to lung and brain endothelium. *Proc Natl Acad Sci U S A*. 2013;110(26):10753-10758. doi:10.1073/pnas.1308345110
95. Abbott NJ, Friedman A. Overview and introduction: the blood-brain barrier in health and disease. *Epilepsia*. 2012;53 Suppl 6:1-6. doi:10.1111/j.1528-1167.2012.03696.x
96. Poduslo JF, Curran GL, Berg CT. Macromolecular permeability across the blood-nerve and blood-brain barriers. *Proc Natl Acad Sci U S A*. 1994;91(12):5705-5709.

doi:10.1073/pnas.91.12.5705
97. Pardridge WM, Kang YS, Buciak JL. Transport of Human Recombinant Brain-Derived Neurotrophic Factor (BDNF) Through the Rat Blood−Brain Barrier in Vivo Using Vector-Mediated Peptide Drug Delivery. *Pharm Res*. 1994;11(5):738-746. doi:10.1023/A:1018940732550
98. Urich E, Schmucki R, Ruderisch N, et al. Cargo Delivery into the Brain by in vivo identified Transport Peptides. *Sci Rep*. 2015;5:1-14. doi:10.1038/srep14104
99. Pasqualini R, Ruoslahti E. Organ targeting in vivo using phage display peptide libraries. *Nature*. 1996;380(6572):364-366. doi:10.1038/380364a0
100. Wang XX, Cho YK, Shusta E V. Mining a yeast library for brain endothelial cell-binding antibodies. *Nat Methods*. 2007;4(2):143-145. doi:10.1038/nmeth993
101. Stebbins MJ, Wilson HK, Canfield SG, Qian T, Palecek SP, Shusta E V. Differentiation and characterization of human pluripotent stem cell-derived brain microvascular endothelial cells. *Methods*. 2016;101:93-102. doi:10.1016/j.ymeth.2015.10.016
102. Sheets MD, Amersdorfer P, Finnern R, et al. Efficient construction of a large nonimmune phage antibody library: the production of high-affinity human single-chain antibodies to protein antigens. *Proc Natl Acad Sci U S A*. 1998;95(11):6157-6162. doi:10.1073/pnas.95.11.6157
103. O'Connell D, Becerril B, Roy-Burman A, Daws M, Marks JD. Phage versus phagemid libraries for generation of human monoclonal antibodies. *J Mol Biol*. 2002;321(02):49-56. doi:10.1016/S0022-2836(02)00561-2
104. Zhou Y, Marks JD. Identification of Target and Function Specific Antibodies for Effective Drug Delivery. *Methods Mol Biol*. 2009;525:145-160. doi:10.1007/978-1-59745-554-1_7
105. Orcutt KD, Ackerman ME, Cieslewicz M, et al. A modular IgG-scFv bispecific antibody topology. *Protein Eng Des Sel*. 2010;23(4):221-228. doi:10.1093/protein/gzp077
106. Poul M a, Becerril B, Nielsen UB, Morisson P, Marks JD. Selection of tumor-specific internalizing human antibodies from phage libraries. *J Mol Biol*. 2000;301(5):1149-1161. doi:10.1006/jmbi.2000.4026
107. Nolan D, Ginsberg M, Israely E, et al. Molecular Signatures of Tissue-Specific Microvascular Endothelial Cell Heterogeneity in Organ Maintenance and Regeneration. *Dev Cell*. 2013;26(2):204-219. doi:10.1016/j.devcel.2013.06.017
108. Wark KL, Hudson PJ. Latest technologies for the enhancement of antibody affinity. *Adv Drug Deliv Rev*. 2006;58:657-670. doi:10.1016/j.addr.2006.01.025
109. Abbott NJ, Rönnbäck L, Hansson E. Astrocyte-endothelial interactions at the blood-brain barrier. *Nat Rev Neurosci*. 2006;7(1):41-53. doi:10.1038/nrn1824
110. Wang L, Boyer JL. The Maintenance and Generation of Membrane Polarity in Hepatocytes. *Sci Front*. 2004:892-899. doi:10.1002/hep.20039
111. Mathiisen TM, Lehre KP, Danbolt NC, Ottersen OLEP. The Perivascular Astroglial Sheath Provides a Complete Covering of the Brain Microvessels : An Electron Microscopic 3D Reconstruction. *Glia*. 2010;1103(October 2009):1094-1103. doi:10.1002/glia.20990
112. Foust KD, Nurre E, Montgomery CL, Hernandez A, Curtis M, Kaspar BK. Intravascular AAV9 preferentially targets neonatal-neurons and adult-astrocytes in

CNS. *Nat Biotechnol*. 2010;27(1):59-65. doi:10.1038/nbt.1515.Intravascular
113. Ullrich O, Reinsch S, Urbé S, Zerial M, Parton RG. Rab11 regulates recycling through the pericentriolar recycling endosome. *J Cell Biol*. 1996;135(4):913-924. doi:10.1083/jcb.135.4.913
114. Ho P, Koendgen H, Campbell N, Haddock B, Richman S, Chang I. Risk of natalizumab-associated progressive multifocal leukoencephalopathy in patients with multiple sclerosis : a retrospective analysis of data from four clinical studies. *Lancet Neurol*. 2017;16(11):925-933. doi:10.1016/S1474-4422(17)30282-X
115. Karaoglu Hanzatian D, Schwartz A, Gizatullin F, et al. Brain uptake of multivalent and multi-specific DVD-Ig proteins after systemic administration. *MAbs*. 2018;10(5):765-777. doi:10.1080/19420862.2018.1465159
116. De Araújo AD, Palomo JM, Cramer J, et al. Diels-Alder ligation and surface immobilization of proteins. *Angew Chemie - Int Ed*. 2005;45(2):296-301. doi:10.1002/anie.200502266
117. Khan F, He M, Taussig MJ. Double-hexahistidine tag with high-affinity binding for protein immobilization, purification, and detection on Ni-nitrilotriacetic acid surfaces. *Anal Chem*. 2006;78(9):3072-3079. doi:10.1021/ac060184l
118. Adams GP, Shaller CC, Chappell LL, et al. Delivery of the α-emitting radioisotope bismuth-213 to solid tumors via single-chain Fv and diabody molecules. *J Inorg Biochem*. 2000;27(4):339-346. doi:10.1016/S0969-8051(00)00103-7
119. Lu RM, Chang YL, Chen MS, Wu HC. Single chain anti-c-Met antibody conjugated nanoparticles for in vivo tumor-targeted imaging and drug delivery. *Biomaterials*. 2011;32(12):3265-3274. doi:10.1016/j.biomaterials.2010.12.061
120. Chen I, Howarth M, Lin W, Ting AY. Site-specific labeling of cell surface proteins with biophysical probes using biotin ligase. *Nat Methods*. 2005;2(2):99-104. doi:10.1038/nmeth735
121. Casi G, Huguenin-Dezot N, Zuberbühler K, Scheuermann J, Neri D. Site-specific traceless coupling of potent cytotoxic drugs to recombinant antibodies for pharmacodelivery. *J Am Chem Soc*. 2012;134(13):5887-5892. doi:10.1021/ja211589m
122. Bernardes GJL, Steiner M, Hartmann I, Neri D, Casi G. Site-specific chemical modification of antibody fragments using traceless cleavable linkers. *Nat Protoc*. 2013;8(11):2079-2089. doi:10.1038/nprot.2013.121
123. Muir T, Sondhi D, Cole P. Expressed protein ligation : A general method for protein engineering. *Proc Natl Acad Sci*. 1998;95(June):6705-6710.
124. Sydor JR, Mariano M, Sideris S, Nock S. Establishment of intein-mediated protein ligation under denaturing conditions: C-terminal labeling of a single-chain antibody for biochip screening. *Bioconjug Chem*. 2002;13:707-712. doi:10.1021/bc025534z
125. Telenti A, Southworth M, Alcaide F, Daugelat S, Jacobs WR, Perler FB. The Mycobacterium xenopi GyrA protein splicing element: Characterization of a minimal intein. *J Bacteriol*. 1997;179(20):6378-6382. doi:10.1128/jb.179.20.6378-6382.1997
126. Reulen SWA, van Baal I, Raats JMH, Merkx M. Efficient, chemoselective synthesis of immunomicelles using single-domain antibodies with a C-terminal thioester. *BMC Biotechnol*. 2009;9:66. doi:10.1186/1472-6750-9-66
127. Muir TW. Semisynthesis of Proteins by Expressed Protein Ligation. *Annu Rev*

Biochem. 2003;72(1):249-289. doi:10.1146/annurev.biochem.72.121801.161900
128. Chong S, Williams KS, Xu M, Wotkowicz C. Modulation of Protein Splicing of the Saccharomyces cerevisiae Vacuolar Membrane ATPase Intein *. *J Biol Chem*. 1998;273(17):10567-10577.
129. Chong S, Mersha FB, Comb DG, et al. Single-column purification of free recombinant proteins using a self-cleavable affinity tag derived from a protein splicing element. *Gene*. 1997;192(2):271-281. doi:10.1016/S0378-1119(97)00105-4
130. Ming-Qun Xu, Henry Paulus SC. Fusion to Self-Splicing inteins for Protein Purifucation. *Methods*. 2000;326:376-418.
131. David R, Richter MPO, Beck-Sickinger AG. Expressed protein ligation: Method and applications. *Eur J Biochem*. 2004;271(4):663-677. doi:10.1111/j.1432-1033.2004.03978.x
132. Hackeng TM, Griffin JH, Dawson PE. Protein synthesis by native chemical ligation: Expanded scope by using straightforward methodology. *Biochem Chem*. 1999;96(August):10068-10073. doi:10.1073/pnas.96.18.10068
133. Villain M, Gaertner H, Botti P. Native Chemical Ligation with Aspartic and Glutamic Acids asC-Terminal Residues: Scope and Limitations. *European J Org Chem*. 2003;2003(17):3267-3272. doi:10.1002/ejoc.200300032
134. Amitai G, Callahan BP, Stanger MJ, Belfort G, Belfort M. Modulation of intein activity by its neighboring extein substrates. *Proc Natl Acad Sci*. 2009;106(27):11005-11010. doi:10.1073/pnas.0904366106
135. Southworth, M. W., K. Amaya, T. C. Evans, M. Xu, Perler FB. Purification of Proteins Fused to Either the Amino or Carboxy Terminus of the Mycobacterium xenopi Gyrase A Intein. *Bio Tech*. 1999;27:110-120. doi:7119991
136. Shusta E V, Raines R T, Pluckthun A WDK. Increasing the secretory capacity of Saccharomyces cerevisiae for production of single-chain antibody fragments. *Nat Biotechnol*. 1998;16(10):291-294. doi:10.1038/nbt0898-773
137. Gietz RD, Schiestl RH. Frozen competent yeast cells that can be transformed with high efficiency using the LiAc/SS carrier DNA/PEG method. *Nat Protoc*. 2007;2(1):1-4. doi:10.1038/nprot.2007.17
138. Robinson AS, Wittrup KD. Constitutive Overexpression of Secreted Heterologous Proteins Decreases Extractable BiP and Protein Disulfide Isomerase Levels in Saccharomyces cerevisiae. *Biotechnol Prog*. 1995;11(2):171-177. doi:10.1021/bp00032a009
139. Cui C, Zhao W, Chen J, Wang J, Li Q. Elimination of in vivo cleavage between target protein and intein in the intein-mediated protein purification systems. *Protein Expr Purif*. 2006;50(1):74-81. doi:10.1016/j.pep.2006.05.019
140. Machova Z, Christiane M, Krauss U, et al. Cellular Internalization of Enhanced Green Fluorescent Protein Ligated to a Human. *CHEMBIOCHE*. 2002;3:672-677.
141. Zhao Z, Lu W, Dun B, et al. Purification of green fluorescent protein using a two-intein system. *Appl Microbiol Biotechnol*. 2008;77(5):1175-1180. doi:10.1007/s00253-007-1233-0
142. Romanelli A, Shekhtman A, Cowburn D, Muir TW. Semisynthesis of a segmental isotopically labeled protein splicing precursor: NMR evidence for an unusual peptide bond at the N-extein-intein junction. *Proc Natl Acad Sci*.

2004;101(17):6397-6402. doi:10.1073/pnas.0306616101
143. Albertsen L, Shaw AC, Norrild JC, Strømgaard K. Recombinant production of peptide C -Terminal α-amides using an engineered intein. *Bioconjug Chem*. 2013;24(11):1883-1894. doi:10.1021/bc4002689
144. Mathys S, Evans TC, Chute IC, et al. Characterization of a self-splicing mini-intein and its conversion into autocatalytic N- and C-terminal cleavage elements: Facile production of protein building blocks for protein ligation. *Gene*. 1999;231(1-2):1-13. doi:10.1016/S0378-1119(99)00103-1
145. Bannister SJ, Wittrup KD. Glutathione excretion in response to heterologous protein secretion Saccharomyces cerevisiae. *Biotechnol Bioeng*. 2000;68(4):389-395. doi:10.1002/(SICI)1097-0290(20000520)68:4<389::AID-BIT4>3.0.CO;2-N
146. Hwang C, Sinskey a J, Lodish HF. Oxidized redox state of glutathione in the endoplasmic-reticulum. *Science (80-)*. 1992;257(5076):1496-1502.
147. Huang D, Gore PR, Shusta E V. Increasing yeast secretion of heterologous proteins by regulating expression rates and post-secretory loss. *Biotechnol Bioeng*. 2008;101(6):1264-1275. doi:10.1002/bit.22019
148. Wentz AE, Shusta E V. Enhanced secretion of heterologous proteins from yeast by overexpression of ribosomal subunit RPP0. *Biotechnol Prog*. 2008;24(3):748-756. doi:10.1021/bp070345m
149. Kobayashi K, Kuwae S, Ohya T, et al. High-level expression of recombinant human serum albumin from the methylotrophic yeast Pichia pastoris with minimal protease production and activation. *J Biosci Bioeng*. 2000;89(1):55-61. doi:Doi 10.1016/S1389-1723(00)88050-0
150. Vila-Perelló M, Liu Z, Shah NH, Willis JA, Idoyaga J, Muir TW. Streamlined expressed protein ligation using split inteins. *J Am Chem Soc*. 2013;135(1):286-292. doi:10.1021/ja309126m
151. Zhao W, Zhang Y, Cui C, Li Q, Wang J. An efficient on-column expressed protein ligation strategy: application to segmental triple labeling of human apolipoprotein E3. *Protein Sci*. 2008;17(4):736-747. doi:10.1110/ps.073383708
152. Miller KD, Weaver-Feldhaus J, Gray SA, Siegel RW, Feldhaus MJ. Production, purification, and characterization of human scFv antibodies expressed in Saccharomyces cerevisiae, Pichia pastoris, and Escherichia coli. *Protein Expr Purif*. 2005;42(2):255-267. doi:10.1016/j.pep.2005.04.015
153. Boado RJ, Hui EKW, Lu JZ, Pardridge WM. CHO cell expression, long-term stability, and primate pharmacokinetics and brain uptake of an IgG-paroxonase-1 fusion protein. *Biotechnol Bioeng*. 2011;108(1):186-196. doi:10.1002/bit.22907
154. Boado RJ, Pardridge WM. Genetic engineering of IgG-glucuronidase fusion proteins. *J Drug Target*. 2010;18(3):205-211. doi:10.3109/10611860903353362
155. Bell R, Ehlers M. Breaching the Blood-Brain Barrier for Drug Delivery. *Neuron*. 2014;81(1):1-3. doi:10.1016/j.neuron.2013.12.023
156. Yan F, Wang Y, He S, Ku S, Gu W, Ye L. Transferrin-conjugated, fluorescein-loaded magnetic nanoparticles for targeted delivery across the blood-brain barrier. *J Mater Sci Mater Med*. 2013;24(10):2371-2379. doi:10.1007/s10856-013-4993-3
157. Tsuchikama K. Antibody-drug conjugates : recent advances in conjugation and linker chemistries. *Protein Cell*. 2018;9(1):33-46. doi:10.1007/s13238-016-0323-0
158. Kumar A, White J, Christie RJ, Dimasi N. *Antibody-Drug Conjugates*. Vol 50. 1st

ed. Elsevier Inc.; 2017. doi:10.1016/bs.armc.2017.08.002
159. Lu H, Wang D, Kazane S, et al. Site-specific Antibody-polymer Conjugates for siRNA Delivery. *J Am Chem Soc*. 2014;135(37):13885-13891. doi:10.1021/ja4059525.Site-specific
160. Senter PD, Springer CJ. Selective activation of anticancer prodrugs by monoclonal antibody – enzyme conjugates. *Adv Drug Deliv Rev*. 2001;53:247-264.
161. Yi G, Son J, Yoo J, Park C, Koo H. Application of click chemistry in nanoparticle modification and its targeted delivery. *Biomater Res*. 2018:1-8.
162. Masserini M. Nanoparticles for Brain Drug Delivery. *ISRN Biochem*. 2013;2013.
163. Dommerholt J, Rutjes FPJT. Strain-Promoted 1,3-Dipolar Cycloaddition of Cycloalkynes and Organic Azides. *Top Curr Chem*. 2016;374(2):1-20. doi:10.1007/s41061-016-0016-4